

Experimentelle Physik

Multi-Pion Production in Deuteron-Proton Collisions at COSY-ANKE

Inaugural-Dissertation
zur Erlangung des Doktorgrades
der Naturwissenschaften im Fachbereich Physik
der Mathematisch-Naturwissenschaftlichen Fakultät
der Westfälischen Wilhelms-Universität Münster

vorgelegt von
Malte Marius Mielke
aus Warendorf

–2014–

Dekan:

Prof. Dr. Christian Weinheimer

Erster Gutachter:

Prof. Dr. Alfons Khoukaz

Zweiter Gutachter:

Prof. Dr. Johannes Wessels

Tag der mündlichen Prüfung:

Tag der Promotion:

Zusammenfassung

Die vorliegende Arbeit liefert einen Beitrag zur Erforschung von Zwei- und Drei-Pionen-Produktionsprozessen in Deuteron-Proton-Kollisionen. Während letztere bislang nur selten Gegenstand von Untersuchungen waren, werden ersteren von Teilchenphysikern seit mehreren Jahrzehnten großes Interesse entgegengebracht. Dies ist vor allem auf den sogenannten ABC-Effekt zurückzuführen, einer markanten Überhöhung des Wirkungsquerschnitts im Bereich niedriger invarianter Massen des Zwei-Pionen-Systems. Bisherige Erkenntnisse deuten stark auf einen Zusammenhang mit dem Auftreten von Nukleonresonanzen hin, kürzlich stattgefunden Experimente bringen den ABC-Effekt sogar mit der Anregung von Dibaryon-Resonanzen in Verbindung.

Die hier präsentierten Ergebnisse der mit dem COSY-ANKE-Aufbau bei einer Überschussenergie von 265 MeV exklusiv nachgewiesenen $d p \rightarrow {}^3\text{He} \pi^+ \pi^-$ -Reaktion sind aufgrund von hoher Statistik und einer guten Impulsauflösung geeignet, vertiefende Details zu Zwei-Pionen-Produktionsprozessen beizusteuern. Zu diesem Zweck wurden Ereignisse mit koinzident nachgewiesenen ${}^3\text{He} \pi^\pm$ und ${}^3\text{He} \pi^+ \pi^-$ Teilchenkombinationen analysiert. Durch die Anwendung verschiedener Selektionsmethoden war es möglich, ein praktisch untergrundfreies Datensample zu extrahieren. Die eingeschränkte geometrische Akzeptanz des ANKE-Detektors für die zu untersuchende Reaktion wurde detailliert analysiert, um eine gut funktionierende Korrekturmethode auszuarbeiten. Auf dieser Grundlage war es möglich differentielle und doppelt-differentielle Wirkungsquerschnitte für einen großen Teil der sich im Schwerpunktsystem rückwärts bewegenden ${}^3\text{He}$ -Kerne zu bestimmen. Neben der wohlbekannten ABC-Überhöhung konnten in den Invariante-Masse-Spektren Unterschiede im Verhalten der positiv und negativ geladenen Pionen mit hoher Präzision bestimmt werden. Zurückgeführt werden diese auf Beiträge zum Isevektor-Kanal des $\pi^+ \pi^-$ -Systems. Die Gesamtdaten werden durch die Modellannahme einer $N^*(1440) \rightarrow \Delta(1232) \rightarrow N$ -Zerfallskette sehr gut beschrieben. Das Modell unterschätzt jedoch überraschenderweise die beobachtete Differenz bei niedrigen invarianten Massen des Zwei-Pionen-Systems. Diese Tatsache wird als Hinweis auf weitere Beiträge zum Isevektor-Kanal interpretiert.

Die anhand desselben Datensatzes durchgeführte Extraktion der Reaktion $d p \rightarrow {}^3\text{He} \pi^+ \pi^- \pi^0$ bei einer Überschussenergie von 130 MeV, knapp unterhalb der Pro-

duktionsschwelle des η -Mesons, ermöglicht eine Untersuchung des Drei-Pionen-Endzustandes ohne Beiträge von Mesonenzerfällen. Eine Abschätzung totaler und differentieller Wirkungsquerschnitte legt nahe, dass die Reaktion nur eine untergeordnete Rolle spielt. Das ist in Übereinstimmung mit der Annahme, dass direkte Drei-Pionen-Produktion bei niedrigen Energien bevorzugt durch eine simultane Anregung der $\Delta(1232)$ - und $N^*(1440)$ -Resonanzen erfolgt.

Abstract

The presented work is a contribution to the research on two- and three pion production in deuteron-proton collisions. Whereas the latter has received very little attention so far, the former is attracting the interest of particle physicists since several decades. An important reason for this is the appearance of the so-called ABC effect, a striking enhancement in the two-pion invariant mass spectrum near its threshold. There is strong evidence that this is related to the presence of nucleons and in the context of recent investigations it is even linked to an excitation of dibaryon resonances.

The here presented results from an exclusive measurement of the $d p \rightarrow {}^3\text{He} \pi^+ \pi^-$ reaction with the COSY-ANKE facility at an excess energy of 265 MeV benefit from high statistics as well as a good momentum resolution. Events with coincidentally detected ${}^3\text{He} \pi^\pm$ and ${}^3\text{He} \pi^+ \pi^-$ combinations were used for the analysis. Various selection steps led to a very clean data sample. The limited geometrical acceptance of the ANKE detector was studied in detail in order to successfully elaborate a reliable correction method. Based on this, it was possible to determine differential and double differential cross sections for a large fraction of the backward ${}^3\text{He}$ hemisphere. The derived invariant mass distributions do allow to illuminate further details of the two-pion production processes. Besides the prominent ABC enhancement, they reveal a significant difference in the behaviour of the positively and negatively charged pions, which is interpreted to be caused by $\pi^+ \pi^-$ isovector contributions. The total results are successfully described in terms of a $N^*(1440) \rightarrow \Delta(1232) \rightarrow N$ decay chain. However, the isobar model surprisingly underestimates the charge difference at low two-pion invariant masses, indicating further contribution to the isovector channel.

Investigations on the simultaneously measured $d p \rightarrow {}^3\text{He} \pi^+ \pi^- \pi^0$ reaction at an energy just below the η meson threshold allow for a study of direct three pion production without any contributions from meson decays. Estimations on total and differential cross sections suggest a very low strength in this energy region. This is compatible with the assumption that at low energies a simultaneous excitation of $\Delta(1232)$ and $N^*(1440)$ resonances is the most important source for the direct generation of a three-pion final state.

“Habe nun, ach!”

Heinrich Faust

Inhaltsverzeichnis

1. Introduction	1
1.1. Two-pion production in nuclear fusion reactions	1
1.1.1. The ABC effect	2
1.1.2. Double pionic fusion beyond the ABC effect	5
1.2. Investigation of the $d p \rightarrow {}^3\text{He} \pi^+ \pi^-$ reaction at COSY-ANKE . . .	9
2. Experimental Setup	11
2.1. COSY	11
2.2. The magnetic spectrometer ANKE	13
2.2.1. Cluster-jet target	14
2.2.2. Forward detection system	16
2.2.3. Positive detection system	17
2.2.4. Negative detection system	17
2.3. Experimental settings used during the beam time	18
2.3.1. COSY settings	19
2.3.2. ANKE settings	20
3. Data analysis	23
3.1. AnalysisTools	23
3.2. Pre-analysis procedures	26
3.2.1. Track reconstruction	26
3.2.2. Failure analysis	27
3.3. Detector calibration	28
3.3.1. Particle momenta	28
3.3.2. Time of flight	34
3.3.3. Energy loss	35
3.4. Particle identification	35
3.4.1. Energy loss - rigidity method	35
3.4.2. Time of flight methods	36
3.5. Identification of multi-pion processes	39
3.6. Efficiency analysis	42
3.6.1. Track efficiencies	42
3.6.2. Calculation of event efficiencies under consideration of different detector combinations	43

3.6.3. Trigger efficiencies	46
4. Determination of cross sections	47
4.1. Luminosity determination via d p elastic scattering	47
4.2. Acceptance analysis for $d p \rightarrow {}^3\text{He} \pi^+ \pi^-$	48
4.2.1. Multidimensional acceptance distribution	49
4.2.2. Model-based acceptance correction	55
4.2.3. Validation of the acceptance correction procedure	61
4.3. Acceptance analysis for $d p \rightarrow {}^3\text{He} \pi^+ \pi^- \pi^0$	64
4.4. Results	68
4.4.1. Invariant mass distributions for $d p \rightarrow {}^3\text{He} \pi^+ \pi^-$	68
4.4.2. Single differential cross section for $d p \rightarrow {}^3\text{He} \pi^+ \pi^-$	71
4.4.3. Three-pion production	73
5. Conclusions and outlook	77
5.1. Two-pion production	78
5.2. Three-pion production	81
A. Appendix	85
A.1. Concepts of relativistic kinematics and associated analysis techniques	85
A.2. Basic properties of two-pion systems produced in fusion reactions of light nuclei	86
A.3. Monte Carlo generated event distributions	89

1. Introduction

The main subject of this work is the investigation of the $d p \rightarrow {}^3\text{He} \pi^+ \pi^-$ reaction. The thesis is therefore opened by a discussion on the current state of research on two pion production in collisions of nucleons and light nuclei, focussing on reactions with a bound nucleus in the exit channel. From this, a motivation for the here presented studies is put forward. Subsequently, the experimental setup and the measuring conditions are specified. The third chapter contains a detailed explanation of the data analysis procedure, including calibration and selection steps, that leads to very clean exclusive data samples of the ${}^3\text{He} \pi^+ \pi^-$ and ${}^3\text{He} \pi^+ \pi^- \pi^0$ final states. Together with a description of the normalisation procedure and a detailed elaboration of the detector acceptance, differential and double-differential cross sections for the $d p \rightarrow {}^3\text{He} \pi^+ \pi^-$ reaction and estimations on cross sections of the $d p \rightarrow {}^3\text{He} \pi^+ \pi^- \pi^0$ reaction are presented in Chapter 4. In the final chapter, conclusions on the results and suggestions on further research are discussed.

1.1. Two-pion production in nuclear fusion reactions

Research on pion production in hadronic collisions provides an important source of information to gain an extensive understanding about properties and dynamics of nucleon resonances. Due to the complexity of final states with more than two particles, theoretical work was so far focused mainly on the generation of single mesons. Progress on the field of two-pion production is accelerated thanks to a significant increase of the experimental database in recent years.

On the basis of an approach by L. Alvarez Ruso, E. Oset and E. Hernández to model two-pion production in proton-proton scattering reactions without a bound nucleus in the final state [AROH98], results from the experiments PROMICE/WASA [B⁺02a, P⁺03], CELSIUS/WASA [S⁺09] and COSY-ANKE [Dym09] can be understood to be driven by excitation processes of conventional nucleon resonances. Non-resonant contributions are found to be small. At low beam energies the direct decay of the Roper resonance $N^*(1440) \rightarrow N (\pi \pi)_{s\text{-wave}}^{I=0}$ plays a dominant role, whereas at higher

energies influences of the channel $N^*(1440) \rightarrow \Delta(1232)\pi \rightarrow N\pi\pi$, the simultaneous excitation of two $\Delta(1232)$ resonances with the process $\Delta\Delta \rightarrow NN\pi\pi$ and higher lying resonances come up [S⁺11].

In case of double-pionic fusion processes, where the outgoing nucleons emerge in a bound state, the situation appears to be more complex. A lot of effort was put into investigations on a peculiar phenomenon, named ABC effect, which is still a matter of debate. Other features of these reaction types were paid less attention to and are hence only scantily illuminated. In the following subsections the current situation is discussed in more detail.

1.1.1. The ABC effect

A characteristic feature which could be observed for various particle combinations is the so-called ABC effect. Named after the authors of the first publication which reported its appearance; A. Abashian, N. E. Booth and K. M. Crowe; it became manifest as an enhancement over phase space in the high momentum region of inclusively detected ${}^3\text{He}$ particles from proton-deuteron collisions [ABC60]. The ${}^3\text{He}$ momentum spectrum for one particular beam energy of the corresponding experiment can be found in Figure 1.1. Through kinematic considerations it could be concluded that this behaviour is equivalent to an excess of events at low invariant masses^a of the undetected two-pion system^b, in the following termed as $m_{\pi\pi}$. The early assumption that the structure is caused by a $\pi\pi$ resonance could soon be discarded, because the position and the width of the observed structure showed a notable angular [BA63] and energy dependence [B⁺73]. Likewise, the hypothesis of a strong s-wave $\pi\pi$ final state interaction [BA63] could be falsified through the determination of a rather small scattering length by theoretical calculations [Wei66] and a corresponding analysis of experimental data of the reaction $\pi^- p \rightarrow \pi^0 \pi^0 n$ [M⁺70].

Numerous experiments which aimed for the investigation of two-pion production processes revealed the ABC effect to appear only in nuclear fusion reactions which allow the outgoing pion-pair to be in an isospin-zero state^c, namely $n p \rightarrow d (\pi\pi)^0$, $p d \rightarrow {}^3\text{He} (\pi\pi)^0$ and $d d \rightarrow {}^4\text{He} (\pi\pi)^0$.^d For these channels, some common phenomenological features could be identified [B⁺73, B⁺06, A⁺11, A⁺12]:

^a A short description of the underlying kinematical concept is given in the Appendix A.1.

^b Due to conservation of charge, the two-pion system is electrically neutral. The individual pions can either be both electrically neutral or oppositely charged.

^c In the following, the synonymus expressions “ $I_{\pi\pi} = 0$ ” and “isoscalar” will also be used.

^d It needs to be stated at this point, that indeed some other reactions also show anomalies in the low $m_{\pi\pi}$ region. However, in these cases the enhancements are usually small or the measured observables differ in some other way from the common ABC effect. Somewhat ambiguous are processes which include the formation of quasi-particles like diprotons. Although clear deviations

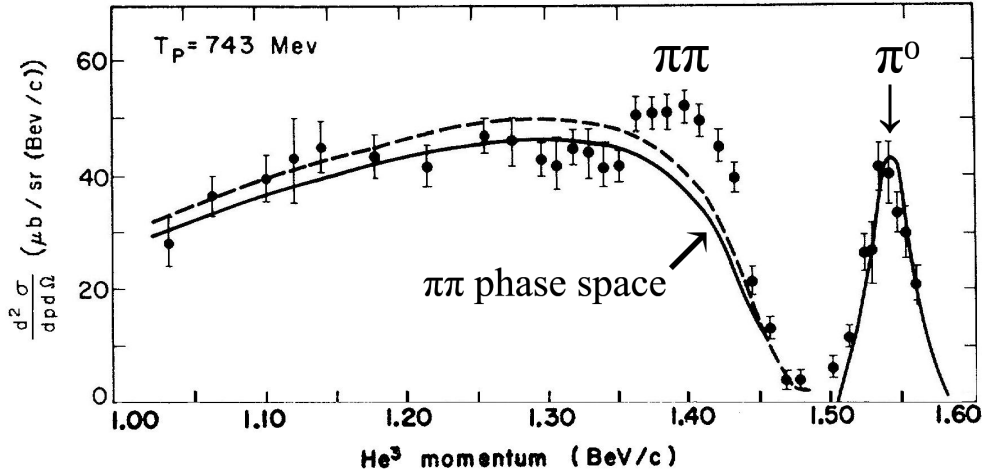


Figure 1.1.: First publication of the ABC effect. Shown are double-differential cross sections of detected ${}^3\text{He}$ particles as function of the reconstructed laboratory momenta. The enhancement above the phase space calculations around 1.4 GeV/c was later referred to as ABC effect. From Reference [ABC60].

(I) On an absolute energy scale, the cross sections show a peak structure in a region close to the production thresholds of one $N^*(1440)$ or two $\Delta(1232)$ resonances. Its width is, particularly in case of proton-neutron scattering, however much smaller than predicted by conventional model calculations (see Figure 1.2). The characteristic $m_{\pi\pi}$ enhancement is only observed in the region of this peak.

(II) The polar-angle distributions of the outgoing nuclei which are associated with the ABC effect show a strong preference of the forward and backward direction in the centre-of-mass frame.

(III) The spectra of the invariant masses of the nuclei and one of the pions exhibit a peak structure, indicating the excitation of Δ resonances.

A detailed conventional explanation of all these phenomena has not been found so far. For the specific case of the $d d \rightarrow {}^4\text{He}(\pi\pi)^0$ reaction a dynamical model, proposed by A. Gårdestig, G. Fäldt and C. Wilkin [GFW98], succeeded in the description of inclusively measured missing-mass distributions, taken at various energies and angles [B⁺76], and the deuteron analysing powers obtained from another experiment [W⁺99]. Moreover one can find a reasonable reproduction of invariant mass and angular distributions from an exclusive measurement by the CELSIUS-

from phase space are seen on condition of particular angular restrictions [D⁺09], these are assumed to be caused by conventional production processes [D⁺09, S⁺11].

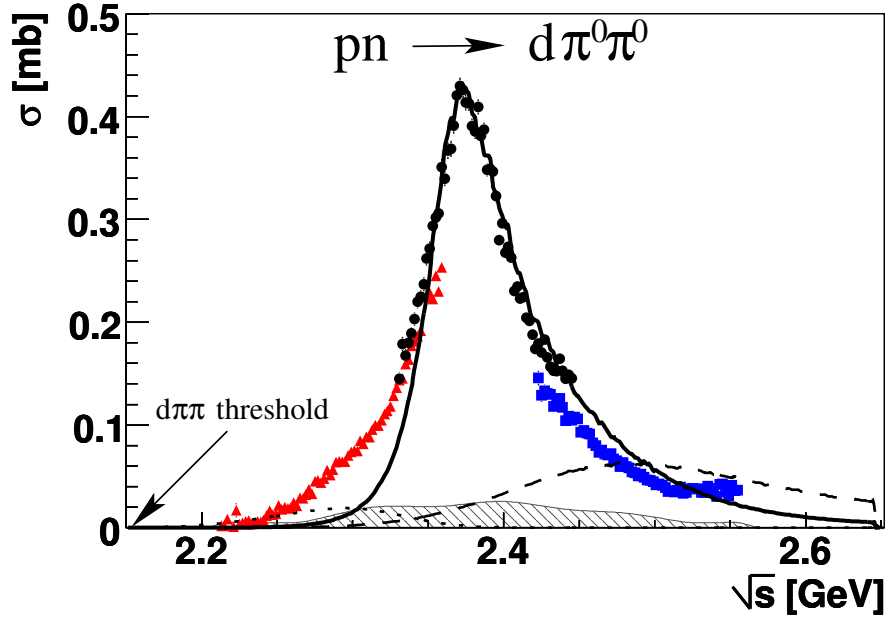


Figure 1.2.: Spectrum of total cross sections of the reaction $pn \rightarrow d\pi^0\pi^0 + p_{\text{spectator}}$ from the WASA-at-COSY experiment. The region of the peak structure is associated with the ABC effect. The solid line represents a calculation of an exotic s -channel resonance of mass $2370 \text{ MeV}/c^2$ and width $70 \text{ MeV}/c^2$. Expected shapes of contributions from conventional $\Delta\Delta$ (dashed) and $N^*(1440)$ (dotted) excitation processes are also shown. From Reference [A⁺11].

WASA collaboration at an excess energy of $Q = 230 \text{ MeV}$,^e for both charged and uncharged pions [K⁺09]. The model follows the idea of a double- Δ excitation with the pions being produced in two independent $NN \rightarrow d\pi$ reactions. Besides the ABC peak it also predicts an enhancement at high $\pi\pi$ invariant masses, as present in the mentioned inclusive data and those from CELSIUS-WASA. However, recent results from WASA-at-COSY for the $dd \rightarrow {}^4\text{He}\pi^0\pi^0$ reaction do not reflect such an enhancement in a broad excess energy range of $Q = 220 - 270 \text{ MeV}$ [A⁺12], leading to an ambiguous situation.

In the course of the publication of the distribution of total cross sections for the $np \rightarrow d\pi^0\pi^0$ reaction measured by the WASA-at-COSY collaboration, the authors suggested the formation of a dibaryon resonance of mass $2370 \text{ MeV}/c^2$ and width $70 \text{ MeV}/c^2$ with the quantum numbers $I(J^P) = 0(3^+)$ [A⁺11] (see also Figure 1.2).

^e The excess energy Q reflects the total kinetic energy in the centre-of-mass frame. It is derived from the total centre-of-mass energy \sqrt{s} via $Q = \sqrt{s} - m_{{}^4\text{He}} - 2m_\pi$.

Similar signatures were identified with the same apparatus in the respective fusion processes to ${}^3\text{He}$ [PdR14a] and ${}^4\text{He}$ [A⁺12]. A clarification of this issue is obviously of high interest and therefore the subject of further intense research. In support of this, an understanding of further nuclear fusion processes which are accompanied by two-pion production could provide valuable information.

1.1.2. Double pionic fusion beyond the ABC effect

The ABC phenomenon has been found to appear dominantly in the $\pi\pi$ isospin $I_{\pi\pi} = 0$ channel of nuclear fusion reactions in a broad excess energy range around $Q = 250$ MeV.^f At significantly lower energies, as well as in the $\pi\pi$ isovector channel (with $\pi\pi$ isospin $I_{\pi\pi} = 1$), the same type of reactions shows a very different behaviour.

Low energy region ($Q < 100$ MeV)

In kinematically complete measurements of $p d \rightarrow {}^3\text{He} \pi^+ \pi^-$ at $Q = 70$ MeV with the COSY-MOMO experiment, where no differentiation between the pion charges was made, a steep rise of the two-pion excitation energy towards higher values was found instead of the ABC enhancement [B⁺99]. The authors interpreted this finding to be linked with a dominance of relative p-waves in the $\pi^+\pi^-$ system. To maintain the symmetry of the total pion wave function, this would lead to a relative isospin $I_{\pi\pi} = 1$.^g Contrary to this, the identity of neutral pions does not allow for a relative angular momentum $l = 1$ in case of $\pi^0\pi^0$. As a consequence, a strong isovector contribution to the charged pion channel should become manifest in the relation of the total cross sections $\sigma_{\pi^+\pi^-}$ and $\sigma_{\pi^0\pi^0}$ as well as in the appearance of the respective invariant mass distributions $m_{\pi^+\pi^-}$ and $m_{\pi^0\pi^0}$. The only published data in this energy region from exclusive measurements of both channels were taken at the CELSIUS accelerator at $Q_{\pi^+\pi^-} = 28$ MeV (and accordingly $Q_{\pi^0\pi^0} = 37$ MeV) [A⁺00]. From a comparison of the extracted total cross sections the ratio $I = 1/I = 0$ of the contributions to the charged pion channel was deduced to be 1.4 ± 0.4 .^h This finding supports the assumption of strong p-wave contributions in the COSY-MOMO data. Also in accordance with COSY-MOMO the $m_{\pi\pi}$

^f The width of the resonance structure associated to the ABC phenomenon is observed to increase with the number of fused nuclei. The WASA-at-COSY collaboration reports values of $\Gamma_2 = 70$ MeV, $\Gamma_3 = 85$ MeV and $\Gamma_4 = 124$ MeV, with Γ_N denoting the total cross section widths for double-pionic fusion reactions to deuterium ($N = 2$), ${}^3\text{He}$ ($N = 3$) and ${}^4\text{He}$ ($N = 4$) [A⁺11, PdR14a, A⁺12]. The authors of the respective publications explain this with effects from Fermi motion and collision damping.

^g See Appendix A.2.

^h Note that one has to account for the cross section ratio $\sigma_{I_{\pi\pi}=0}(\pi^+\pi^-) = 2\sigma(\pi^0\pi^0)$. See also Appendix A.2.

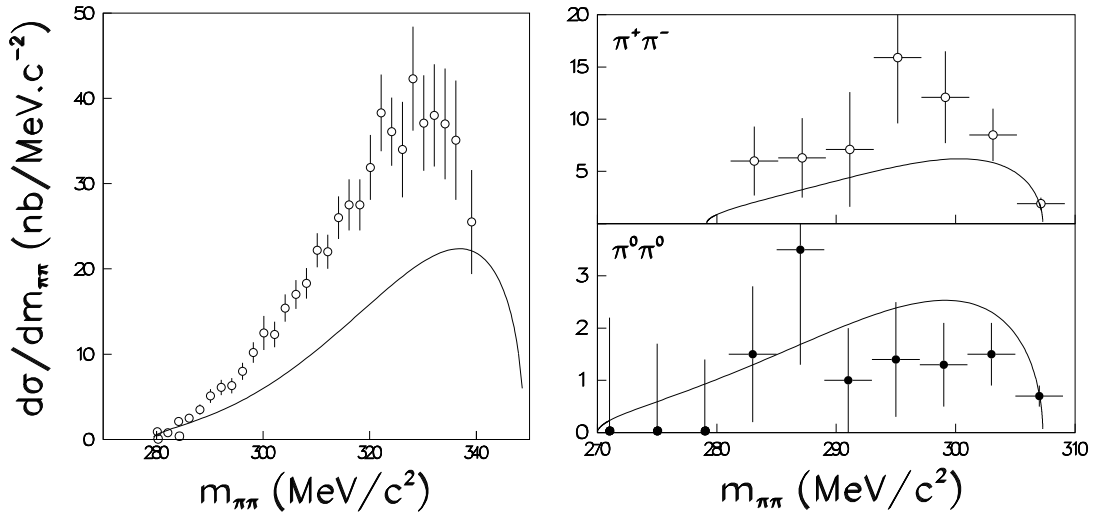


Figure 1.3.: Predictions of the FGW-model in comparison with experimental data of the $pd \rightarrow {}^3\text{He} \pi^+ \pi^-$ reaction from COSY-MOMO (left) and the $pd \rightarrow {}^3\text{He} \pi^+ \pi^- / \pi^0 \pi^0$ reactions from CELSIUS (right). From Reference [FGW00].

distributions show no sign of an ABC effect. However, because of low statistics it is hardly possible to draw definitive conclusions on the shape of the spectra.

An attempt by G. Fäldt, A. Gärdestig and C. Wilkin (FGW) to describe the proton-deuteron fusion processes with isoscalar two-pion production in terms of sequential single-pion production succeeded in reproducing the suppression at low $\pi\pi$ masses [FGW00]. Figure 1.3 shows the calculations in comparison to the results from COSY-MOMO and CELSIUS. The model however completely neglects influences of isovector contributions and therefore the possibility of odd $\pi\pi$ partial waves. In addition the authors ruled out the possibility of a simple model extension that could lead to a $\pi\pi$ p-wave dominance.

For fusion reactions of proton-neutron and deuteron-deuteron combinations no exclusively measured $\pi\pi$ data at low energies are available. In the case of inclusively detected deuterons at $Q_{\pi^+\pi^-} = 70$ MeV by C. L. Hollas and collaborators [H⁺82], an enhancement at high missing-mass values points towards a similar behaviour as observed in the fusion to ${}^3\text{He}$. L. Alvarez-Ruso explained the results in terms of an interference of two decay channels of the Roper resonance, namely $N^*(1440) \rightarrow \Delta(1232)\pi \rightarrow N\pi\pi$ and $N^*(1440) \rightarrow N(\pi\pi)_{s\text{-wave}}^{I=0}$ [AR99]. The spectra produced by the latter process are similar to phase space, whereas an inclusion of the decay through the Delta resonance leads to the observed rise towards high $m_{\pi\pi}$. The model succeeds in describing the general features of the Hollas data. However,

it implies a dominance of isoscalar pion pairs and does therefore not provide an explanation of the large isovector contributions indicated by the measurements of the $p d \rightarrow {}^3\text{He} \pi \pi$ reaction at CELSIUS and COSY-MOMO.

Investigations on the $d d \rightarrow {}^4\text{He} (\pi \pi)^0$ reactions could help to shed more light on the question of $\pi \pi$ isospin contributions at low energies, since in this case the pions are in a pure $I_{\pi\pi} = 0$ state.ⁱ A large deviation from the ${}^3\text{He}$ data would corroborate the evidence for the $I_{\pi\pi} = 1$ dominance seen by CELSIUS and COSY-MOMO. Published data from measurements with inclusively detected ${}^4\text{He}$ particles at $Q_{\pi^+\pi^-} = 20$ MeV [B⁺97] and $Q_{\pi^+\pi^-} = 57$ MeV [C⁺66] show no clear deviations from phase space. However, since both datasets suffer from a lack in statistics the results do not allow to completely rule out a shift towards high missing-mass values. As pointed out by G. Fäldt, U. Tengblad and C. Wilkin, there is up to now no agreed model which allows for a proper description of these data [FTW06].

In summary, it can be stated that knowledge about two-pion production in nuclear fusion reactions at low energies ($Q < 100$ MeV) is still ambiguous. The existing theoretical explanations adequately reproduce the experimentally reconstructed features of the reactions $n p \rightarrow d \pi \pi$ and $p d \rightarrow {}^3\text{He} \pi \pi$, but imply a dominance of isoscalar pion pairs. This conflicts with experimental evidence for a strong isovector contribution at least in the ${}^3\text{He}$ case. However, the database is too thin for drawing firm conclusions. The same holds for the fusion to ${}^4\text{He}$, where isospin conservation requires the two pions to be in a pure isospin-zero state. Provided that $I_{\pi^+\pi^-} = 1$ plays an important role at small energies, one could assume it to be relevant in the ABC region as well. There is however the challenge to extract its ratio in the presence of the strong isoscalar contribution of the ABC effect.

Isovector contributions in the ABC region

Explicit investigations on the isovector channel are possible with pion combinations $\pi^\pm \pi^0$, because in this case the third component of isospin can only couple to ± 1 .^j Exclusive data of measurements on the reaction $p p \rightarrow d \pi^+ \pi^0$ at an excess energy of 213 MeV show indications for the influence of $\Delta(1232)$ resonances in the $d\pi$ invariant mass spectra [K⁺10]. As expected for $I_{\pi\pi} = 1$, no ABC-like enhancement at low $m_{\pi\pi}$ is seen. The authors describe the results in terms of a conventional $\Delta\Delta$ excitation model [RS73] which is supplemented by an isovector-channel operator. The calculations provide a good overall description of the data, but slightly underestimate the peak widths in the $m_{d\pi}$ spectra. Due to the high energy, which is needed for

ⁱ See Appendix A.2.

^j In principle two pions can also couple to $I_{\pi\pi} = 2$. As shown in the Appendix A.2, isospin conservation forbids this coupling in each of the possible fusion processes of nucleons and/or deuterons to stable particles.

1. Introduction

the excitation of two simultaneously excited $\Delta(1232)$ particles ($2m_\Delta - 2m_N = 310$ MeV/ c^2), it is, despite a full width of $\Gamma_\Delta = 120$ MeV/ c^2 , anyway unlikely that this process plays a notable role at significantly lower energies. It is therefore no candidate for the influences discussed in Section 1.1.1.

The double-pionic fusion process of protons and deuterons to tritons and $\pi^+\pi^0$ pairs was studied in the context of the original ABC experiments at $Q_{\pi^+\pi^0} = 188$ MeV [BAC61] and later at the Saclay synchrotron Saturne at $Q_{\pi^+\pi^0} = 337$ MeV and $Q_{\pi^+\pi^0} = 354$ MeV [B⁺73]. In both cases the results were used to identify the isospin nature of the ABC enhancement in the ${}^3\text{He}$ production processes at similar kinematic conditions. At low $m_{\pi\pi}$ values the isoscalar part was found to be above 90%, revealing the effect to be dominantly in the $\pi\pi$ isospin $I_{\pi\pi} = 0$ channel. Nevertheless the ${}^3\text{H}$ momentum spectra did show evidence for a notable $I_{\pi\pi} = 1$ contribution even at low two-pion masses. Unfortunately, neither angular dependences nor total cross sections of this reaction are known. Hence it is hardly possible to draw further theoretical conclusions on the basis of the currently available information.

Alternatively, the amount of the isovector contribution can be studied by comparison of the $d p \rightarrow {}^3\text{He} \pi^+ \pi^-$ and the $d p \rightarrow {}^3\text{He} \pi^0 \pi^0$ reactions, as done in the case of the CELSIUS measurements at $Q_{\pi^+\pi^-} = 28$ MeV [A⁺00] (see Section 1.1.2). For $Q_{\pi^+\pi^-} = 269$ MeV, where the strength of the ABC effect reaches its maximum, substantial information on this topic was provided by the CELSIUS-WASA collaboration [B⁺06]. As can be seen from the left hand side of Figure 1.4, the data show that the enhancement at low $m_{\pi\pi}$ is significantly more pronounced in the $\pi^0\pi^0$ than in the $\pi^+\pi^-$ spectrum. In part this arises from the mass difference of charged and uncharged pions, hampering an exact isospin evaluation near the two-pion threshold. Nevertheless, the different shapes of the distributions do suggest some $I_{\pi\pi} = 1$ contribution in the overall $m_{\pi^+\pi^-}$ spectrum. An according extraction led to an isovector ratio of $\approx 10\%$, mainly assigned to the high mass region. However, as a consequence of the uncertainties in the relative normalisation, the principal author considers the possibility of a relative contribution up to two times larger [Bas06, Bas14].

A possibility to study influences of the isospin-one $\pi\pi$ production without uncertainty regarding relative normalisations is given by a comparison of the ${}^3\text{He} \pi^+$ and ${}^3\text{He} \pi^-$ invariant mass distributions. In the case of the purely isoscalar combination $\pi^0\pi^0$, the fact that the two pions are indistinguishable particles causes the two $m_{{}^3\text{He}\pi}$ distributions to be necessarily identical. Hence, any deviation between $m_{{}^3\text{He}\pi^+}$ and $m_{{}^3\text{He}\pi^-}$ can be ascribed to the influence of the amplitudes for producing $I_{\pi\pi} = 1$ systems and their interferences with the $I_{\pi\pi} = 0$ amplitudes. Such a difference was found in the CELSIUS-WASA data, as can be gathered from the corresponding spectrum displayed on the right hand side of Figure 1.4. However, the

results did suffer from a rather coarse mass resolution and no quantitative analysis of this effect was performed.

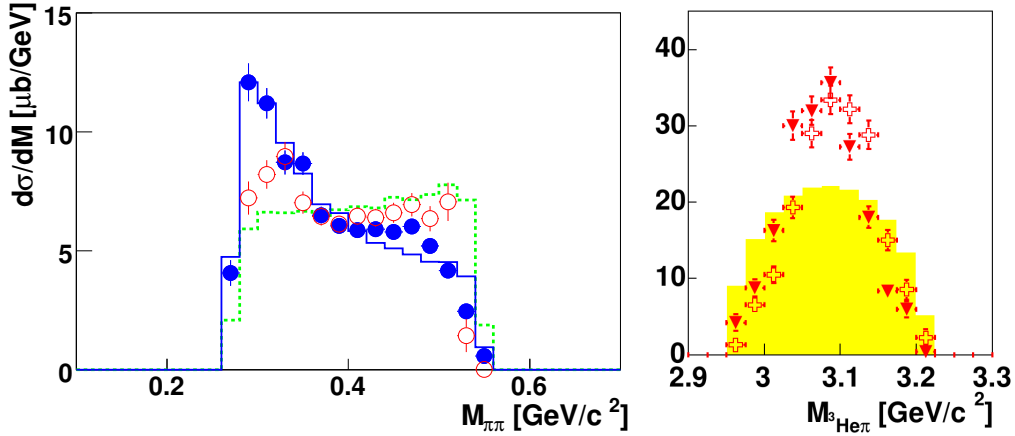


Figure 1.4.: Evidence for isovector contribution in data of the $p d \rightarrow {}^3\text{He} (\pi \pi)^0$ reaction taken in the ABC energy region at CELSIUS-WASA.

Left: Comparison of the $m_{\pi\pi}$ distributions for $\pi^0\pi^0$ (full symbols) and $\pi^+\pi^-$ (open symbols). To account for the isospin relation between both channels in the isoscalar case the $\pi^+\pi^-$ cross section was divided by a factor of two.

Right: Comparison of the $m_{3\text{He}\pi}$ distributions for ${}^3\text{He} \pi^+$ (open crosses) and ${}^3\text{He} \pi^-$ (filled triangles). The yellow bars denote a distribution according to simple phase space calculations.

From Reference [B⁺06].

To conclude, various different experimental approaches point towards relevant contributions to the isovector channel in the ABC energy region. However, these are neither understood quantitatively nor qualitatively.

1.2. Investigation of the $d p \rightarrow {}^3\text{He} \pi^+ \pi^-$ reaction at COSY-ANKE

It has been shown in the previous section that two-pion production in fusion processes of light nuclei is a lively field of research, where still a number of open questions exist. In particular, there is little substantiated knowledge about the role of the isospin-one $\pi\pi$ channel. There is evidence from experimental data on the $d p \rightarrow {}^3\text{He} \pi^+ \pi^-$ reaction, that it plays a prominent role at lower excess energies

1. Introduction

($Q < 100$ MeV), although this is not finally clarified. At higher energies the ABC effect begins to dominate, which is associated with an isospin-zero state of the two pions. However, different experimental results additionally indicate relevant $\pi\pi$ isovector contributions. Knowledge about these is very poor, but would be appropriate to deepen the insight into the dynamics of double-pionic fusion processes.

Various approaches were presented in the previous section to study $I_{\pi\pi} = 1$ contribution and its relative strength in comparison with the $I_{\pi\pi} = 0$ production intensity. Among these, the determination of the ${}^3\text{He } \pi^+ / {}^3\text{He } \pi^-$ mass difference in the $d p \rightarrow {}^3\text{He } \pi^+ \pi^-$ reaction, which depends on interference effects of the isospin amplitudes, has the advantage of an increased sensitivity in comparison to methods that depend only on the relative $I_{\pi\pi} = 1 / I_{\pi\pi} = 0$ production intensities. As a further benefit, it is independent on relative normalisations, since solely a single reaction needs to be studied. However, such an attempt requires, besides an exclusive reconstruction of the reaction, a very fine resolution of the derived invariant mass distributions.

These conditions are fulfilled by a rich data sample of the reaction $d p \rightarrow {}^3\text{He } \pi^+ \pi^-$, taken with the COSY-ANKE experiment. The excess energy of 265 MeV is very close to that of the CELSIUS-WASA measurement of the same reaction. The use of a magnetic spectrometer however significantly increases the momentum resolution of the reconstructed particles. As will be shown in this work, the high precision of the results allows to shed more light on the effects of isoscalar and isovector contributions in the ABC energy region. The benefit of high statistics is utilised to furthermore extract the ${}^3\text{He } \pi^+ / {}^3\text{He } \pi^-$ mass difference in a restricted range of low $\pi^+ \pi^-$ invariant masses. Here the $I_{\pi\pi} = 1$ part is expected to be small, because $I_{\pi\pi} = 1$ is related to relative $\pi\pi$ p-waves. The question, to what degree it still affects the $m_{{}^3\text{He}\pi^\pm}$ mass difference is a subject of the presented investigation. Conclusions on the results will be drawn on the basis of a description, which attempts to model the observed charge difference in terms of the sequential decay $N^*(1440) \rightarrow \Delta(1232)\pi \rightarrow N\pi\pi$.

2. Experimental Setup

An extensive investigation of the reaction $d p \rightarrow {}^3\text{He} \pi^+ \pi^-$ makes high demands on the experimental equipment. For an analysis of two particle invariant mass distributions it is indispensable to have access to momentum information of all three involved final state particles. Considering the law of momentum conservation, the kinematical properties of a single particle can be calculated with the knowledge of the other ones. Thus at least two ejectiles of the reaction need to be coincidentally detected. The fact that the ABC effect appears at an energy considerably above the production threshold of $d p \rightarrow {}^3\text{He} \pi^+ \pi^-$ implies a large phase space for the reaction. The momentum and angular acceptance of the detector must therefore be good enough to cover a kinematical region which enables general conclusions. Additionally the search for potentially small differences in the ${}^3\text{He} \pi$ invariant mass spectra affords a high momentum resolution and a sufficient amount of statistics.

The experiment was conducted using the ANKE facility, which is located at an internal target station of the particle accelerator COSY. It consists of a magnetic spectrometer and several high resolution detector systems for positively and negatively charged particles. It meets therefore important requirements for a systematic measurement of the reaction of interest.

This chapter contains an overview of the COSY accelerator, the relevant components of the ANKE detector system and the experimental settings of the measurement.

2.1. COSY

The COoler SYnchrotron COSY [Mai97], schematically depicted in Figure 2.1, is a medium-energy accelerator and storage ring which is located at the Forschungszentrum Jülich. It provides unpolarised as well as polarised proton and deuteron beams of momenta up to $3.7 \text{ GeV}/c$ and has the possibility to store up to $5 \cdot 10^{10}$ unpolarised or $1 \cdot 10^{10}$ polarised beam particles at revolution frequencies of $0.26 - 1.6 \text{ MHz}$.

2. Experimental Setup

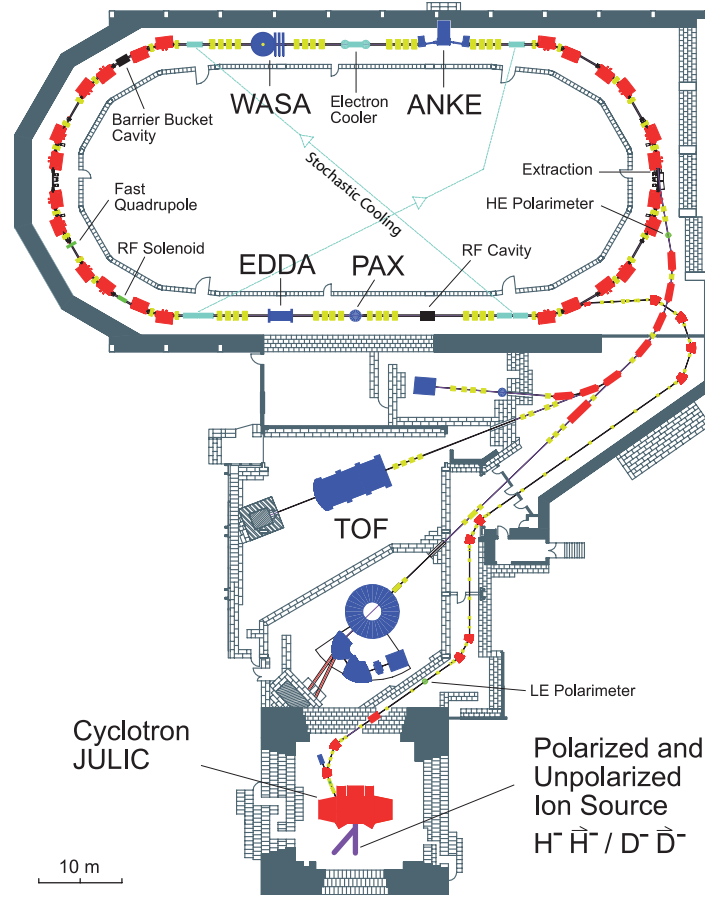


Figure 2.1.: The COSY accelerator facility. Polarised or unpolarised proton and deuteron beams from the cyclotron JULIC are injected into the synchrotron ring. The accelerated beam can be extracted to the external target stations or stored for measurements at the internal experiments. This is a modified version of a sketch provided by the Institute for Nuclear Physics (IKP) of Forschungszentrum Jülich, taken from Reference [Gos13].

The name Cooler Synchrotron refers to the two integrated cooling mechanisms [P⁺00], which improve the beam momentum resolution from $\Delta p/p = 10^{-3}$ to $\Delta p/p = 10^{-4}$. At injection energy the appropriate tool is an electron cooler, whereas for higher beam momenta ($> 1.5 \text{ GeV}/c$) the technique of stochastic cooling can be used.

Another device that is applicable for improvement of the beam quality is the broadband barrier bucket (bb) cavity [S⁺08]. In contrast to the cooling mechanisms, which mainly affect on the transversal momentum components, the bb cavity can be used to control the longitudinal beam dynamics. This allows to stabilise the mean value of the beam momentum over time.

For measurements with polarised beams, the internal experiment EDDA, originally optimised for the investigation of elastic proton-proton scattering processes, can be used as a fast beam polarimeter [Sch99]. It is equipped with a carbon fibre target and two shells of scintillating detector material.

An important tool for the manipulation of polarised beams is the radio frequency (rf) solenoid. By generating weak longitudinal magnetic fields within a frequency range of 0.5 – 1.5 MHz it allows to induce spin-direction reversals (spin flips) of the COSY beam particles.

2.2. The magnetic spectrometer ANKE

The magnetic spectrometer ANKE (**A**pparatus for **S**tudies of **N**ucleon and **K**aon **E**jectiles [B⁺01b]) is an internal experiment of the COSY storage ring, placed at one of its two straight sections. It consists of a variety of applicable targets, a magnetic system comprising three dipole magnets, and several detection systems for charged particles. A sketch of the installation is shown in figure 2.2.

The experimental design is driven by the aim of identifying any kind of charged ejectile from the beam-target interaction zone and determining its momentum with high accuracy. For that matter the central dipole magnet D2 is of particular importance. It separates the reaction products from the unscattered beam particles and guides them, according to their charge and momentum, onto the different detector systems. The curvature of its flight path then allows to precisely deduce the particle's ratio of momentum and charge, termed rigidity. The spatial track information needed for that is provided by multiwire drift- and proportional chambers (MWDC/MWPC). For the purpose of particle identification Čerenkov and plastic scintillation counters can be used.

To optimise the geometrical acceptance for the respective reaction of interest, the D2 magnet and parts of the surrounding detectors can be moved perpendicular to the beam direction. This affects on the deflection angle α of the beam. To guide the unscattered beam particles back into the beam pipe, there is a defined value of α for each combination of beam momentum and D2 field strength. The maximum values for deflection angle and flux density are $\alpha = 10.6^\circ$ and $B = 1.57$ T.

Depending on the requirements of the measurement, ANKE can be equipped with either a solid strip target [K⁺01], a polarised gas target [M⁺13] or an unpolarised cluster-jet target [K⁺99]. The first is used for investigation of reactions with heavy nuclei, whereas the two latter ones provide hydrogen or deuterium as target material. Deuterium can be also used for experiments on a quasi-free neutron target [Sch12]. In this scenario a low energy spectator proton is emitted, which can be detected

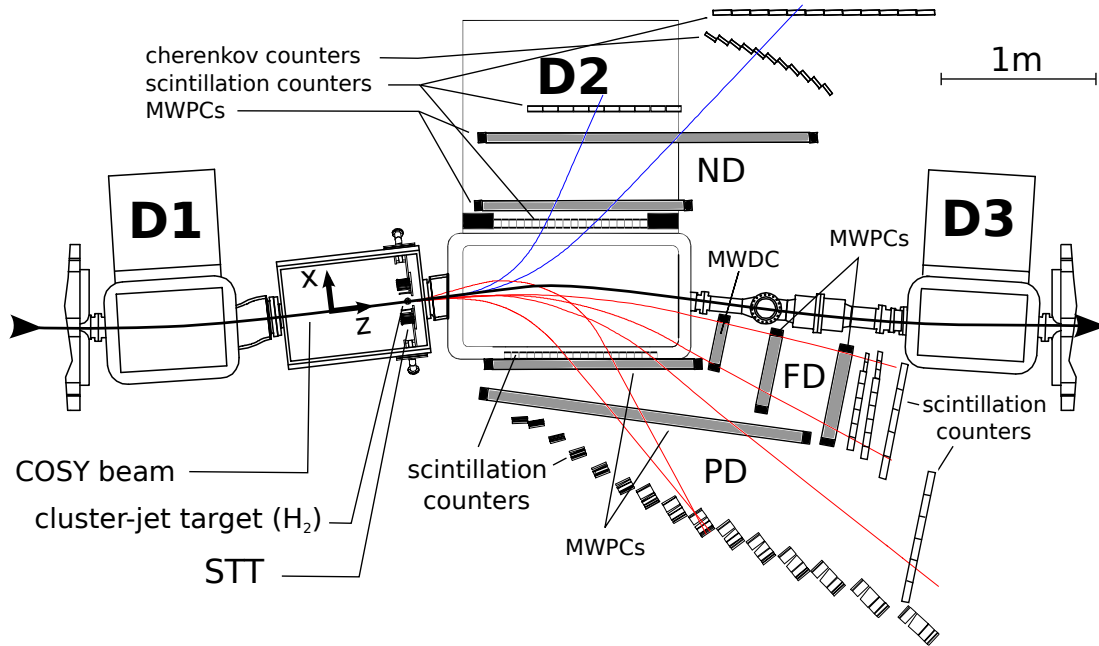


Figure 2.2.: Top view of the ANKE spectrometer. The beam, coming from the left, is deflected by the dipole magnets D1 and D3 onto the target and back to the nominal orbit. The spectrometer magnet D2 separates the reaction products from the beam and guides them onto the various detector systems for positively and negatively charged particles. This is a modified version of a sketch provided by the Institute for Nuclear Physics (IKP) of Forschungszentrum Jülich.

with the silicon tracking telescopes (STT), a set of vertex detectors consisting of silicon strip counters.

For the investigation of the reaction $d p \rightarrow {}^3\text{He} \pi^+ \pi^-$ the forward (FD), positive (PD), and negative (ND) detector systems were used in combination with a hydrogen cluster-jet target. In the following sections these components are described in more detail.

2.2.1. Cluster-jet target

The technique of cluster jet beams is ideally suited to meet the requirement of an unpolarised proton target at an internal accelerator experiment. It provides material of very high purity with a time-invariant density distribution; its areal density can be continuously regulated up to 10^{15} atoms/cm² and the cluster beam

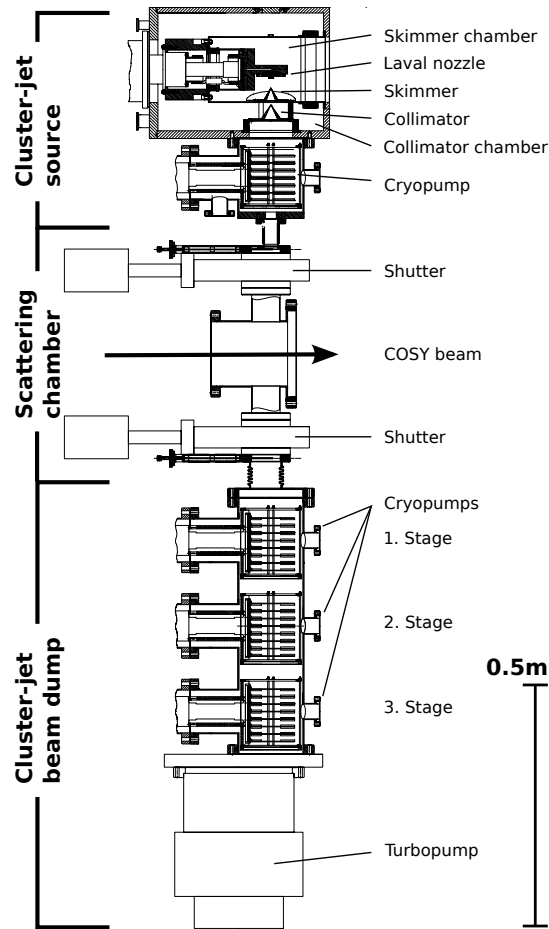


Figure 2.3.: Setup of the cluster-jet target at ANKE. This is a modified version of a sketch provided by A. Khoukaz, taken from Reference [Gos13].

is spatially well defined, which allows to accurately determine the vertex region of a reaction.

Thanks to the very successful operation during more than 15 years at ANKE [K⁺99] and COSY-11 [D⁺97], Münster type cluster-jet targets have proven their high suitability for modern experiments in particle physics. Current developments of enhanced types are scheduled to be used for laser-induced ion acceleration [Gri14] and for the future PANDA experiment at the accelerator facility FAIR in Darmstadt [T⁺11, Her13, Köh].

To produce a cluster beam, hydrogen or deuterium gas of pressures between 10 and 20 bar is cooled down to a temperature of 20 to 35 K and pressed through a nozzle

with a convergent-divergent profile, a so-called Laval nozzle. The highest target densities are observed for high pressures in combination with low temperatures. The formation process of the clusters depends on the vapour pressure conditions of the hydrogen. Investigations from the Münster cluster target group have shown that for the typical measuring conditions at the ANKE experiment the cluster beam can be interpreted as a spray of liquid hydrogen [Köh10, Täs12].

Figure 2.3 illustrates the setup of the ANKE cluster-jet target. It is composed of a cluster source and a beam dump, which are connected through the scattering chamber. Originating in the nozzle, the beam is separated from the residual gas by a conical orifice, called skimmer. A further orifice, the collimator, defines the final shape of the cluster jet that interacts with the accelerator beam. The passage into the high vacuum of the scattering chamber is accomplished by several pumping stages using roots-, rotary vane-, turbo molecular- and cryopumps. This method of differential pumping is also applied in the beam dump.

2.2.2. Forward detection system

Compared with the beam particles, positively charged ejectiles with a high longitudinal momentum are only slightly deflected by the spectrometer. To measure them the so called forward detection system is placed close to the beam pipe, almost fully utilising the gap of 1.6 metre length between the magnets D2 and D3. It consists of one multi-wire drift chamber (MWDC), two multi-wire proportional chambers (MWPC) and a scintillation hodoscope. The latter is originally composed of two layers, but can optionally be complemented by a third one. For this purpose usually one of the layers from the side wall of the positive detector system is used (see section 2.2.3). An illustration of the arrangement can be found in Figure 2.2.

The development of the forward detector system was driven by the motivation to achieve a good momentum resolution at high particle fluxes, despite small curvatures of the ejectile tracks and the fact that the space between the chambers is necessarily small. As a consequence of that, no scintillation counters were placed close to the exit window of the D2 magnet, which would have facilitated time of flight measurements for single particles.

The proportional chambers each include two modules; one of them is vertically orientated, the other horizontally. Both are constructed of one strip and two wire planes. The former is used as active cathode inclined by 18° with respect to the wire orientation. The latter are anode planes shifted against each other, such that their individual wire spacing of 2 mm enables an effective spatial resolution of 1 mm. As the proportional chambers, the drift chamber is composed of two modules. The first one consists of three planes where vertical anode and cathode wires are

arranged alternately. In the second module are four planes with wires inclined by 30° . With chambers of this type spatial resolutions of up to $200\ \mu\text{m}$ can be achieved. By using all three wire chambers a rigidity resolution of $\approx 1\%$ is possible.

The scintillation hodoscope is built up of two modules with eight, respectively nine, vertically orientated panels of plastic scintillation material. These have a height of 360 mm, a width of 40 to 80 mm and a thickness of 15 to 20 mm, depending on their distance to the beam pipe. Each counter is read out by photomultiplier tubes located at the upper and lower ends, providing timing (TDC) and amplitude (ADC) signals. Mean timer modules are used to reduce the time dependence on the vertical hit position.

2.2.3. Positive detection system

Positively charged particles with relatively low momenta ($< 1.1\ \text{GeV}/c$) have tracks with a strong curvature and mostly do not pass the forward detector system. They can be detected in the positive system, which was basically designed for the purpose of kaon investigation. 15 telescopes, equipped with scintillation counters, passive degraders and in part Čerenkov counters, are placed along the focal surface of the spectrometer magnet, each one covering a defined momentum range of roughly $30\ \text{MeV}/c$ [B⁺02b]. For particle identification Čerenkov light, veto, energy loss and timing information are accessible. In combination with the start signals from the plastic scintillators located directly at the exit window, time of flight information for single tracks can be extracted. To limit multiple scattering effects on the track reconstruction the start counters have a thickness of only 0.5 to 2 mm. Heights of 270 mm and widths of 50 mm are identical for all 23 layers. For particles with momenta outside the telescope acceptance the so-called side-wall is installed, two layers of five and six scintillators with a width of 100 mm, a height of 1000 mm and a thickness of 10 mm. For the measurement of the reaction $d\ p \rightarrow {}^3\text{He}\ \pi^+\ \pi^-$ the layer with six counters was moved to the forward detector system to improve the ${}^3\text{He}$ selection by energy loss cuts.

To enable track reconstruction two multi-wire proportional chambers are placed between the start counters and the telescopes. Both have three planes, arranged vertically and inclined by $\pm 30^\circ$ respectively. A wire spacing of 2.54 mm allows for a pion momentum determination with an accuracy of 2-3 %.

2.2.4. Negative detection system

This detector system was designed for the measurement of negatively charged kaons and pions which are deflected to the outside direction of the accelerator ring. It

is composed of two multi-wire proportional chambers, Čerenkov detectors as well as two layers of scintillation counters. A large part of it is placed inside the iron yoke of the D2 magnet. The 22 start counters each have a width of 50 mm, a height of 270 mm and a thickness of 2 mm. Owing to the lack of space inside the yoke, the layer with stop counters is subdivided into two parts. For the first 12 counters the dimensions are 350 mm · 80 mm · 10 mm (height · width · thickness), for the other 10, which are located outside the dipole, 250 mm · 150 mm · 20 mm. The two multi-wire proportional chambers between the scintillation layers are of identical construction as the chambers in the positive system. The accuracy of the momentum reconstruction is accordingly similar. Additionally 11 curved Čerenkov counters are installed for pion–kaon separation at high momenta.

2.3. Experimental settings used during the beam time

The principal aim of the experimental proposal leading to the measurement of the $d p \rightarrow {}^3\text{He} \pi^+ \pi^-$ reaction was the determination of the η meson mass. The choice of the experimental settings resulted therefore mainly from the corresponding requirements. In this section they are briefly summarised, with a focus laid on the aspects that are relevant for the presented analysis. A comprehensive description can be found in the PhD thesis of P. Goslawski [Gos13].

The idea of η meson mass determination applied here, makes use of the special kinematic properties of two-body final states. In these cases the centre-of-mass (CM) momenta of the involved ejectiles have, as a consequence of momentum conservation, identical absolute values. For a particular reaction, their magnitude depends solely upon the total CM energy \sqrt{s} . In case of a beam incident on a target at rest, this is defined by the beam momentum and the masses of the involved particles. Provided that the masses of three of the four particles are known, the mass of the fourth one can thus be calculated for any CM energy above the production threshold from the respective combination of beam and ejectile momentum ($p_{\text{beam}}, p_{\text{ejectile}}$).

An appropriate reaction for the determination of the η meson mass with the ANKE spectrometer at the COSY facility is $d p \rightarrow {}^3\text{He} \eta$. The masses of the involved light nuclei are well known, the momentum of the doubly charged ${}^3\text{He}$ particle $p_{{}^3\text{He}}$ can be precisely measured with the forward detector system, and an accurate determination of the deuteron beam momentum p_d is possible thanks to the so-called resonant depolarisation technique (see section 2.3.1).

For kinematical reasons the optimal precision is gained if the reaction threshold can be ascertained. The best way to achieve this is a measurement of multiple ($p_d, p_{{}^3\text{He}}$)

pairs at low excess energies. The knowledge of the functional relation between p_d and $p_{3\text{He}}$ allows then to extrapolate the beam momentum towards the threshold at $p_{3\text{He}} = 0$.

The resulting experimental strategy, as well as the required settings of the COSY accelerator and the ANKE spectrometer, are treated in the following subsections.

2.3.1. COSY settings

In total, the experiment was carried out at 18 closely-spaced total energies between 3.353 and 3.374 GeV, alternately subdivided into three blocks. Subsequent to the preparation of the beam energies, the measurements of the beam momenta and those at the ANKE spectrometer were performed separately from each other. Whereas for the former the usage of a polarised beam is indispensable, the latter was operated with unpolarised particles in order to ensure a sufficiently high luminosity.

Settings for the beam momentum measurement

At the beginning of each block the resonant depolarisation technique was applied to determine the beam momenta. At the end of the first and second block this was repeated for the sake of studying systematic effects. The procedure makes use of the effect that a polarised accelerator beam can be depolarised by induction of a horizontal radio frequency magnetic field, in this case created by an appropriate rf solenoid (see section 2.1). The depolarisation frequency coincides with that of the spin precession in the ring and depends linearly on the kinematic γ -factor of the beam [D⁺80]. The position of the resonance for a certain beam momentum could be identified by measuring the polarisation with the EDDA detector in dependence of the solenoid field frequency. In combination with the knowledge of the beam revolution frequency, obtained by analysis of the so-called Schottky noise [M⁺01], this allowed to calculate the beam momentum with an accuracy of $\Delta p/p = 3 \cdot 10^{-5}$.

A more detailed explanation of the resonant depolarisation technique and its application for the determination of beam momenta at the COSY accelerator can be found in the diploma thesis from P. Goslawski [Gos08].

Accelerator settings for the scattering experiment

For the measurements with the ANKE spectrometer the beam energies grouped into one block were set up in a supercycle. This enabled an automatic switch of the machine settings after each injection. The length of a single cycle was set to 206 seconds. The lowest beam energy of 1.765 GeV appeared two times each in the first and in the second supercycle to allow for background studies for the reaction $d p \rightarrow {}^3\text{He} \eta$ on the basis of high statistics. From ten days of data acquisition in total for the first two blocks of energies, two and a half fell upon this setting.

In order to provide a constant average beam momentum over the whole cycle time the barrier bucket cavity (see section 2.1) was switched on after finishing the acceleration process.

2.3.2. ANKE settings

The setup for the measurements with the ANKE spectrometer was primarily adjusted to optimise the acceptance, the detection efficiency and the momentum resolution in the forward detector system for ${}^3\text{He}$ particles from the reaction $d p \rightarrow {}^3\text{He} \eta$ close to the production threshold. With a supplementary use of the two side detector systems, allowing for the measurement of positively and negatively charged pions, this ensured very good conditions for gaining a valuable data sample of the reaction $d p \rightarrow {}^3\text{He} \pi^+ \pi^-$.

The general settings were already approved in two previous ANKE experiments, which aimed for an investigation of the η - ${}^3\text{He}$ final state interaction [M⁺07, P⁺14]. The D2 spectrometer magnet was positioned such, that the beam was deflected by 5.9° from its nominal orbit. In combination with the chosen beam momenta this involved magnetic flux densities between 1.403 and 1.440 T. In the context of a previous diploma thesis, it could be shown that these parameters are also very well suited for an investigation of the double pion production [Mie07].

The main trigger T1, used to initiate the readout process of all three detector systems by the data acquisition system (DAQ), was based on information of energy loss in the scintillation counters of the forward detector system. As a consequence of the higher mass and double charge, the ${}^3\text{He}$ particles deposit significantly more energy compared to protons and deuterons. Therefore a coincident request of high amplitude signals in all three hodoscope layers was applied to suppress a large part of the non- ${}^3\text{He}$ background.

A second trigger T2 was used to record also events with protons or deuterons in the Fd system, by requesting coincident low amplitude signals in the first two hodoscope layers. To limit the increasing of DAQ dead time the trigger was pre-scaled by a

factor of 1024. By this the total data transfer rate only increased by approximately 10%. The resulting data served for detector calibration and normalisation purposes, as described in chapters 3.3 and 4.

Scaler information, like the beam current signal from the accelerator and trigger rates were read out periodically every 100 ms with a further trigger T4.

Special triggers for the coincidental detection of pions and ^3He particles were not necessary, because all events of interest for the investigation of the $d p \rightarrow ^3\text{He} \pi^+ \pi^-$ reaction were already included in the main trigger T1.

2. *Experimental Setup*

3. Data analysis

The investigation of isospin effects in the reaction $d p \rightarrow {}^3\text{He} \pi^+ \pi^-$, with the data taken at the ANKE experiment, involved a number of extensive analysis steps. To provide basic information of the registered events, the raw detector output needed to be inspected and converted into physical values; like particle momenta, energy losses and times of flight. The corresponding procedures, including track reconstruction as well as detector calibration, are explained in sections 3.2 and 3.3. Subsequently, the individual particles detected in each detector system and finally the reaction of interest as a whole, were identified by various selection methods, which are described in sections 3.4 and 3.5. To enable the extraction of differential and double differential cross sections, the impact of detector and data acquisition inefficiencies needed to be quantified on an event-by-event basis (section 3.6).

3.1. AnalysisTools

Transformation of the raw digitised information from modern particle detector systems into physically interpretable results cannot be achieved without an interplay of complex computer programmes. The software used for the processing of the data from the presented measurements will be outlined in this section, especially focusing on a new library, which was developed in cooperation with other contributors and in the context of this thesis.

All applied programmes are based on the platforms “ROOT” or “Geant4”. Both of them were written in the programming language C++ and are commonly used for analysis and detector simulation problems in particle physics and other fields of activity. The software generally used for the handling of the data from the ANKE detector is the “RootSorter” [HHM02]. It provides a number of essential standard methods, such as track reconstruction and chamber efficiency determination. An important application is the online monitoring of running measurements. An appropriate tool for the simulation of the detector response to reactions of interest is AnkeGeant4 [Mus04], which accesses the same setup information as the analysis software. As a source for primary particles the ROOT-based event generator PLUTO [F⁺07] is mostly used.

To ensure equal treatment of the measured and simulated data it is advisable to use, at least from a particular stage of the analysis, a code that allows to process both kinds of input sources in the same way. In the Münster part of the ANKE collaboration it has become well established to use the RootSorter for a preselection of the raw data, including a determination of particle momenta, and to treat its output with the same software that is applied on the files produced with AnkeGeant4.

The construction of an adequate framework, which is suited to establish a standardised foundation for extensive analyses, was initiated by M. Papenbrock [Pap] and developed further in cooperation with several members of the group. The library package “Reconstruction” makes use of the concept of object-orientated programming and supports the work with a modular structure. As a consequence the user code may be subdivided into various individual parts, which can be easily added to or removed from the analysis procedure.

All modules that build on the “Reconstruction” library obligatory contain four basic methods:

- ↓ startProcessing
- ↓ processCut
- ↓ processEvent
- endProcessing

The program flow is organised such that each of these is processed successively for the implemented modules. The first method is called before the event loop starts, enabling for example the initialisation of variables and declaration of spectra. Within the event loop, “processCut” and “processEvent” are executed. This two-step procedure allows to define whether the current event fulfills certain conditions, and to continue its processing accordingly. Any action that is to be done after the event loop, like fit procedures and further analysis steps, is then part of the “endProcessing” method.

Access to the data and communication between the different modules is provided through the so-called “Event classes”. These offer a large number of predefined methods that enable the user to receive all relevant kinds of experimental information, regardless of whether they originate from simulations or real measurements. However, the input files have to be of AnkeGeant4 or RootSorter nature, with a structure specifically adjusted for the usage with the Reconstruction library. The addition of supplemental variables to the read-in routine is nevertheless easily possible.

The retrieval of data is considerably facilitated by making use of the concept of inheritance. The principle can be illustrated with the structure diagram shown in

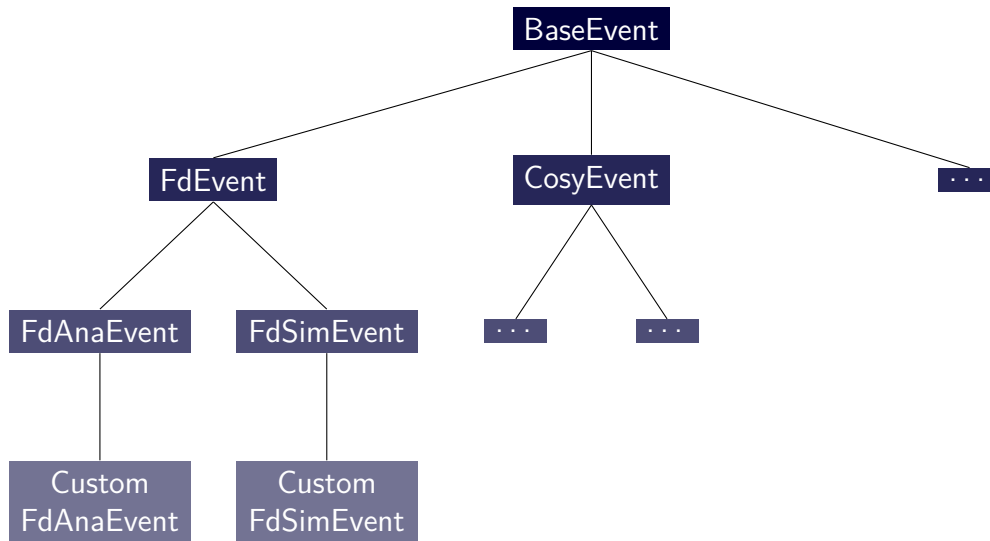


Figure 3.1.: Diagram of the inheritance structure for the “Event classes” in the “Reconstruction” library. Apart from minor changes adopted from Reference [Fri14].

Figure 3.1. All involved classes have a common framework, which is defined in the “BaseEvent” class. It contains methods and variables that are relevant for any kind of subclass, like particle masses or placeholders and getter functions for momentum vectors. At the secondary level a distinction is made between the different hardware components the requested data can be assigned to. This stage of subclasses was not a part of the original software concept, since its original design goal was focused on the analysis of Fd data solely. The new sublevel was implemented during the studies of the reaction $d p \rightarrow {}^3\text{He} \pi^+ \pi^-$, primarily in order to simplify the inclusion of Pd and Nd data in the analysis. Each detector is now accessible individually through a dedicated “DetectorEvent” class which provides access to respective raw signals and preprocessed data. General information, like beam properties or trigger numbers, can be obtained through the “CosyEvent” class. The possibility to easily add further detector systems to the analysis was for instance used by D. Schröder in the course of the examination of data measured with the ANKE silicon tracking telescope [Sch12].

Reading in the actual data happens then at the third hierarchy level. In most cases it is not necessary to directly address these classes, since the overlying “HardwareEvents” already know whether they work with simulated or measured data. Only methods that request information existing for solely one of the two have to be explicitly called from here. Moreover it is possible to derive further subclasses according to the needs of an individual analysis. In figure 3.1 they are termed “CustomEvents”. These do also serve as testing grounds for the development of

new methods.

3.2. Pre-analysis procedures

Before conducting the main analysis, the measured data were pre-processed and pre-selected by use of the RootSorter software. Through the appliance of the ^3He trigger (see section 2.3.2) a large part of the deuteron and proton induced background in the forward detector system had already been suppressed on the hardware level. For a kinematically complete analysis of the reaction $d p \rightarrow ^3\text{He} \pi^+ \pi^-$ the properties of at least two ejectiles needed to be experimentally determined. Hence a request of coincident hits in the forward and one of the side detector systems could be used to further reduce the amount of data. Besides signals from the top and bottom photomultipliers of at least one counter in each scintillation hodoscope layer, the condition for evidence of a hit implied the reconstruction of valid particle tracks.

3.2.1. Track reconstruction

The track finder algorithm uses the positions of the wires and the counters that were hit by a particle to interpolate a straight line between the chambers. To withdraw background contribution from particles that were rescattered from the poles of the D2 magnet or other material, the localisations and gradients of the lines are checked for consistency. In vertical direction this is mainly done by rejecting unrealistic correlations between the Y-values of the points where the tracks cross the chambers.^a The criteria for the horizontal direction depend on the detection system. The straight tracks reconstructed in the forward detector need to cross the exit window region of the D2 magnet, which defines therefore a geometrical acceptance limit. In the side detectors only certain combinations of start and stop counters are allowed. For the presented analysis the number of excluded combinations was complemented with the help of AnkeGeant4 simulations of the reaction $d p \rightarrow ^3\text{He} \pi^+ \pi^-$. More detailed information about the general track reconstruction mechanisms at ANKE can be found in the references [D⁺04, Jun00].

^a “Unrealistic” can here be understood such that the reconstructed track would not pass the beam-target overlap region. Since the y-component of the particle momentum is almost unaffected by the spectrometer field, consistency can be checked without time-consuming calculations.

3.2.2. Failure analysis

Despite great efforts and an excellent qualification of the people who contribute to a large experiment like ANKE, it is almost unavoidable that a minor part of the detector outputs does not have a perfect quality. In most cases this does not affect the reliability of the results, as long as the defects are carefully examined and considered in the analysis. The noticed problems and the respective solutions concerning the presented data are itemised in the following according to the affected detector system.

Forward detector system

The absolute values of the amplitude and timing signals from the hodoscope were found to shift during the first runs of the first supercycle. For the rest of the beam time no further fluctuations appeared. Because less than 3% of the total amount of relevant data were affected, these have been taken out of the analysis.

Positive detector system

For one of the start counters in the high momentum region the amplitude threshold had been set too high. As a consequence some of the pion induced signals were not registered. The counter was excluded from the analysis.

Negative detector system

Owing to an inappropriate delay setting, the mean timer signals from the start counters were not completely stored. For the analysis the timing was hence calculated by averaging the time information from the up and bottom photomultipliers, in the following sections referred to as “software mean timing”. Compared to the hardware mean timing the resolution is slightly worse. However, this affects only marginally on the quality of the final analysis.

As a result of temporary outages of the corresponding high voltage power supply, one of the stop counters was inactive for several runs. Approximately 8% of the runs were affected and therefore taken out of the analysis.

For one stop counter in the very low momentum region, the upper photomultiplier had been inactive. The counter was excluded from the analysis.

3.3. Detector calibration

A prerequisite for the identification and evaluation of the reaction of interest is the transformation of the detector output into physical information about the involved particles. Although there exist established standard procedures for the handling of the raw signals, the complex measuring conditions of each specific experiment make it necessary to perform individual detector calibrations. A description of the handling of track and scintillator information is provided in this chapter.

3.3.1. Particle momenta

Magnetic spectrometers like ANKE are adequate tools for precision measurements of ejectile momenta. They make use of the fact that charged particles moving through a magnetic field experience a defined deflection according to the Lorentz force. An effective momentum determination can be obtained by tracing the reconstructed straight tracks through the magnetic field up to the beam-target interaction zone by use of the Runge-Kutta method [MB79]. Other approaches adopted for the ANKE experiment are the boxfield and polynomial approximation techniques [Mer03, D⁺04]. In the context of the presented analysis they were solely used to generate start parameters for the most precise Runge-Kutta method.

However, the accuracy of the momentum reconstruction depends strongly on the exact knowledge of the relevant experimental parameters; namely the magnetic field strength, the orientation of the beam axis, the position of the vertex point and the coordinates and orientation of the wire chambers. Each of these was already known to a certain extent from experience, calculations or individual measurements. To reach the aimed exactness, it was nevertheless necessary to perform a fine adjustment by use of data registered during the analysed beam time. Since it is hardly possible to find an algorithm to calibrate all parameters individually that influence the reconstructed particle momenta, an established approach is the introduction of effective parameters. It is based on the assumption that a convenient combination of these compensates for all possible deviations. Adequate effective parameters are selected according to the size of their uncertainty and their sensitivity on the respective calibration method.

The explanations of the applied procedures are given in the following, subdivided according to the respective detector system.

Forward detector system

For several reasons, the calibration of the forward system was the most crucial one. To get an absolute accuracy that is comparable to that from the side detectors, the high momenta of the particles covered by the Fd acceptance necessitate accordingly a better relative accuracy. On the other hand, high momenta go along with small track curvatures, thus creating a greater sensitivity on the experimental parameters. Moreover, since all hardware triggers required a hit in the forward detector, it was the only one that could be calibrated independently. The attainable quality of the momentum determination in the side detectors is therefore limited by the achieved Fd precision. Since a high accuracy was also of central importance for the investigation of the η mass, an elaborate calibration was conducted under support of S. Dymov, a collaboration member who is highly specialised on this topic. A detailed description of his contribution is documented in a separate report [Dym09]. In the following the main aspects will be summarised and commented.

Besides the measurements performed under regular conditions, some calibration data were additionally taken with the spectrometer magnet D2 switched off. At this setting the accelerator beam remains on its nominal orbit, which is equivalent to a deflection angle $\alpha = 0^\circ$. The absence of influences from a magnetic field allows the straight tracks, reconstructed from the chamber information, to be extrapolated directly to the vertex position. The coordinates of the latter are fixed, while the X and Y positions of the chamber centres, as well as one rotation angle each, are used as parameters to optimise the χ^2 of a straight line fit. The precision of this procedure is mainly limited by the uncertainty of the vertex coordinates.

A second calibration step was performed with the regular data at $\alpha = 5.9^\circ$. Kinematical variables of several well identifiable reference reactions were used to adjust the X coordinate of the vertex point and the rotation angle of the forward detector platform.^b The χ^2 was derived through the residuals from the expected values. Most of the relevant final control spectra are shown and explained in Figure 3.2. A consideration of shifts in the missing-mass spectra as a result of unequal smearings of the reconstructed momentum components, as figured out by T. Mersmann [M⁺07] and P. Goslawski [Gos13], was thereby not made. In case of individually checked momentum components, possible if all ejectiles of a reaction were detected, this effect does not occur. These variables provide thus the most reliable verification of the calibration. As can be seen in the right column of Figure 3.2, the mean position of each of the distributions deviates by less than 1 MeV/c from the expected value.

^b In this context, the so-called missing-mass-technique was used. Its basic principle is explained in the Appendix A.1.

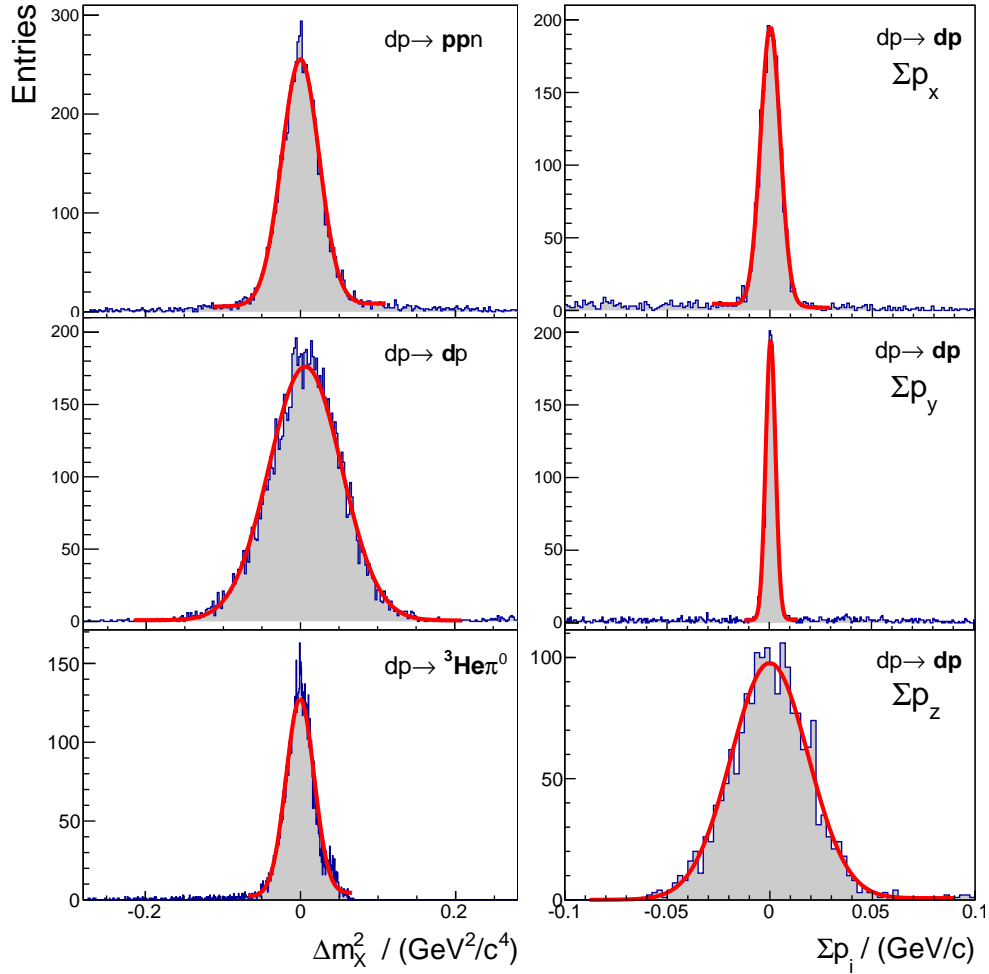


Figure 3.2.: Final control spectra for the momentum calibration of the forward system. The reaction equations each denote the considered process. Detected particles are marked with a bold font. The spectra on the left hand side show the variance of the squared missing-mass value of the undetected particle from the expected result. The red lines show fits, combining a Gaussian with a straight line function, intended to incorporate background contribution. The slight deviation in the control spectrum of the reaction $d p \rightarrow {}^3\text{He} \pi^0$ can mostly be explained by a shift of the peak caused by smearing effects (see text).

In case of the elastic $d p$ scattering with slow emitted deuterons, both ejectiles could be detected. This allowed to check four-momentum conservation, as illustrated on the right hand side for the three momentum components. For lack of space the total energy distribution of the same reaction is not shown.

The highly nonlinear correlation between the detector settings and the reconstructed kinematical variables makes it necessary to test a detector setting at a large variety of momentum and angular regions. This is the reason why a selection of very different reactions was included into the calibration process. Nevertheless the accuracy of the results varies with the momentum scale of the studied reaction. C. Fritzsche performed with the same dataset, for normalisation purposes, an analysis of the dp elastic scattering process with fast deuterons detected in the forward system [Fri14].^c Although the average value of the resulting missing-mass agreed with the proton mass within $3 \text{ MeV}/c^2$, he found non-negligible variations when he compared the corresponding distributions for different momentum transfer regions. This shows, that for tracks with very small curvatures already tiny imperfections of the relevant parameters can lead to an imprecise momentum reconstruction.^d

To assure a high quality of the η mass determination, for which the same dataset was used, an improvement of the calibration was performed through a careful consideration of all kinematically accessible momentum combinations of the reaction $dp \rightarrow {}^3\text{He} \eta$ [Gos13]. This was possible, because of the full geometrical acceptance of ANKE at energies close to the production threshold. The resulting uncertainties of the absolute values of the centre-of-mass particle momenta were estimated to be in the region of $0.2 \text{ MeV}/c$. The variations from the original calibration were of the same order. From that, it could be concluded that in the rigidity region of the ${}^3\text{He}$ particles from the $dp \rightarrow {}^3\text{He} \eta$ reaction, the original calibration provides a high accuracy. Since the ${}^3\text{He}$ particles from the $dp \rightarrow {}^3\text{He} \pi^+ \pi^-$ reaction have similar momenta, the parameters for the energy setting below the η threshold could be used without further considerations.

Positive detector system

With an elaborated momentum calibration of the forward system at hand, the alignment of the MWPCs in the positive system appeared less complex. Particles which were detected there, especially the pions due to their low mass, experienced a relatively strong effect of the spectrometer field. Consequently the reconstruction of the momenta is not exceedingly sensitive on the experimental parameters. Nevertheless, to enable an accuracy of $3 \text{ MeV}/c^2$ for the final invariant mass calculations, the positions of the chambers need to be adjusted by use of calibration reactions.

^c See also the description of the normalisation in Chapter 4.1.

^d A principal inconsistency might originate from the straight track reconstruction algorithm, which does not account for fringe field effects in the region of the drift chamber. In general this has a minor effect, which can be balanced by an adequate choice of effective calibration parameters. However, for strongly diverging track rigidities, like for the fast elastically scattered deuterons compared to all other calibration processes, it could lead to a difference in the optimal settings.

An appropriate calibration reaction is the process $d p \rightarrow p p n$, with the beam proton acting as a spectator particle. Moving with around half the deuteron beam momentum it was practically always detected in the forward system, thus providing a good geometrical acceptance. For the scattered target proton, the accepted momentum range in the positive system lay between 0.3 and 1.5 GeV/c^2 . This allowed to consider different kinematical conditions for the test of the calibration, making the result more reliable. The position of the neutron missing-mass was hence tested for small ($p^{\text{Proton(Pd)}} < 0.5 \text{ GeV}/c$), medium ($0.5 < p^{\text{Proton(Pd)}} < 1.0 \text{ GeV}/c$) and high ($p^{\text{Proton(Pd)}} > 1.0 \text{ GeV}/c$) momenta of the protons detected in the positive system. The adjustment of only one calibration parameter, in this case Z of the second chamber, was sufficient to get satisfactory results. The control spectra for the final detector settings are presented and explained in Figure 3.3. Assuming only small effects on the peak position from the present minor background, the variations from the expected values do not exceed 2 MeV/c^2 .

Negative detector system

A specific calibration for the reconstruction of particle momenta in the negative system was not expected to be necessary. The associated wire chambers are entirely placed on the platform of the D2 magnet. Since they were moreover never moved for other reasons, their position in the ANKE coordinate system most likely remained constant since many years. Alignments gained from calibration procedures of earlier beam times could be considered as suitable for the analysed data. Nevertheless this assumption needed to be verified on the basis of kinematical variables of a control reaction. Since the beam energy was not high enough to allow the production of charged kaon pairs, very few processes remained that could be used for this check. One of them was the three pion production via $d p \rightarrow {}^3\text{He} \pi^+ \pi^- \pi^0$. However, the number of reconstructed events which could be used to identify the π^0 missing-mass was so small, that the determination of the peak position suffered from a high uncertainty. Details on the investigation of the three pion production are explained in chapter 3.5.

The only reaction that was found to provide a sufficient amount of statistics, apart from the analysed $d p \rightarrow {}^3\text{He} \pi^+ \pi^-$, was the single pion production process with three final protons $d p \rightarrow p p p \pi^-$. Information from all three detector systems were needed to reconstruct the mass of the missing proton. The resulting distributions were, similar to the procedure of the Pd calibration, separated according to the determined pion momenta. Despite the influence of some background in the low momentum region, it can be asserted that the spectra, displayed in Figure 3.4, show an excellent agreement with the expected results and each other. This confirms, that the determination of momenta with the negative system provides very accurate

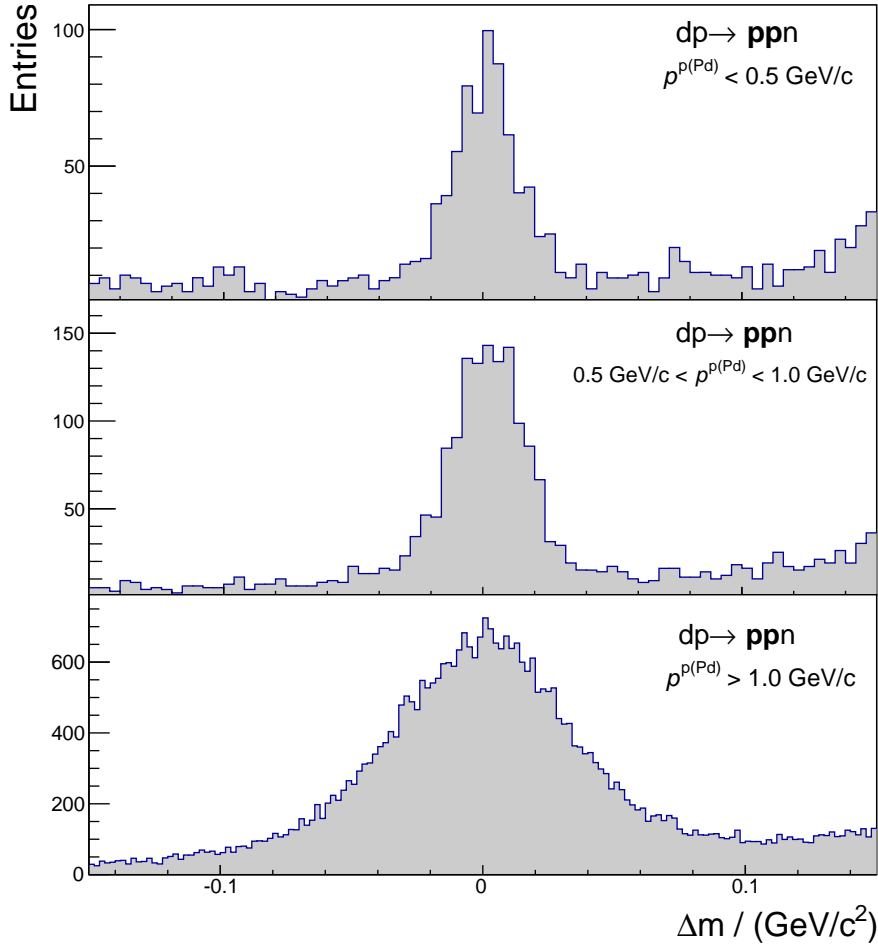


Figure 3.3.: Final control spectra for the momentum calibration of the positive system. Plotted are deviations of the mean value of the missing-mass distributions from the nominal neutron mass for events with coincident hits in the forward and positive detectors, separated according to the momenta reconstructed in the latter. The background shows a slightly increasing tendency towards higher mass values. This leads to a tiny shift of the peak position into the same direction. A rough estimation of this effect has been considered sufficient for the aimed precision of the calibration.

For the highest proton momenta a remarkably larger width compared to the other kinematical regions can be observed. The particles contributing to this distribution have very high transversal momenta towards the positive system ($\approx 0.5 \text{ GeV}/c$), whereas the detector design was optimised to provide primarily a good resolution of the longitudinal component.

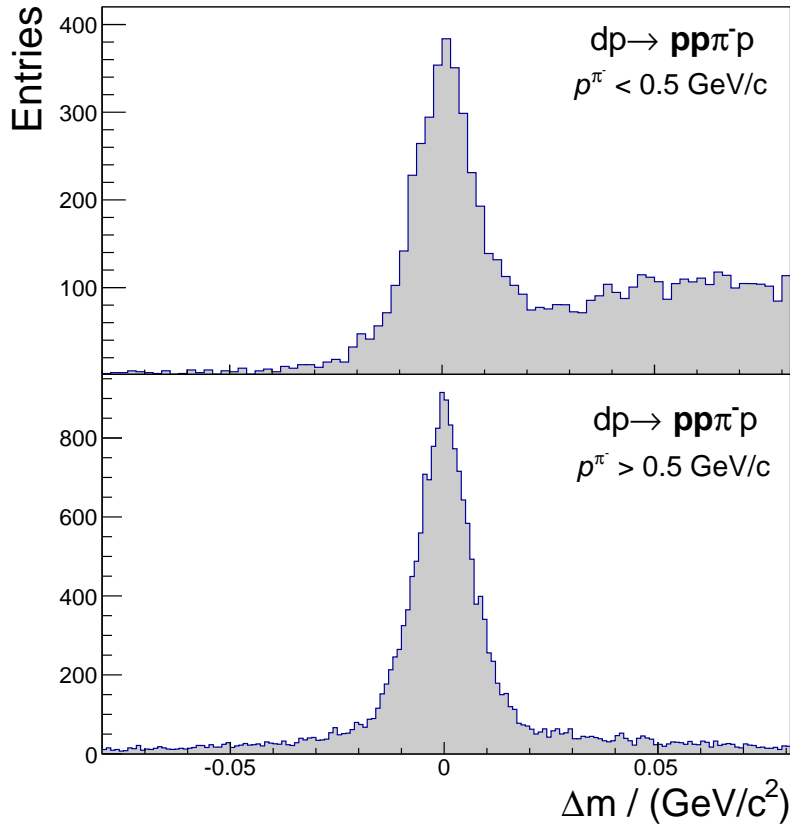


Figure 3.4.: Final control spectra for the momentum calibration of the negative system. Plotted are deviations of the missing-mass distributions from the nominal proton mass for events with coincident hits in the forward, positive and negative detectors, separated according to the momenta reconstructed in the latter.

mean values, as is the case with the two other detector systems after the execution of the respective calibration procedures.

3.3.2. Time of flight

Timing information of particles, that penetrated through the scintillation material of the hodoscope layers, is accessible in the form of TDC signals. For the detectors of the ANKE experiment, one TDC channel equates to a timing width of 44 ps. Offsets between different counters, caused by differences in mean timer delays, response times of the photomultipliers and runtimes of the dedicated signals, made it necessary to perform an appropriate adjustment. Of particular importance in

that respect was a relative calibration of counters from different detector systems (see Section 3.4).

The applied method makes use of the fact, that the Runge-Kutta track reconstruction algorithm provides, besides a calculation of the particle momentum, precise information about the respective path length between the vertex point and each hit detector module. For identified particles with known masses it is thus possible to calculate the time difference between hits in arbitrary counter combinations purely from track information. A comparison to the same observable obtained from TDC values gives then access to the accumulated offset parameter $\Delta t_{ij} = \Delta t_i + \Delta t_j$, with i and j denoting the involved counters. In order to get the counter-specific offset parameters Δt_i and Δt_j , one particular counter is selected for which Δt_i is set to zero. All other offsets can be deduced out of this. In the present analysis an Fd counter served as a reference.

3.3.3. Energy loss

The ADC information from the scintillation counters is a quantity, that is proportional to the energy deposited by a penetrating particle. Similar to the case with the TDC signals, differences in thresholds and amplification factors for the individual counters lead to outputs that are not directly comparable with each other. In the course of the Bachelor's thesis of C. Fritzsche, an energy loss calibration for the hodoscope of the ANKE forward system was performed [Fri11]. The applied method relies on a comparison of the detector signals to the output of AnkeGeant4 simulations.

Energy loss information from the side detectors was not used during the analysis of the reaction $d p \rightarrow {}^3\text{He} \pi^+ \pi^-$. Therefore no corresponding calibration was done.

3.4. Particle identification

For a selection of events from the $d p \rightarrow {}^3\text{He} \pi^+ \pi^-$ reaction a clear identification of the involved particles was necessary. The applied methods made use of energy loss, timing, momentum and track length information.

3.4.1. Energy loss - rigidity method

According to the Bethe-Bloch formula, the energy which a heavy relativistic particle deposits in a particular material depends quadratically on its charge. Hence, the

double charged ${}^3\text{He}$ nuclei have a high chance to produce significantly stronger signals in the scintillation counters than deuterons or protons. This circumstance had already been used to set up an effective ${}^3\text{He}$ online trigger for the measurements (see Section 2.3.2). Since the energy loss moreover shows a heavy dependency on the particle's speed, a consideration of the reconstructed momenta enables a more precise selection in the offline analysis. To illustrate this, Figure 3.5a shows, as an example for one of the counters of the second layer in the forward hodoscope, the according event distribution as function of the deposited energy and the associated ejectile rigidity. Each particle type can be identified by means of a characteristic band. However, as a consequence of the huge amount of protons, the energy loss regions associated with ${}^3\text{He}$ particles are significantly populated with background.

To reduce the complexity of the selection constraints, the energy loss variable ΔE was replaced by the product $\beta^2\Delta E$. For the velocities of the measured ${}^3\text{He}$ particles its value is nearly momentum-independent, as indicated by Figure 3.5b. This allowed to define constant limits of $\beta^2\Delta E$ for each of the three Fd hodoscope layers. By requiring the condition to be fulfilled for at least one counter of each layer, a large fraction of the background could be suppressed. A representative result of this threefold cut is shown in Figure 3.5c. The fact that a small part of ${}^3\text{He}$ events was also rejected, has been accounted for by applying identical cuts to the Monte Carlo data used in the estimation of the acceptance corrections (see Section 4.2). A further reduction of the proton background was achieved by a time-of-flight-analysis, which will be discussed in the following section.

3.4.2. Time of flight methods

Another very efficient tool for particle identification is provided in terms of the TDC information from the hodoscopes. In particular this applies to pions, which move considerably faster than any other hadrons with comparable momenta. Hence cuts on the basis of the time of flight (TOF) between start and stop counters of the side detectors could be performed. Because the respective time differences vary with the particle velocities and the path lengths between the counters, each start-stop combination had to be considered individually. Even without the use of calibrated values, as can be seen from Figure 3.6 for a selected counter combination, this allowed for a very clear separation of the positively charged pions from proton and random background with a 3σ cut. In the negative system no relevant amounts of other particles than pions were observed. Nevertheless the same cuts like in the positive system were applied to reject random background.

In contrast to the situation with the clearly separable pions, an identification of ${}^3\text{He}$ particles based on timing information is much more challenging. Their momenta are twice as high as proton or deuteron momenta with identical rigidities. As a

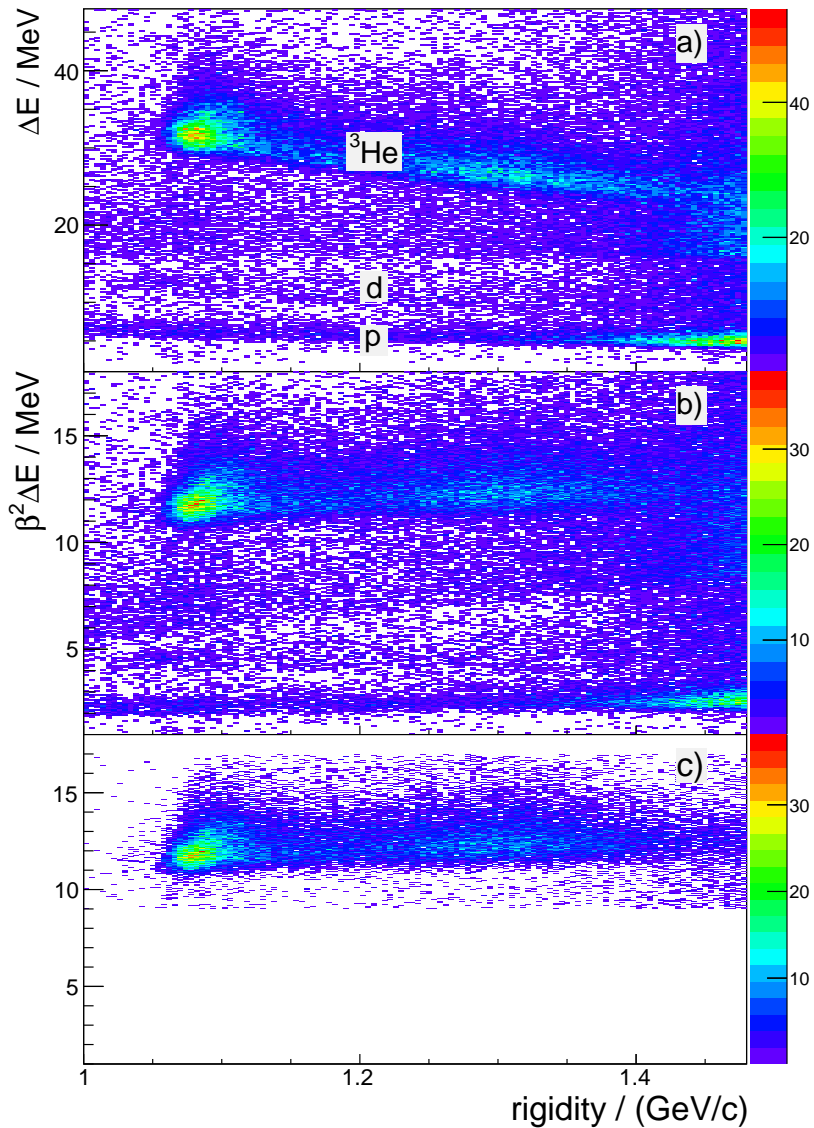


Figure 3.5.: (a) ΔE versus rigidity in preselected data before cuts. The reconstructed particle rigidity is recorded on the abscissa. The ordinate shows the energy deposited in the second scintillator wall of the forward detector. The edge at about 16 MeV is a consequence of the hardware trigger cut.

(b) Same data with ΔE multiplied by the square of the particle speed, on the assumption that this is a ${}^3\text{He}$ nucleus.

(c) The same spectrum as in (b) after making cuts on the ${}^3\text{He}$ band for each of the three hodoscope layers.

A modified version of this figure has been published in Reference [M⁺14].

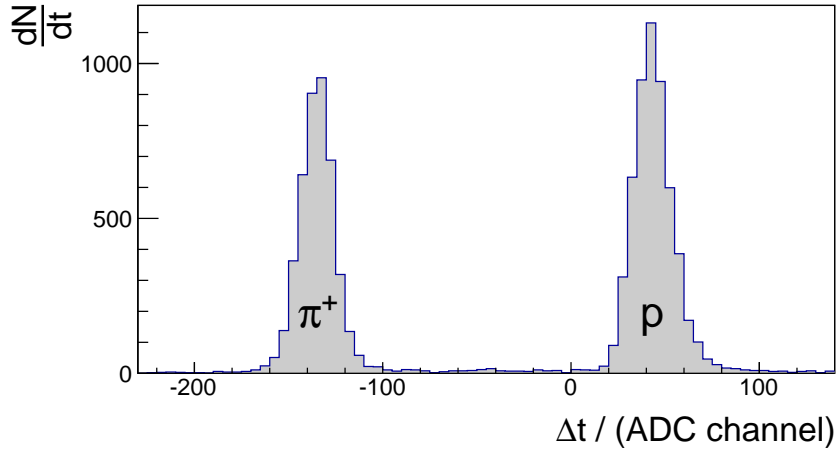


Figure 3.6.: Example of a time of flight difference between a pair of start and stop counters in the positive detector. A modified version of this figure has been published in Reference [M⁺14].

consequence, the compared ${}^3\text{He}$ nuclei have only slightly smaller velocities than the protons, and are faster than the corresponding deuterons. Since moreover the path length distances between the layers are small and the timing resolution especially of the sidewall counters is insufficient, a particle separation solely based on TDC information of the forward hodoscopes is hardly achievable. However, an improvement of the selectivity is possible if timing information of the different detector systems is combined. The applied procedure is based on the approach used for the relative calibration of the TDC signals (see Section 3.3.2). The time difference between hits in the forward and the respective side detector system was calculated from track information, assuming an associated ${}^3\text{He}\pi$ combination (Δt_{calc}), and compared to the time difference measured with the scintillation counters (Δt_{meas}). The resolution of the latter was improved by averaging the times recorded in the first two forward hodoscope layers. If the variables are then plotted against each other in a histogram, a distribution around the bisecting line should appear for correctly assumed particle combinations, as can be seen in the two spectra on the left hand side of Figure 3.7. As a cut parameter, the difference $\Delta t_{meas} - \Delta t_{calc}$ was chosen. The respective distributions are shown on the right hand side of the same Figure 3.7. For the selection, a 3σ limit was used, thus rejecting large parts of the proton and random background.

Due to the use of the software instead of the hardware mean timer values of the negative system (see Section 3.2.2), the corresponding distributions suffer from a slightly worse resolution compared to those which were created with data from the positive system. The resulting overlap suggests a still non-negligible amount of

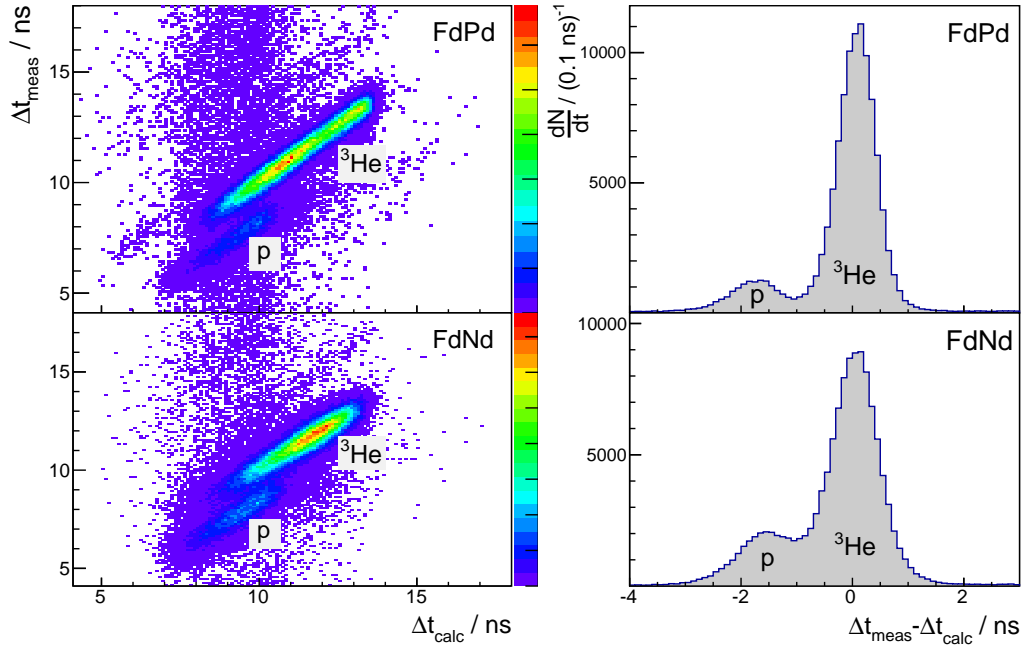


Figure 3.7.: (Left hand side) Times of flight measured between the forward hodoscope and the start counter of a side detector, plotted against those calculated from momentum information on the assumption of ${}^3\text{He}\pi$ particle combinations. In case of consistency the events are distributed around the bisecting line. The main background appears as an individual band, resulting from protons in the forward detector system that were previously misidentified as ${}^3\text{He}$ nuclei by the ΔE –rigidity cut. (Right hand side) Difference between the same variables. The main proton background is placed close to the ${}^3\text{He}$ peak, which is centred at the origin. A modified version of a part of the figure has been published in Reference [M⁺14].

background. However, a further reduction of the proton background was effected through the subsequent missing-mass-analysis (Section 3.5) and a cut on the ${}^3\text{He}$ scattering angle (Section 4.2).

3.5. Identification of multi-pion processes

As a result of the methods applied for particle identification, events with coincidentally detected ${}^3\text{He}\pi^+$, ${}^3\text{He}\pi^-$ and ${}^3\text{He}\pi^+\pi^-$ combinations could be extracted

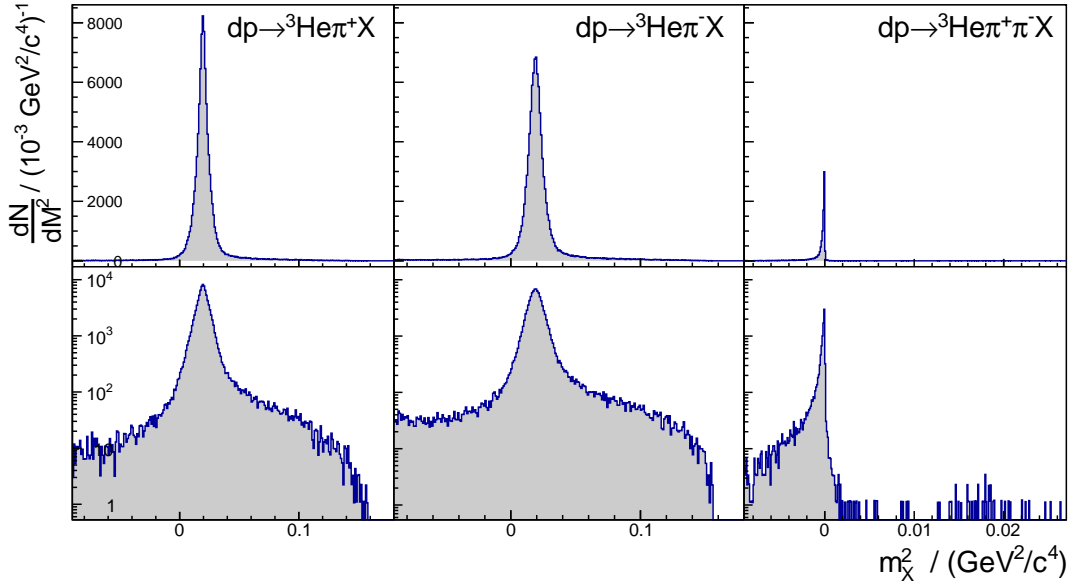


Figure 3.8.: Distributions in the squares of the missing masses for $dp \rightarrow {}^3\text{He}\pi^+X$, $dp \rightarrow {}^3\text{He}\pi^-X$ and $dp \rightarrow {}^3\text{He}\pi^+\pi^-X$ reactions. All channels are dominated by two-pion production. The semi-logarithmic plots reveal contributions from three-pion production and background events, most probably caused by misidentified protons in the forward system. As a consequence of the different TDC signal resolutions of the positive and the negative system (see Section 3.4.2), the background contribution is slightly lower for detected ${}^3\text{He}\pi^+$ than for ${}^3\text{He}\pi^-$ combinations.

from the dataset. At a total energy of 3.353 GeV, these may be associated with either two- or three-pion production processes. A discrimination between these, as well as a further suppression of the remaining background of misidentified particles, could be achieved with a missing-mass analysis. For the three different combinations of detected particles, the respective distributions are illustrated in Figure 3.8 as function of the squared missing-mass.

In the spectra corresponding to the ${}^3\text{He}\pi$ coincidences, clear peaks appear at the charged pion mass ($m_{\pi^\pm}^2 = 0.020 \text{ GeV}^2/c^4$), which result unambiguously from two pion production events. The contribution of three-pion production in terms of the reaction $dp \rightarrow {}^3\text{He}\pi^+\pi^-\pi^0$, kinematically allowed above squared masses of $(m_{\pi^\pm} + m_{\pi^0})^2 = 0.075 \text{ GeV}^2/c^4$, is in contrast too small to be identified on the background. However, in the spectrum of the less numerous three-particle coincidences, where the signal-to-background ratio is even better, a very small number of events is found in the vicinity of the squared π^0 mass. From simulations it can be found that the

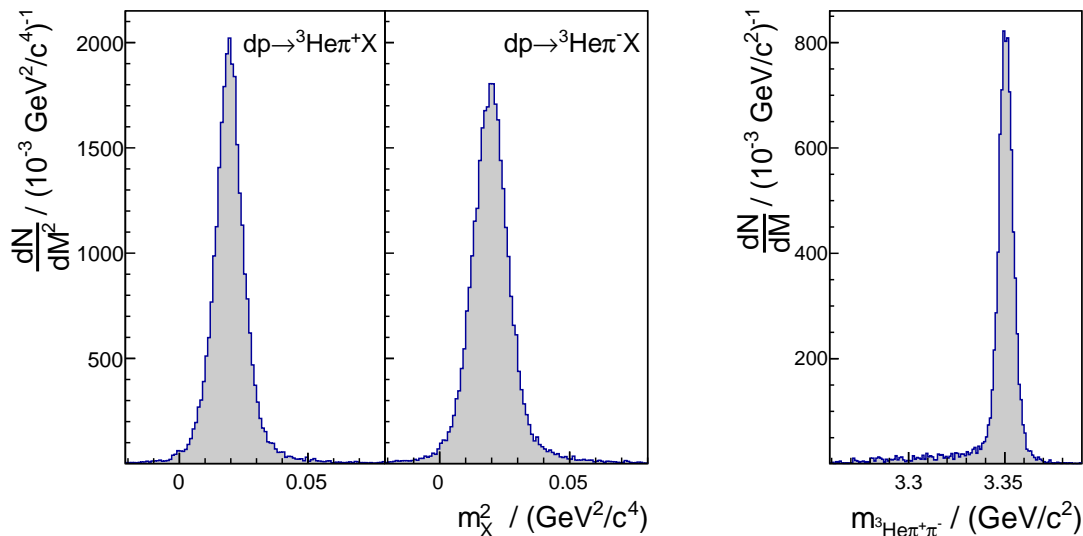


Figure 3.9.: Event distributions which were used to set the cut conditions based on missing-mass and invariant-mass information. For the case that all final state particles were detected, the resulting peak position corresponds to the total energy of 3.35 GeV.

half-width of the corresponding peak is $\sigma = 0.0025 \text{ GeV}^2/c^4$. Within a 3σ region around the mean position, 40 events can be assigned to the $d p \rightarrow {}^3\text{He} \pi^+ \pi^- \pi^0$ reaction on the assumption of a negligible background contribution. An estimation of the cross section will be given in Chapter 4.4.

For the final analysis of the reaction $d p \rightarrow {}^3\text{He} \pi^+ \pi^-$, only events with ${}^3\text{He}$ particles scattered backwards in the centre-of-mass frame were used. A motivation for this is given in the context of the acceptance analysis (see Section 4.2). Most of the background visible in Figure 3.8 results from processes involving a break-up of the beam deuteron, causing the incident protons to be mostly scattered at small angles and detected in the forward system. Hence, the amount of background actually relevant for the analysis is even further reduced by the ${}^3\text{He}$ angle cut.

Because the peaks in the missing-mass spectra of the ${}^3\text{He} \pi$ combinations deviate from a Gaussian peak shape, a manual estimation of reasonable cut limits was carried out. This led to an acceptance of events within a mass range of $\pm 0.03 \text{ GeV}^2/c^4$ around the mean position of the charged pion.

Due to the strongly asymmetric missing-mass distribution for detected ${}^3\text{He} \pi \pi$ combinations, the respective events were instead selected using a 4σ cut on the invariant-mass of all ejectiles. The relevant distributions, after a restriction to CMS

^3He production angles from 143° to 173° , are shown in Figure 3.9. In total, a number of $\approx 81,500$ events remained, subdivided into 34,000 $^3\text{He} \pi^+$, 39,000 $^3\text{He} \pi^-$ and 8,500 $^3\text{He} \pi^+ \pi^-$ combinations. The ratio of lost events from the $d p \rightarrow ^3\text{He} \pi^+ \pi^-$ reaction for all three cuts is smaller than 0.5%. The overall background is estimated to be below 1%.

3.6. Efficiency analysis

Even if a particle completely passed through a detector, inefficiencies of the detectors or the data acquisition system might have prevented its recording. As a consequence, estimations of the amount and the properties of accordingly lost events are required in order to determine cross sections.

3.6.1. Track efficiencies

Any particle, of which a valid track was reconstructed in the course of the $d p \rightarrow ^3\text{He} \pi^+ \pi^-$ analysis, had been registered in all scintillation counters and MWPC chambers of the respective detector system. To get the probability of particles with similar kinematic properties to be undetected due to a missing detector signal, the inefficiencies of all relevant detector parts need to be considered.

For the used scintillation counters, appropriate tests under laboratory conditions had proven a probability of detection close to 100 %. In contrast, the wire chambers show notable and moreover spatially inhomogeneous inefficiencies. In the case of the side detectors these are determined by means of data from the start-stop (SaSo) counter combinations, which define passing areas for the ejectiles. Since the efficiencies vary with the respective stopping power, which depends on the type of the passing particle, an appropriate identification is necessary. Events with pions, verified purely by time-of-flight and energy loss information, allow for a determination of an MWPC efficiency distribution as function of the SaSo combinations by checking for correspondingly reconstructed tracks:

$$\varepsilon_{SaSo} = \frac{N_{Tracks}(SaSo)}{N_{Pions}(SaSo)}. \quad (3.1)$$

For both side detector systems efficiencies between 89% and 98% were calculated. In the final analysis each track was weighted with the inverse value of its associated counter combination.

In the forward system, where no start counters exist and a spatial track classification according to particle momenta lacks from ambiguity, an individual method for efficiency determination is used [D⁺04]. It builds on the fact that tracks may still be reconstructed if information from one arbitrary wire plane is missing. Each of the planes is subdivided into $20 \cdot 20$ squares. Efficiency maps are created by comparing the numbers of tracks which pass a certain square (i, j) , reconstructed with and without consideration of the particular plane (pl):

$$\varepsilon_{pl,ij} = \frac{N_{Tracks}(pl, ij)}{N_{Tracks}(\cancel{pl}, ij)}. \quad (3.2)$$

To derive out of this the probability of detection for a certain track, the efficiency of each passed cell needs to be considered. It was found to be mostly above 97%. A complication of the calculation is given by the fact, that not necessarily all planes were required to be hit. A similar issue is treated in the following chapter, where the determination of event efficiencies out of the track efficiencies is discussed.

3.6.2. Calculation of event efficiencies under consideration of different detector combinations

For a kinematically complete reconstruction of events from the reaction $d p \rightarrow {}^3\text{He} \pi^+ \pi^-$ it is necessary to have direct momentum information of at least two particles. Since the trigger condition required hits in the hodoscope counters of the forward detector, this means that the number of reconstructed events (in the following N^{rec}) is a sum of three track combinations:

$$N^{rec} = N_{FdNd}^{rec} + N_{FdPd}^{rec} + N_{FdNdPd}^{rec}. \quad (3.3)$$

Which detectors are hit by a certain momentum composition depends on the geometrical acceptance and on the MWPC efficiency. For the calculation of total event efficiencies (ε) it has to be considered which information is necessary for a kinematically complete reconstruction. In case that only two particles can geometrically be accepted, detection of both is indispensable for the analysis. Consequently the event efficiencies ε_{FdNd} and ε_{FdPd} are simply the products of the detection probabilities of the individual tracks:

$$\begin{aligned} \varepsilon_{FdNd} &= \varepsilon_{Fd} \cdot \varepsilon_{Nd} \\ \varepsilon_{FdPd} &= \varepsilon_{Fd} \cdot \varepsilon_{Pd} \end{aligned} \quad (3.4)$$

3. Data analysis

Provided that all three particles are covered by the ANKE acceptance, event reconstruction is possible with all three tracks, but also if one in negative or positive system is missing due to MWPC inefficiency. The resulting efficiency ε_{2+} is therefore a sum of the probabilities for these occurrences:

$$\begin{aligned}
\varepsilon_{2+} &= \varepsilon_{Fd} \cdot \varepsilon_{Nd} \cdot \varepsilon_{Pd} \\
&+ \varepsilon_{Fd} \cdot \varepsilon_{Nd} \cdot (1 - \varepsilon_{Pd}) \\
&+ \varepsilon_{Fd} \cdot \varepsilon_{Pd} \cdot (1 - \varepsilon_{Nd}) \\
&= \varepsilon_{Fd} \cdot (\varepsilon_{Nd} + \varepsilon_{Pd} - \varepsilon_{Nd} \cdot \varepsilon_{Pd}).
\end{aligned} \tag{3.5}$$

The following acronyms will be used in the further explanations for clarification:

$$\begin{aligned}
\varepsilon_{FdNdPd} &= \varepsilon_{Fd} \cdot \varepsilon_{Nd} \cdot \varepsilon_{Pd} \\
\varepsilon_{FdNd\cancel{Pd}} &= \varepsilon_{Fd} \cdot \varepsilon_{Nd} \cdot (1 - \varepsilon_{Pd}) \\
\varepsilon_{Fd\cancel{Pd}Nd} &= \varepsilon_{Fd} \cdot \varepsilon_{Pd} \cdot (1 - \varepsilon_{Nd}).
\end{aligned} \tag{3.6}$$

Based on the previous considerations, the number of events after correction for efficiency N^{total} would be composed of:

$$N_{FdNd}^{total} = \sum_i^{N_{FdNd}^{rec}} \frac{1}{\varepsilon_{FdNd,i}}. \tag{3.7a}$$

$$N_{FdPd}^{total} = \sum_j^{N_{FdPd}^{rec}} \frac{1}{\varepsilon_{FdPd,j}}. \tag{3.7b}$$

$$N_{FdNdPd}^{total} = \sum_k^{N_{FdNdPd}^{rec}} \frac{1}{\varepsilon_{2+,k}} = \sum_k^{N_{FdNdPd}^{rec}} \frac{1}{\varepsilon_{FdNdPd,k} + \varepsilon_{FdNd\cancel{Pd},k} + \varepsilon_{Fd\cancel{Pd}Nd,k}}. \tag{3.7c}$$

However, in the actual analysis it is not possible to decide whether a missing particle was undetected due to lacking geometrical acceptance or as a result of chamber inefficiency. The events associated with the two latter summands in the denominator of equation 3.7c are thus identified as two-particle coincidences. As a consequence ε_{FdNd} or ε_{FdPd} respectively are assigned to them instead of the correct ε_{2+} . These wrongly attributed efficiencies would have an effect on the shape of the invariant

mass spectra and the quantity of the differential cross sections. However, it is possible to correct for this by exploitation of information that can be extracted from the reconstructed three-track events.

As a first step a quantification of events with misallocated efficiencies is necessary. This can be done on the basis of the reasonable assumption, that the efficiency distribution shows only small fluctuations. By this means it is possible to group events with nearly constant efficiencies ε^* to a quantity N^{rec*} , such that

$$\sum_k^{N^{rec*}} \frac{1}{\varepsilon_k^*} = N^{rec*} \cdot \frac{1}{\varepsilon^*} = N^{total*}. \quad (3.8)$$

With equation 3.8 it is possible to express the amount of events with misallocated efficiencies as individual summands (bold font) of a number of reconstructed events:

$$N_{FdNd}^{rec*} = N_{FdNd}^{total*} \cdot \varepsilon_{FdNd}^* + \mathbf{N}_{\mathbf{FdNdPd}}^{total*} \cdot \varepsilon_{\mathbf{FdNdPd}}^* \quad (3.9a)$$

$$N_{FdPd}^{rec*} = N_{FdPd}^{total*} \cdot \varepsilon_{FdPd}^* + \mathbf{N}_{\mathbf{FdNdPd}}^{total*} \cdot \varepsilon_{\mathbf{FdPdNd}}^* \quad (3.9b)$$

$$N_{FdNdPd}^{rec*} = N_{FdNdPd}^{total*} \cdot \varepsilon_{FdNdPd}^* \quad (3.9c)$$

These can be written as:

$$N_{FdNdPd}^{total*} \cdot \varepsilon_{FdNdPd}^* \stackrel{3.9c}{=} N_{FdNdPd}^{rec*} \cdot \frac{\varepsilon_{FdNdPd}^*}{\varepsilon_{FdNdPd}^*} = N_{FdNdPd}^{rec*} \cdot \frac{1 - \varepsilon_{Pd}^*}{\varepsilon_{Pd}^*} \quad (3.10a)$$

$$N_{FdNdPd}^{total*} \cdot \varepsilon_{FdPdNd}^* \stackrel{3.9c}{=} N_{FdNdPd}^{rec*} \cdot \frac{\varepsilon_{FdPdNd}^*}{\varepsilon_{FdNdPd}^*} = N_{FdNdPd}^{rec*} \cdot \frac{1 - \varepsilon_{Nd}^*}{\varepsilon_{Nd}^*} \quad (3.10b)$$

For the efficiency correction on an event-by-event basis the quantity is included in terms of a probability by setting $N_{FdNdPd}^{rec} = 1$ and then multiplied with the difference between the wrongly attributed and the correct efficiency correction factor:

$$\begin{aligned} \varepsilon_{corr} &= \frac{1 - \varepsilon_{Pd}}{\varepsilon_{Pd}} \cdot \left(\frac{1}{\varepsilon_{FdNd}} - \frac{1}{\varepsilon_{2+}} \right) \\ &+ \frac{1 - \varepsilon_{Nd}}{\varepsilon_{Nd}} \cdot \left(\frac{1}{\varepsilon_{FdPd}} - \frac{1}{\varepsilon_{2+}} \right). \end{aligned} \quad (3.11)$$

ε_{corr} was added to all efficiencies of events with a three-particle coincidence and provided therefore a correction of the misallocated efficiencies occurring for some of the events with two detected particles.

3.6.3. Trigger efficiencies

A significant reduction ($\approx 60\%$) of the effective count rate of the triggered events was caused by dead time of the ANKE data acquisition system. Access to trigger input and output rates (N_{in} and N_{out} respectively) is provided in terms of the scaler events (see Section 2.3.2). Based on these, the dead time τ was calculated as

$$\tau = 1 - \frac{N_{out}}{N_{in}}. \quad (3.12)$$

To account for fluctuations of the rates and therefore the dead times, an appropriate correction was done on an event-by-event basis. It has to be regarded that each trigger setting leads to an individual dead time rate. Hence, a separate correction procedure was applied on the data used for normalisation purposes, because these were recorded with a different trigger setting than the reactions of interest.

4. Determination of cross sections

The measurements of the reaction $d p \rightarrow {}^3\text{He} \pi^+ \pi^-$ at the ANKE experiment led, in conjunction with the presented calibration and identification methods, to a very clean data sample with high statistics and a very good momentum resolution. To draw firm and valuable conclusions out of this selection, it is necessary to transform the obtained information into differential observables. This requires corrections for the limited detector acceptance and its finite momentum resolution, as well as an absolute normalisation of the data. The latter has been done by analysing a reference reaction with well known cross sections, as described in the following section. Subsequent to that, the procedure of the acceptance correction for the $d p \rightarrow {}^3\text{He} \pi^+ \pi^-$ reaction is elaborated. In a further section, the ANKE acceptance for the $d p \rightarrow {}^3\text{He} \pi^+ \pi^- \pi^0$ reaction is studied. Final results are shown in Section 4.4.

4.1. Luminosity determination via $d p$ elastic scattering

The normalisation was accomplished by using the simultaneously measured elastic scattering reaction $d p \rightarrow d p$ for a determination of the integrated luminosity^a on the basis of calibration data from References [D⁺68, G⁺91, I⁺83, V⁺88, W⁺80]. These provide differential cross sections as function of the Lorentz-invariant Mandelstam variable t , also termed as four-momentum transfer. For small values of t , this correlation is almost insensitive on the centre-of-mass energy of the experiment and provides therefore a reliable comparability of results obtained at different beam energies. For a corresponding analysis of the ANKE data, C. Fritsch extracted

^a The luminosity L is the quantity which relates the cross section σ of a reaction with the event rate \dot{N} through $\dot{N} = L \sigma$. For internal fixed-target experiments at ring accelerators like COSY-ANKE, it corresponds to the product of the target density ρ_{target} , the number of stored beam particles n_{beam} and the revolution frequency f_0 : $L = \rho_{target} n_{beam} f_0$. By the use of a reference reaction with known cross sections, it is possible to determine L_{int} , the luminosity integrated over time. This quantity has the advantage over L , that it does not rely on time-resolved information on the beam current, the target density and its areal distribution as well as the size of the beam-target overlap region.

events with high-momentum deuterons from the data recorded with trigger T2, which required hits in both layers of the first scintillator hodoscope (see also Section 2.3.2). These allowed for an almost background-free extraction of the reaction by use of the missing-mass technique.^b On this basis it was possible to study the luminosity in a wide momentum transfer range of $0.08 < |t| < 0.26$ (GeV/c)² with a resolution of 0.01 (GeV/c)², thus gaining a good understanding on systematic effects. The resulting integrated luminosity of the data used for the analysis of the $d p \rightarrow {}^3\text{He} \pi^+ \pi^-$ reaction amounts to $L_{int} = (3143 \pm 17_{\text{stat}} \pm 190_{\text{syst}}) \text{ nb}^{-1}$, with the latter number denoting a systematic uncertainty of 6%. This value composes of contributions from direct uncertainties of the reference results, uncertainties of parameters of fits on the reference data and of uncertainties in the deuteron momentum reconstruction. As was pointed out in Section 3.3.1, the weak deflection of the large momentum particles in the spectrometer field causes a high sensitivity on the knowledge of the ANKE setup parameters.

A detailed description of the various analysis steps applied, as well as a presentation of all results can be found in C. Fritzsche's master's thesis [Fri14]. In addition to the extraction of luminosities, the rich data sample is currently analysed further with regard to an enhancement of the database on differential cross sections of the $d p$ elastic scattering reaction. This also implies analyses on reactions, which are applicable for an independent normalisation. According studies had earlier been carried out on the reaction $d p \rightarrow {}^3\text{He} \pi^0$ [Eve12]. The current focus is set on the $d p \rightarrow d \pi^0 p_{\text{spec}}$ process, where the spectator proton p_{spec} is only passively involved in the reaction [Fri14], since this reaction was already successfully used for normalisation purposes by other members of the ANKE collaboration [Mch13].

4.2. Acceptance analysis for $d p \rightarrow {}^3\text{He} \pi^+ \pi^-$

For a spectrometer experiment like ANKE, the geometrical acceptance is in general maximal for measurements close to the production threshold of a reaction. The excess energy for $d p \rightarrow {}^3\text{He} \pi^+ \pi^-$ lies at $Q = 265$ MeV for the data with the lowest beam momentum, and is thus significantly above the ideal kinematical region for this detector. As will be shown in this section, an accurate acceptance analysis on the basis of AnkeGeant4 simulations nevertheless allows to overcome the associated limitations if dedicated kinematical confinements are applied and an appropriate data description is used for the correction.

^b The kinematical basis of this analysis method is explained in the Appendix A.1.

4.2.1. Multidimensional acceptance distribution

For processes with a three-body final state of identified particles, there are in total nine degrees of freedom. Through four-momentum conservation the number of independent observables is reduced to five. Since furthermore unpolarised reactions show isotropic distributions in the azimuthal angle, four parameters remain to be considered in the context of an acceptance analysis. It is convenient to use variables which are also the subjects of the actual investigation. An adequate choice in the context of the analysis of the reaction $d p \rightarrow {}^3\text{He} \pi^+ \pi^-$ are the invariant masses of the ${}^3\text{He} \pi^-$ and the $\pi^+ \pi^-$ systems,^c the ${}^3\text{He}$ production angle $\vartheta_{3\text{He}}$, and the orientation of the ejectile plane relative to the beam axis, denoted as $\vartheta_{\text{plane}}^{CMS}$. For the first three of these, previous experiments conducted under similar conditions have found significant deviations from simple phase space behaviour [B⁺73, B⁺06]. It is therefore essential to carefully identify the kinematical regions covered by the ANKE acceptance. For this purpose the detector response to the $d p \rightarrow {}^3\text{He} \pi^+ \pi^-$ reaction was simulated on the initial assumption of a uniformly filled phase space.

First conclusions can be drawn on the basis of two-dimensional plots of the ${}^3\text{He}$ production angles against the other chosen parameters, as shown in Figure 4.1. The $m_{\pi^+\pi^-}$ spectrum covers a mass range from $0.28 \text{ GeV}/c^2$ to $0.57 \text{ GeV}/c^2$. That entire region is seen by ANKE for ${}^3\text{He}$ particles moving backwards in CMS with $143^\circ < \vartheta_{3\text{He}}^{CMS} < 173^\circ$. Under consideration of this angular constraint, the distributions of the variables $m_{3\text{He}\pi^-}$ and $\vartheta_{\text{plane}}^{CMS}$ are also completely within the ANKE acceptance. Hence it is indicated to focus in the following analysis on this region.

A similar check for dependences of the detectable invariant mass distributions on $\vartheta_{\text{plane}}^{CMS}$ is illustrated in Figure 4.2. For events with $143^\circ < \vartheta_{3\text{He}}^{CMS}$ the $\vartheta_{\text{plane}}^{CMS}$ angles range for geometrical reasons only from 50° to 130° . A full coverage of the two-dimensional spectrum is given for $70^\circ < \vartheta_{\text{plane}}^{CMS} < 110^\circ$.

More detailed acceptance studies can be done by subdividing all four relevant degrees of freedom into a specific number of bins, thus allowing to create a four-dimensional acceptance matrix. The basic principle of the applied method is described in Reference [B⁺01a]. According to this, each matrix element is filled with the ratio of generated and reconstructed events from the Monte Carlo simulations,

^c Note that for a three-body final state the invariant mass of any two-particle combination can be expressed as a function of the other two-particle invariant masses according to $m_{3\text{He}\pi^-}^2 + m_{3\text{He}\pi^+}^2 + m_{\pi^+\pi^-}^2 = s + m_{3\text{He}}^2 + m_{\pi^-}^2 + m_{\pi^+}^2 = \text{const}$, with the Mandelstam variable s denoting the squared centre-of-mass energy. The choice of particle combinations is from that point of view in principal arbitrary. However, as a consequence of the huge mass difference between pions and ${}^3\text{He}$ nuclei, there is an almost linear correlation between $m_{3\text{He}\pi^-}$ and $m_{3\text{He}\pi^+}$, implying a large number of events to be close to the boundary of the respective two-dimensional distribution. In combination with the finite momentum resolution, this effectively causes a low sensitivity on $m_{\pi^+\pi^-}$ in the $m_{3\text{He}\pi^-}$ vs $m_{3\text{He}\pi^+}$ plot. Hence, the choice of $m_{\pi^+\pi^-}$ as one of the parameters is convenient.

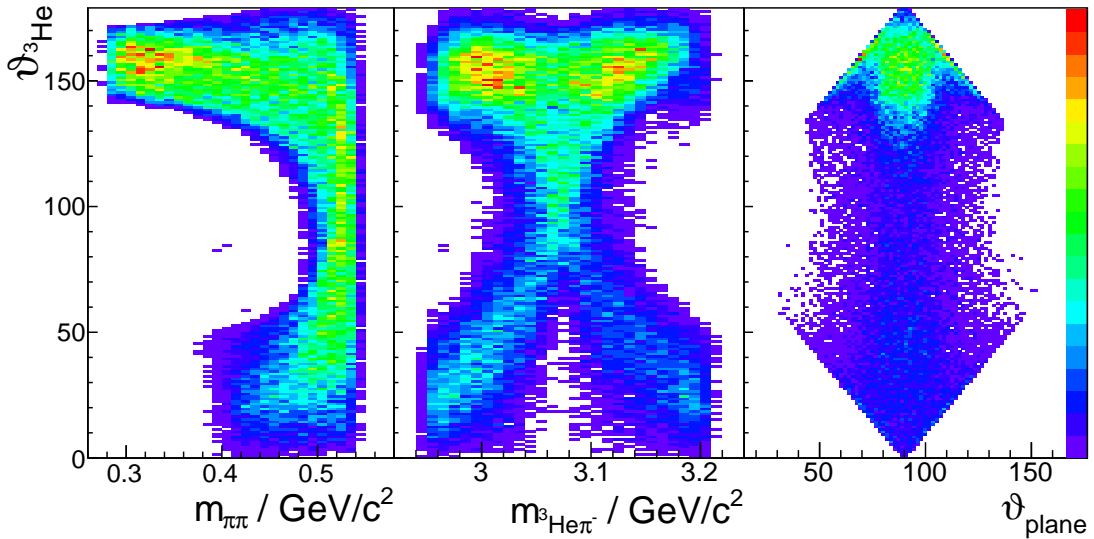


Figure 4.1.: Monte Carlo generated distributions of events accepted by the ANKE detector system. Shown are the correlations between the ${}^3\text{He}$ production angle and the other three chosen independent variables $m_{\pi^+\pi^-}$, $m_{3\text{He}\pi^-}$ and $\vartheta_{\text{plane}}^{CMS}$ on the assumption of a simple three body phase-space behaviour. The coloured scale is linear, starting at 0. The maximum values of the three distributions, indicated by red colours, are not necessarily identical. Corresponding generated distributions without any acceptance restrictions are shown in the Appendix A.3.

thus defining the relative acceptance in this explicit area of phase space. The derived values also account for the finite detector and tracking resolution, since the reconstructed momenta imply an accordant smearing. The bin widths of the invariant masses were set to $30 \text{ MeV}/c^2$, those of the angles to 5° . Figure 4.3 illustrates the map as slices of the two-dimensional invariant mass distributions. For its calculation, 300 million events were generated over the whole ${}^3\text{He}$ angular range, thus 58 million for $143^\circ < \vartheta_{3\text{He}}^{CMS} < 173^\circ$. On average, this implies about 10000 generated events per bin.^d

For the regarded angular combinations, the spectra show for almost every bin a non-vanishing acceptance. However, for some areas significant fluctuations become apparent. Especially at high $m_{\pi^+\pi^-}$ ($\approx 0.5 \text{ GeV}/c^2$) in combination with central

^d The total number of accepted simulated events is about 25 times higher than the number of accepted events from the measurement. The statistical uncertainties associated with the Monte Carlo simulations are thus of minor importance in comparison to those arising from the experimental data.

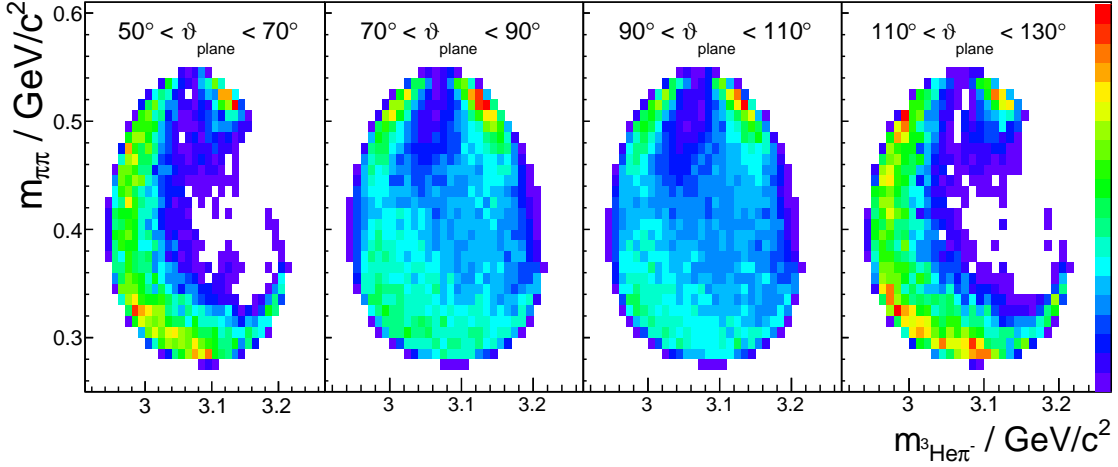


Figure 4.2.: Monte Carlo generated distributions of events accepted by the ANKE detector system, with the confinement $143^\circ < \vartheta_{^3\text{He}}^{CMS} < 173^\circ$. Shown are the correlations between $m_{\pi^+\pi^-}$ and $m_{^3\text{He}\pi^-}$ for different angular regions of $\vartheta_{\text{plane}}^{CMS}$. The coloured scale is linear, starting at 0. The maximum values of the distributions, indicated by red colours, are not necessarily identical. The corresponding generated distribution for the entire $\vartheta_{\text{plane}}^{CMS}$ range, but with the restriction $143^\circ < \vartheta_{^3\text{He}}^{CMS} < 173^\circ$, is shown in the Appendix A.3.

$m_{^3\text{He}\pi^-}$ values ($\approx 3.05 \text{ GeV}/c^2$) the acceptance undergoes a steep drop. An implication of this is that the acceptance distribution within a single bin can not be assumed to be on a constant level, causing a potentially strong local model dependence. A use of this acceptance matrix for a correction of the measured data might therefore lead to the appearance of significant binning effects. A reduction of the bin width could in principle help to reduce these, but would in return create empty bins in the measured data. One possibility to avoid such problems is an exclusion of the region where $3.03 \text{ GeV}/c^2 < m_{^3\text{He}\pi^-} < 3.09 \text{ GeV}/c^2$ and $m_{\pi^+\pi^-} > 0.43 \text{ GeV}/c^2$ from the analysis. Since such a restriction would considerably reduce the significance of the results, a modification of the approach has been developed.

The general idea of the revised procedure is to make assumptions on the actual physical behaviour of specific observables or even the reaction process as a whole, allowing to integrate over areas of incomplete acceptance. It is self-evident that the reliability of by this means derived results may depend strongly on the correctness of the drawn assumptions and requires therefore a careful estimation of associated systematic uncertainties. The model presented in the following subsection replaces the uniform phase-space distributions used for the AnkeGeant4 simulations by a description which aims to reproduce the main characteristics of the data. On this basis, the acceptance correction is performed binwise for each of the invariant mass

4. Determination of cross sections

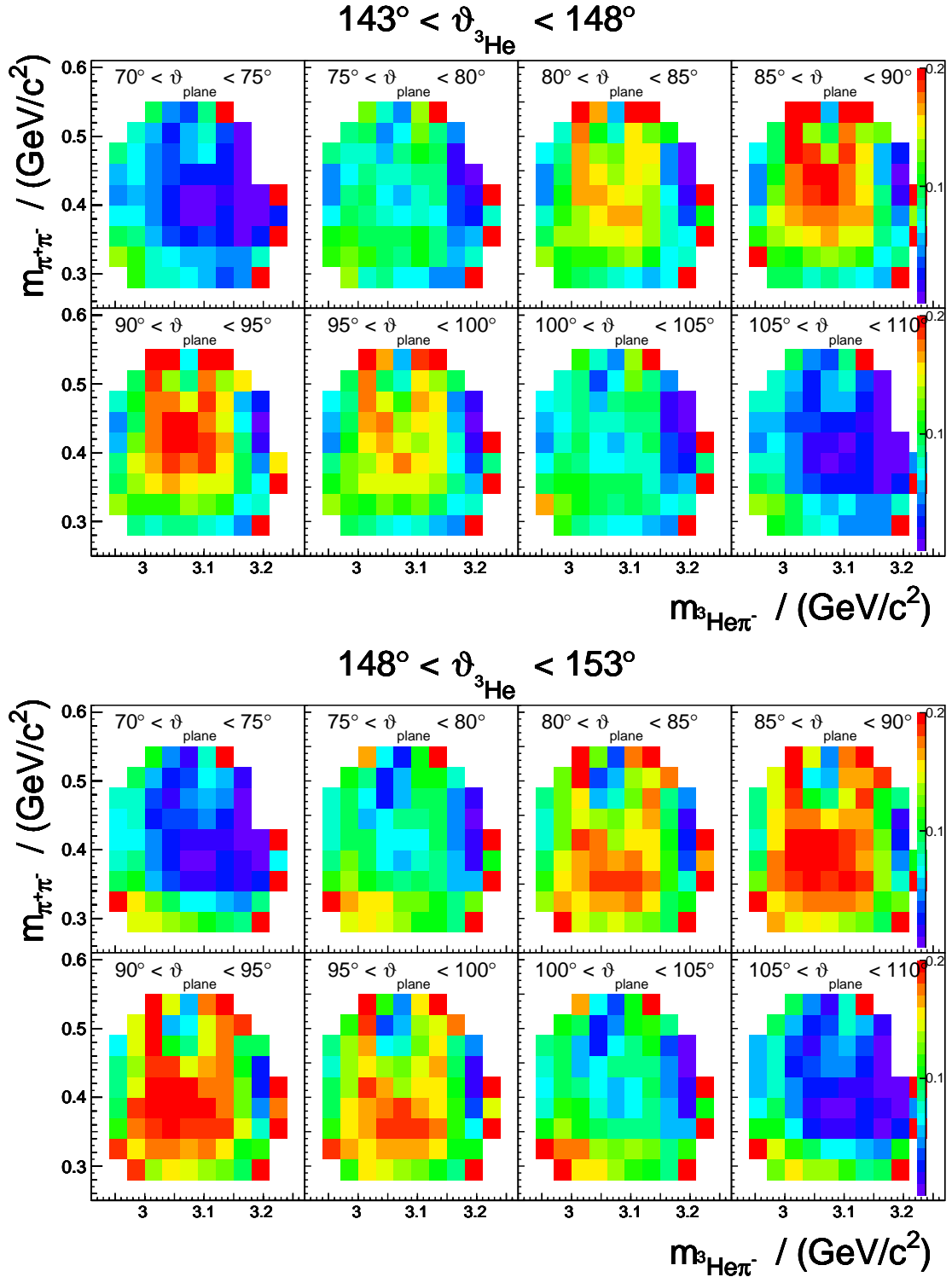


Figure 4.3.: Two-dimensional slices of the ANKE acceptance matrix for the reaction $d p \rightarrow ^3\text{He} \pi^+ \pi^-$. The numbers were calculated as the ratio of detected and generated events per bin. Red bins mark acceptances around 20 %, blue bins of 2 % and less.

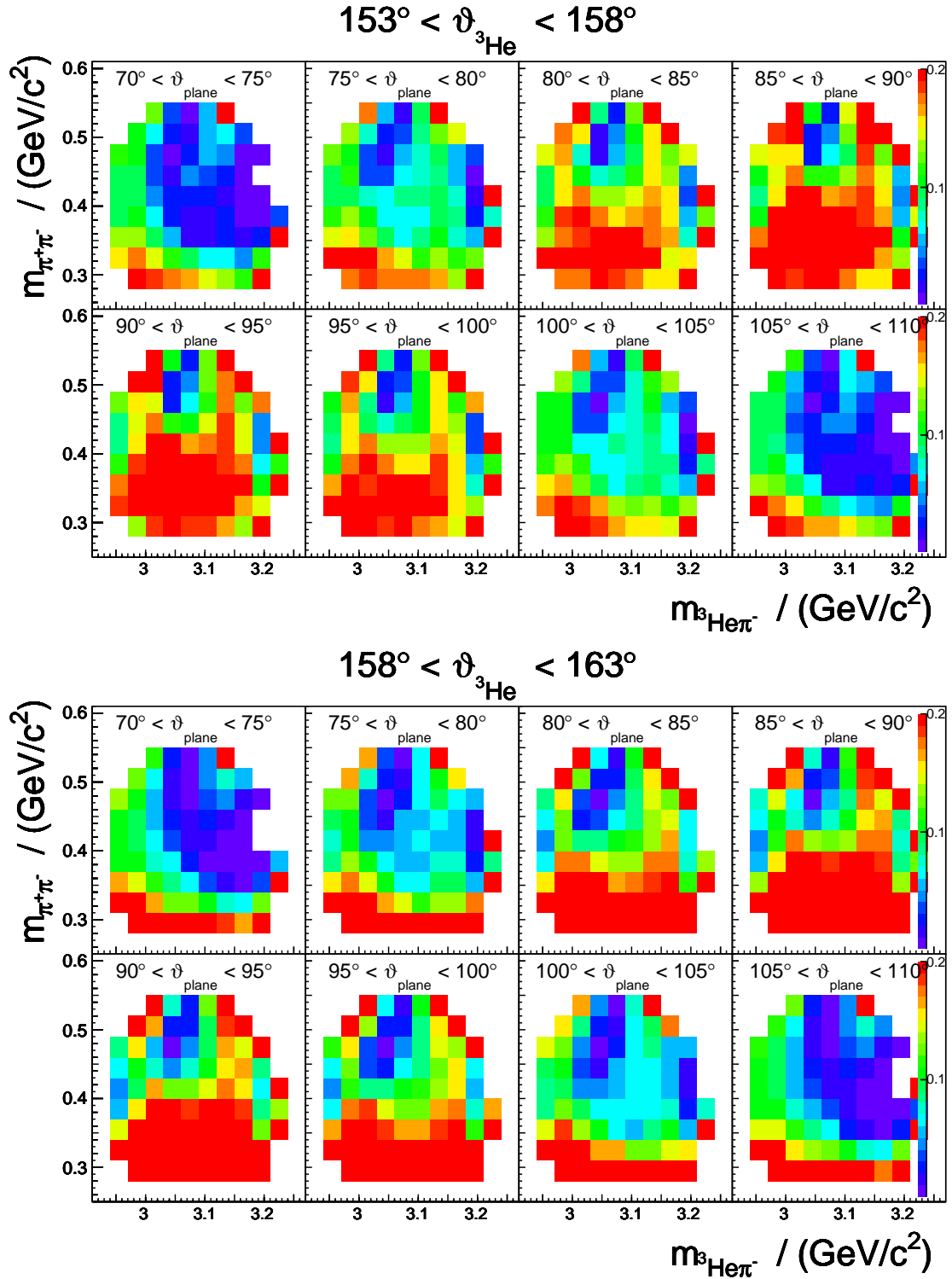


Figure 4.3.: (Continued)

4. Determination of cross sections

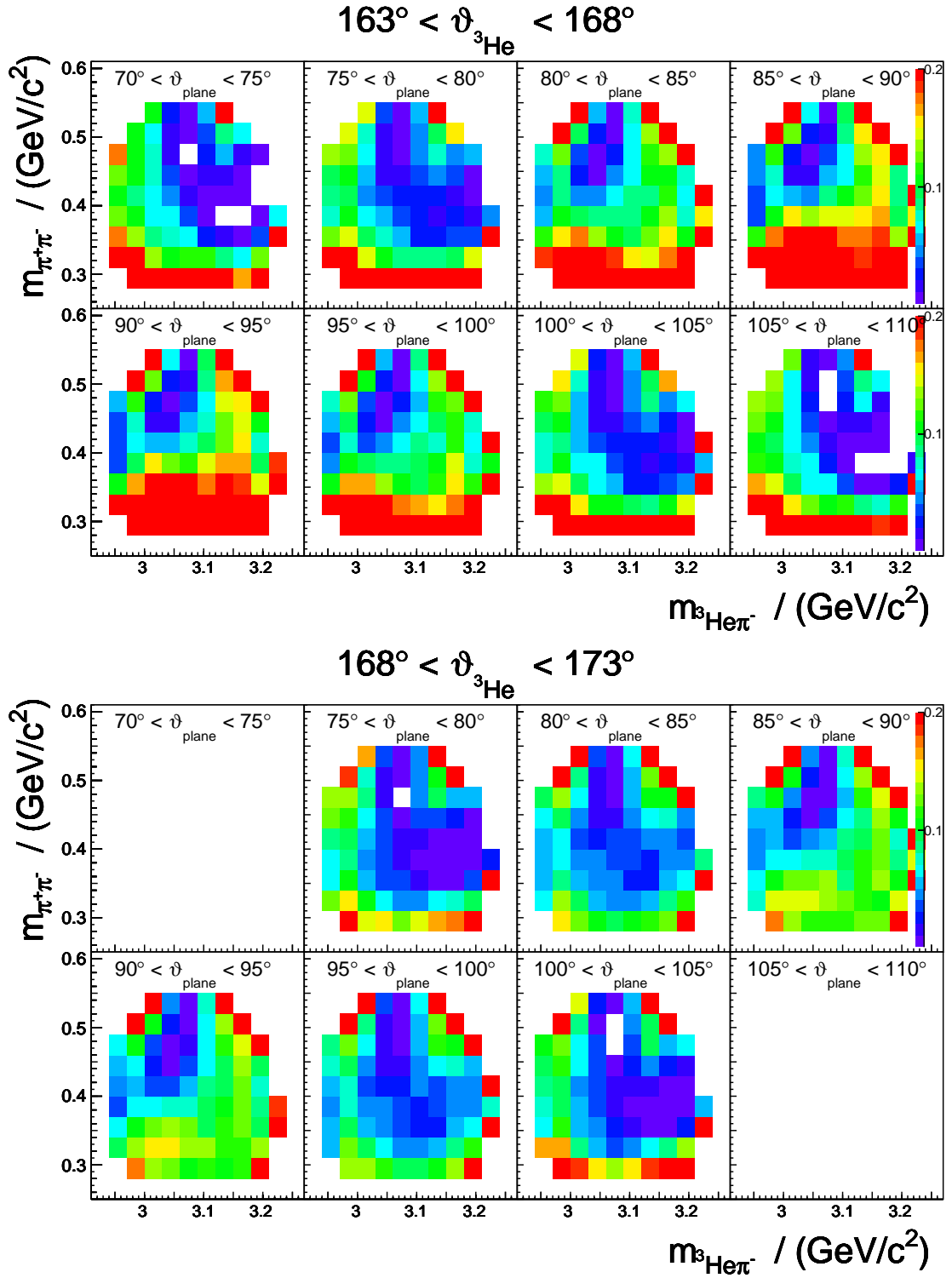


Figure 4.3.: (Continued)

spectra. A test of the reliability of the results gained by this means is possible with the help of the here presented matrix method.

4.2.2. Model-based acceptance correction

The attempt to overcome the model dependence of the acceptance correction by choosing a multi-dimensional approach leads to an unfavourable restriction of kinematically accessible regions. To overcome this limitation, it is necessary to make assumptions on the actual physical behaviour of the observed variables, enabling to downsize the dimensionality of the correction matrix. The required features of a data description can be deduced through a thorough examination of the measured distributions under consideration of the detector acceptance. The treatment of the different variables will be discussed in the following.

The confinement on ${}^3\text{He}$ production angles $143^\circ < \vartheta_{3\text{He}}^{CMS} < 173^\circ$, introduced in the previous subsection, needs to be kept up since a consideration of the full angular region would require too many assumptions on interdependences of the observables. The resulting small range of $\vartheta_{3\text{He}}$, in conjunction with the fact that the corresponding acceptance distribution is relatively smooth, justifies the use of a distribution which is flat in $\cos(\vartheta_{3\text{He}})$. Since furthermore there are no signs for significant deviations from phase space in the polar angle of the production plane ϑ_{plane}^{CMS} , the model development can be focused on a proper reconstruction of the invariant mass spectra and their interdependences. Prominent features that need to be reflected are the characteristic ABC enhancement at low $m_{\pi\pi}$ and a peak-like structure in the central region of the $m_{3\text{He}\pi}$ spectra, including a tail to higher masses for the combination with the positively charged pion.

The evaluation of a data description is done with the help of the uncorrected two-dimensional distribution of the invariant masses of $m_{\pi^+\pi^-}$ and $m_{3\text{He}\pi^-}$. Results of a χ^2 test of the Monte Carlo output serve as a quantification of the level of agreement with the data. Besides an optimisation of the reduced χ^2 (in the following termed as χ_{red}^2), a bin-wise χ^2 analysis can be used to systematically improve a tested approach. In Figure 4.4 an example of the procedure is given through a comparison with a simulated distribution according to phase space. As expected, the strong deviation between the plots is clearly visible in the χ^2 distribution and consequentially leads to a high value of χ_{red}^2 .^e

^e It should be noted here, that the absolute values of χ^2 depend on the size of the Monte Carlo sample and converge only in the case of exceedingly high statistics. To permit a comparison between different data descriptions, the number of simulated events is the same for any χ^2 test. The integrated number of accepted simulated events that contribute to the spectrum is 130,000.

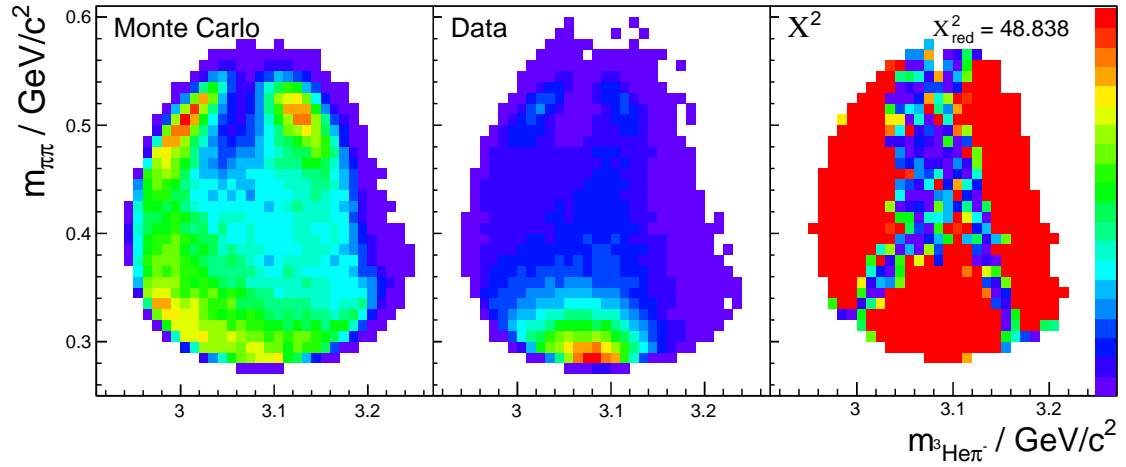


Figure 4.4.: χ^2 test to verify the quality of data reproduction by a Monte Carlo distribution according to phase space. Shown is the correlation between $m_{\pi^+\pi^-}$ and $m_{^3\text{He}\pi^-}$ for events accepted by the ANKE detector system, with the confinement $143^\circ < \vartheta_{^3\text{He}}^{CMS} < 173^\circ$. The coloured scale is linear and for the χ^2 distribution it covers a range from 0 to > 8 . The corresponding generated distribution with the restriction $143^\circ < \vartheta_{^3\text{He}}^{CMS} < 173^\circ$ is shown in the Appendix A.3.

In the following, different data descriptions will be presented and tested accordingly.

First attempt: Effective $\Delta\Delta$ model

Up to now there exists no agreed model for $d p \rightarrow ^3\text{He} \pi^+ \pi^-$. For the similar exit channel with $\pi^0 \pi^0$ instead of $\pi^+ \pi^-$ the WASA-at-COSY collaboration uses a description based on the simultaneous appearance of two $\Delta(1232)$ resonances,^f which are either excited directly or as a decay product of an exotic resonance. The model was originally developed to provide an explanation for data from the WASA-at-COSY experiment on the reaction $n p \rightarrow d \pi^0 \pi^0$ [A⁺11]. A modified version was later used to describe data from the same experiment on $p d \rightarrow ^3\text{He} \pi^0 \pi^0$ [PdR14a]. Detailed information about the application of the model can be found in the given references. The excitation of two Δ resonances, represented by corresponding Breit-Wigner terms, results in the observed peaking at central $m_{^3\text{He}\pi^-}$. A further effect are enhancements at low and high values in the $m_{\pi\pi}$ spectrum.

^f Properties of the $\Delta(1232)$ resonance according to the Particle Data Group (PDG) [B⁺12]: $I(J^P) = 3/2(3/2^+)$; Breit Wigner mass (mixed charges) = 1230 to 1234 MeV/ c^2 ; Breit Wigner full width (mixed charges) = 114 to 120 MeV/ c^2 ; Main decay mode: $N \pi$ (Fraction: 100 %).

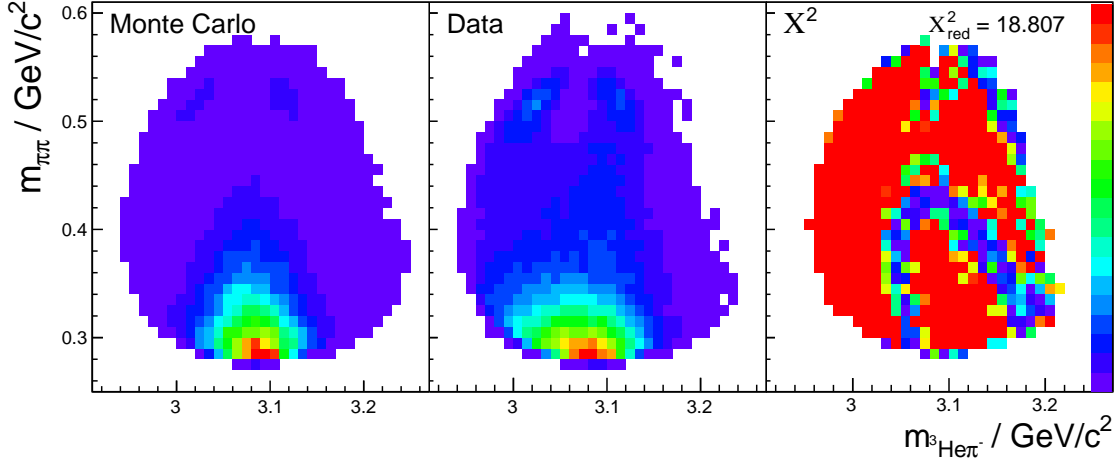


Figure 4.5.: χ^2 test to verify the quality of data reproduction by a Monte Carlo distribution according to the ABC resonance model by the WASA-at-COSY collaboration [PdR13]. Shown is the correlation between $m_{\pi^+\pi^-}$ and $m_{^3\text{He}\pi^-}$ for events accepted by the ANKE detector system, with the confinement $143^\circ < \vartheta_{^3\text{He}}^{CMS} < 173^\circ$. The coloured scale is linear and for the χ^2 distribution it covers a range from 0 to > 8 . The corresponding generated distribution with the restriction $143^\circ < \vartheta_{^3\text{He}}^{CMS} < 173^\circ$ is shown in the Appendix A.3.

An implication of the assumed dibaryon resonance is a form factor that leads to a suppression of high two-pion invariant masses, providing thus an explanation for the ABC effect [A⁺11]. However, since the description aims to explain solely the production of pure isospin-zero states of the two pions, as is the case with $\pi^0 \pi^0$, it does not imply isovector contributions and associated interference effects that are relevant for the $\pi^+ \pi^-$ state. Hence, on this basis there is no possibility to reproduce the observed difference between $m_{^3\text{He}\pi^+}$ and $m_{^3\text{He}\pi^-}$. A comparison of the ANKE data to the model calculations, as shown in Figure 4.5, moreover reveals that the inclusion of two Δ propagators leads to too small peak widths in these spectra. Since the acceptance correction for the $d p \rightarrow {}^3\text{He} \pi^+ \pi^-$ reaction at ANKE exhibits a considerable sensitivity on the shape of the simulated $m_{^3\text{He}\pi}$ distributions, the use of a more precise data description is unavoidable.

Second attempt: Sequential Roper decay via Δ resonance

A better reproduction of the two-particle invariant mass spectra is feasible through an alternative ansatz, based on the idea of excitations of the resonance $N^*(1440)$,

4. Determination of cross sections

also known as the Roper resonance.[§] Up to 40 % of its branching ratio is associated with the formation of two pions. Away from the threshold region of two-pion production, as in the presented case, this proceeds dominantly through the channel $N^* \rightarrow \Delta \pi \rightarrow N \pi \pi$ [AROH98, S⁺09]. Because each step of the decay chain is associated with a change of the nucleon spin ($\Delta J = 1$), both of the pions emitted in relative p-wave to the nucleon. The description used here was developed in collaboration with C. Wilkin along general lines of a theoretical study of two-pion production in nucleon-nucleon collisions by L. Alvarez Ruso, E. Oset and E. Hernández [AROH98, AR99]:

$$\sigma \propto \left| [m_\pi^2 + B \vec{k}_1 \cdot \vec{k}_2] (3\Delta^{++} + \Delta^0) \right|^2. \quad (4.1)$$

The scalar product of the pion momenta \vec{k}_i in the centre-of-mass frame is intended to reflect the double p-wave transition. It leads to a preference of parallel and antiparallel momentum combinations and thus enhancements at high and low $\pi\pi$ invariant masses. To strengthen the central $m_{\pi\pi}$ region, the effect is reduced by the presence of a second summand, for which the scalar is replaced by the constant value of the squared pion mass m_π^2 . The complex parameter B allows for a relative adjustment of both contributions. An appropriate ratio of its real and imaginary part produces furthermore the observed preference of low compared to high values of $m_{\pi\pi}$.

The appearance of the $\Delta(1232)$ resonance, excited by the decay of the $N^*(1440)$, is described by Breit-Wigner functions of the form [Pil67]

$$\Delta(k_{\pi N}, \Gamma) = \frac{\sqrt{m_\Delta \Gamma / k_{\pi N}}}{m_{\pi N}^2 - m_\Delta^2 + im_\Delta \Gamma}, \quad (4.2)$$

with $k_{\pi N}$ being the absolute momentum in the πN system and

$$\Gamma(k_{\pi N}) = b \frac{\gamma R^2 k_{\pi N}^3}{1 + R^2 k_{\pi N}^2}, \quad (4.3)$$

the energy-dependent width. The constant $\gamma = 0.74$ denotes a “reduced width”, $R = 6.3 \text{ c/GeV}$ the interaction range. Further explanations about γ and R can be found in Reference [Pil67], page 121, and references therein. The laboratory nucleon momentum, needed for the calculation of $k_{\pi N}$ and the invariant mass $m_{\pi N}$, is taken as one third of the ^3He momentum. Effects which cause a broadening of the

[§] Properties of the $N(1440)$ resonance according to the PDG [B⁺12]: $I(J^P) = 1/2(1/2^+)$; Breit Wigner mass = 1420 to 1470 MeV/ c^2 ; Breit Wigner full width = 200 to 450 MeV/ c^2 ; Main decay modes: $N \pi$ (Fraction: 55-75 %), $N \pi \pi$ (Fraction: 30-40 %).

4.2. Acceptance analysis for $d p \rightarrow {}^3\text{He} \pi^+ \pi^-$

	$N^{*+} \rightarrow \Delta^{++} \pi^-$	$N^{*+} \rightarrow \Delta^0 \pi^+$	$N^{*0} \rightarrow \Delta^+ \pi^-$	$N^{*0} \rightarrow \Delta^- \pi^+$
I	1/2 3/2 1	1/2 3/2 1	1/2 3/2 1	1/2 3/2 1
I_3	+1/2 +3/2 -1	+1/2 +3/2 -1	+1/2 +3/2 -1	+1/2 +3/2 -1
CG	$\sqrt{1/2}$	$\sqrt{1/6}$	$\sqrt{1/6}$	$\sqrt{1/2}$
	$\Delta^{++} \rightarrow p \pi^+$	$\Delta^0 \rightarrow p \pi^-$	$\Delta^+ \rightarrow n \pi^+$	$\Delta^- \rightarrow n \pi^-$
I	3/2 1/2 1	3/2 1/2 1	3/2 1/2 1	3/2 1/2 1
I_3	+3/2 +1/2 1	-1/2 +1/2 -1	+1/2 -1/2 1	-3/2 -1/2 -1
CG	1	$\sqrt{1/3}$	$\sqrt{1/3}$	1
CG_{total}	$\sqrt{1/2}$	$\sqrt{1/18}$	$\sqrt{1/18}$	$\sqrt{1/2}$

Table 4.1.: Overview of channels related to the Roper decay via a Δ resonance. For each process, the isospins I and their third components I_3 of the involved particles are given. These allow an assignment of the Clebsch-Gordan coefficients CG. The bold value CG_{total} marks the coefficient for the whole decay chain.

width for bound isobars in comparison to free ones, like Fermi motion and multiple scattering, are considered in terms of the factor b . Its size was estimated with the help of data on pion scattering on light nuclei. Since no such information for the case of ${}^3\text{He}$ particles is available, a rough interpolation of the extracted widths from pion-proton [P⁺78], pion-deuteron [P⁺78] and pion- ${}^4\text{He}$ [W⁺73] scattering experiments was conducted. From that, the ratio $\Gamma({}^3\text{He}) : \Gamma(p)$ was deduced to be in the range 1.3 - 1.4. On this basis the value for b was determined in the course of an optimisation of the data description. The same holds for the Breit-Wigner mass of the Δ resonance in the ${}^3\text{He}$ nucleus. Fits on the mentioned data on pion-nucleus scattering indicated it to be a few MeV/c^2 higher than the nominal value.

As will be explained later on, both m_Δ and b become relevant quantities with respect to the difference in the $m_{{}^3\text{He}\pi}$ spectra, due to the ratio 3 : 1 of the Δ^{++} and Δ^0 propagators. This difference in the excitation probability of differently charged Δ resonances can be understood through a study of the relevant decay channels of the excited nucleon under consideration of the isospin correlations. The participation of protons and neutrons in the reaction enables four different possibilities to induce the production of a $\pi^+ \pi^-$ final state through the decay of an $N^*(1440)$ via a $\Delta(1232)$ resonance. These are illustrated in Table 4.1 in combination with a deduction of the respective Clebsch–Gordan coefficients.

In the case of positively charged Roper resonances, the Clebsch-Gordan coefficient for channels where the Δ resonance decays into a $\pi^+ N$ combination is $(1/2)^{1/2}$ and thereby exceeds that of the decay into $\pi^- N$ of $(1/18)^{1/2}$ by a factor of three, resulting in a factor of nine difference in the the cross section. For neutral Roper

4. Determination of cross sections

resonances it is exactly the other way round. The two protons and one neutron which form the ${}^3\text{He}$ nucleus lead, on the assumption of a charge independent nucleon excitation, to the total Clebsch-Gordan ratio

$$\frac{\Delta \rightarrow N\pi^+}{\Delta \rightarrow N\pi^-} = \frac{2 \cdot \sqrt{1/2} + \sqrt{1/18}}{\sqrt{1/2} + 2 \cdot \sqrt{1/18}} = \frac{7}{5}. \quad (4.4)$$

As a consequence of this, the excitation of Roper resonances would cause a higher number of events in the $m_{{}^3\text{He}\pi^+}$ spectrum to be directly linked with Δ decay processes than in the $m_{{}^3\text{He}\pi^-}$ spectrum. Since the excitation function of the $\Delta(1232)$ has a tail to higher masses^h, its influence would result in a different appearance of the two $m_{{}^3\text{He}\pi}$ distributions. A further contribution to a relative shift between these is given by the Breit-Wigner mass of the $\Delta(1232)$. With $m_\Delta = 1232 \text{ MeV}/c^2$, the peak position is $m_{{}^3\text{He}} - m_p + m_\Delta = 3108 \text{ MeV}/c^2$ and therefore slightly higher than the centre of the $m_{{}^3\text{He}\pi}$ distribution at $3080 \text{ MeV}/c^2$ ⁱ, thus strengthening the effect of a Δ excess in the $m_{{}^3\text{He}\pi^+}$ spectrum. An increment of m_Δ , as motivated above, leads to a further divergence. In contrast, a large Δ width, realisable in terms of a high value of b , reduces the importance of this effect, since it causes the $m_{{}^3\text{He}\pi}$ distributions to smear out.

On the basis of the deduced CG factor of $7/5$ it is however not possible to adequately reproduce the difference observed in the data. This deficiency can be overcome by a complete neglect of the influence of neutral Roper resonances. A physical manifestation of this scenario could be realised through a consideration of an initial process of the form $d p \rightarrow d N^*$. After the decay via $N^* \rightarrow \Delta^{++} \pi^- \rightarrow p \pi^+ \pi^-$ the proton would be captured by the deuteron to form the ${}^3\text{He}$.^j With the resulting weighting factors 3 and 1 for $\Delta^{++} (\rightarrow p\pi^+)$ and $\Delta^0 (\rightarrow p\pi^-)$ in combination with the values $m_\Delta = 1238 \text{ MeV}/c^2$, $b = 1.35$ and $B = 0.2 + 0.3i$ the measured invariant mass distributions and their interdependences can be reasonably described. The optimisation of the parameters was mainly driven by the above discussed χ^2 test. The final results of this procedure are shown in Figure 4.6. The bin-wise determination of χ^2 values allows to localise the kinematical regions of the persisting deviations from the data, which are found to be predominantly at $m_{\pi^+\pi^-} < 0.42 \text{ GeV}/c^2$. As can be seen from Figures 4.2 and 4.3, the geometrical acceptance in this region is relatively high and does not suffer from major relative fluctuations. It will be demonstrated in the following section that the presented data description hence

^h This asymmetry follows from the energy-dependence of the width Γ , denoted in Equation 4.3.

ⁱ At an excess energy of $Q = 265 \text{ MeV}$ this value is derived through $m_{{}^3\text{He}} + m_{\pi^\pm} + \frac{Q}{2} = 3080 \text{ MeV}/c^2$.

^j Since the primary purpose of the used approach is to enable a proper estimation of the acceptance correction, no further implications of this assumption will be discussed at this point. Conclusions on the model and its validity will be drawn in Section 5.1.

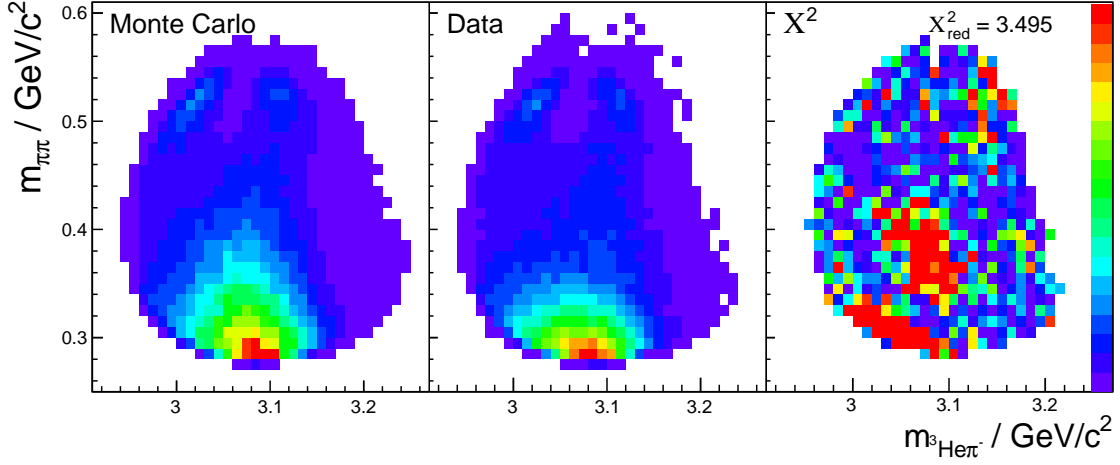


Figure 4.6.: χ^2 test to verify the quality of data reproduction by a Monte Carlo distribution according to the presented isobar production model (see also Reference [M⁺14]). Shown is the correlation between $m_{\pi^+\pi^-}$ and $m_{^3\text{He}\pi^-}$ for events accepted by the ANKE detector system, with the confinement $143^\circ < \vartheta_{^3\text{He}}^{CMS} < 173^\circ$. The coloured scale is linear and for the χ^2 distribution it covers a range from 0 to > 8 . The corresponding generated distribution with the restriction $143^\circ < \vartheta_{^3\text{He}}^{CMS} < 173^\circ$ is shown in the Appendix A.3.

allows for an adequate acceptance correction of the ANKE data on the the reaction $d p \rightarrow {}^3\text{He} \pi^+ \pi^-$.

4.2.3. Validation of the acceptance correction procedure

Despite the fact that the data description presented in the previous section enables a convenient reproduction of the measured invariant mass distributions and their interdependences, the great sensitivity of the acceptance correction on the input model still affords a serious examination to justify its application. For this reason two independent approaches were used to study the model dependence in detail. These are discussed in the following.

Effects of model variations

Provided that the simple isobar model according to Equation 4.1 reproduces the measured data sufficiently well to enable the determination of reliable acceptance

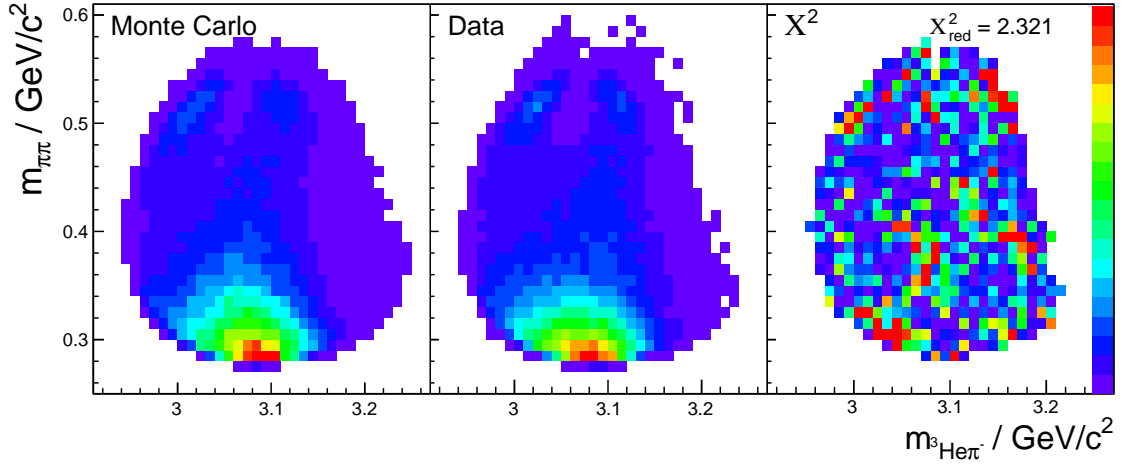


Figure 4.7.: χ^2 test to verify the quality of data reproduction by a Monte Carlo distribution according to a modified version of the presented isobar production model (for details see text). Shown is the correlation between $m_{\pi^+\pi^-}$ and $m^3_{He\pi^-}$ for events accepted by the ANKE detector system, with the confinement $143^\circ < \vartheta_{3He}^{CMS} < 173^\circ$. The coloured scale is linear and for the χ^2 distribution it covers a range from 0 to > 8 . The corresponding generated distribution with the restriction $143^\circ < \vartheta_{3He}^{CMS} < 173^\circ$ is shown in the Appendix A.3.

correction factors, deviating descriptions of comparable quality should lead to similar results. For this purpose, a considerable modification of the original ansatz of the form

$$\sigma \propto |3\Delta^{++} + \Delta^0|^2 P(M_{\pi^+\pi^-}), \quad (4.5)$$

where the term $[m_\pi^2 + B\vec{k}_1 \cdot \vec{k}_2]$ is replaced by an artificially introduced third order polynomial $P(m_{\pi^+\pi^-})$, was used to study acceptance effects. With the parameters

$$P(x) = 1.00 - 6.05x + 12.52x^2 - 8.65x^3, \quad (4.6)$$

where the masses are measured in GeV/c^2 , it was possible to accurately reproduce the shape of the $m_{\pi^+\pi^-}$ distribution. Results of the corresponding χ^2 test are shown in Figure 4.7, revealing an even better agreement with the data than the description according to Equation 4.1.

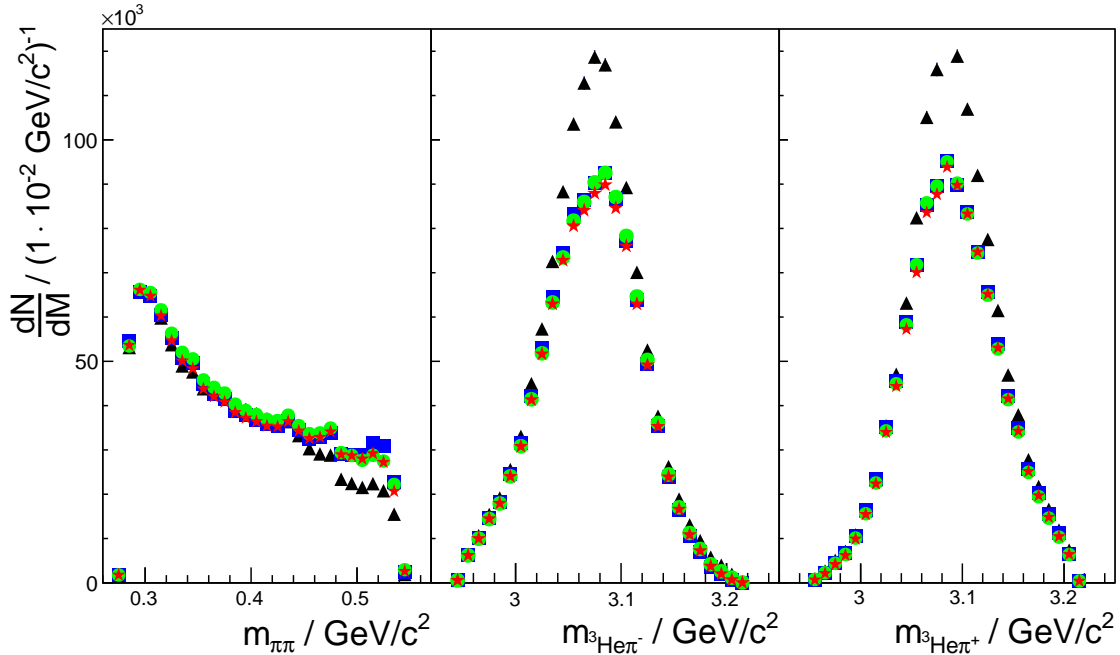


Figure 4.8.: Measured invariant mass distributions after individual (one-dimensional) correction for acceptance with models according to Equations 4.1 (blue squares), 4.5 (red stars), Equation 4.1 with $(7\Delta^{++} + 5\Delta^0)$ (green circles) and simple phase space (black triangles). Statistical uncertainties are displayed, but mostly these are smaller than the markers. All differences are purely a result of unequal acceptance correction factors.

A comparison of individually (\cong one-dimensionally) acceptance-corrected invariant mass distributions on the basis of different models can be found in Figure 4.8. Besides the discussed variation it also includes an attempt with simple phase space, as well as another modification of Equation 4.1 where a ratio $\Delta^{++}/\Delta^0 = 7/5$ in line with the actual Clebsch-Gordan coefficients is considered.^k

The effect on the acceptance corrected results is in agreement within 3 % for the three model variations, whereas the phase space corrected distributions diverge significantly from the rest. Moreover, the integrals of the three different invariant mass distributions coincide within 3 % in all cases except for the phase space correction, where the number of events in the $m_{\pi\pi}$ spectrum is $\approx 20\%$ smaller than in the $m_{3\text{He}\pi}$ spectra. These findings indicate that a one-dimensional acceptance correction based on Equation 4.1 leads to reliable results. To corroborate this

^k As discussed above, this ratio does not allow to enable a proper reproduction of the measured invariant mass distributions. A χ^2 test of this parametrisation resulted in a value of 6.58 for the reduced χ^2 .

assumption further, the investigation is complemented by a comparison with a multidimensional acceptance correction.

Comparison with multidimensional approach

As discussed in Section 4.2.1, a four-dimensional acceptance map allows in principle for a model-independent correction of the measured data, but leads in return to various restrictions on the kinematic coverage. Whereas this fact is rather problematic with respect to the determination of cross sections, it still provides a method to test the applicability of a data description for a one-dimensional correction. In addition to the confinement of the ${}^3\text{He}$ scattering angle, cuts on the polar angle of the normal to the ejectile plane ϑ_{plane}^{CMS} and the two-dimensional $m_{\pi^+\pi^-}$ vs $m_{{}^3\text{He}\pi^-}$ relation are necessary to avoid systematic effects on the resulting invariant mass distributions. The following regions are excluded on the basis of Figure 4.3:

$$\begin{aligned} \vartheta_{plane}^{CMS} < 80^\circ \quad \vartheta_{plane}^{CMS} > 100^\circ. \\ (3.03 \text{ GeV}/c^2 < m_{{}^3\text{He}\pi^-} < 3.09 \text{ GeV}/c^2) \wedge (m_{\pi^+\pi^-} > 0.43 \text{ GeV}/c^2). \end{aligned} \quad (4.7)$$

In the case of the multidimensional approach, the correction factors are determined individually for each event, according to the position of its kinematic parameters in the acceptance matrix. In contrast, with the one-dimensional model based procedure the correction factors are determined for the particular bins of each spectrum. A comparison of the results of the two different methods is shown in Figure 4.9. Due to the two-dimensional invariant mass cuts, the distributions are not smooth. For $m_{\pi^+\pi^-}$ and $m_{{}^3\text{He}\pi^-}$ the affected intervals are directly visible, whereas for $m_{{}^3\text{He}\pi^+}$ the corresponding events are spread over a wider mass range. In these regions the distributions of the data points in $m_{{}^3\text{He}\pi^\pm}$ tend to exhibit marginally lower event numbers for the case of the multidimensional approach. This may, at least partly, be caused by edge effects. Apart from that, the two methods lead to a very good agreement of the results. The integrals of the distributions are consistent within 3%. Hence it can be stated that, as far as they are comparable, no principal deviations between the two methods can be found.

4.3. Acceptance analysis for $d p \rightarrow {}^3\text{He} \pi^+ \pi^- \pi^0$

Besides a detailed investigation of the $d p \rightarrow {}^3\text{He} \pi^+ \pi^-$ reaction, the procedure of the data analysis according to Chapter 3 also enables a study on the ${}^3\text{He} \pi^+ \pi^- \pi^0$

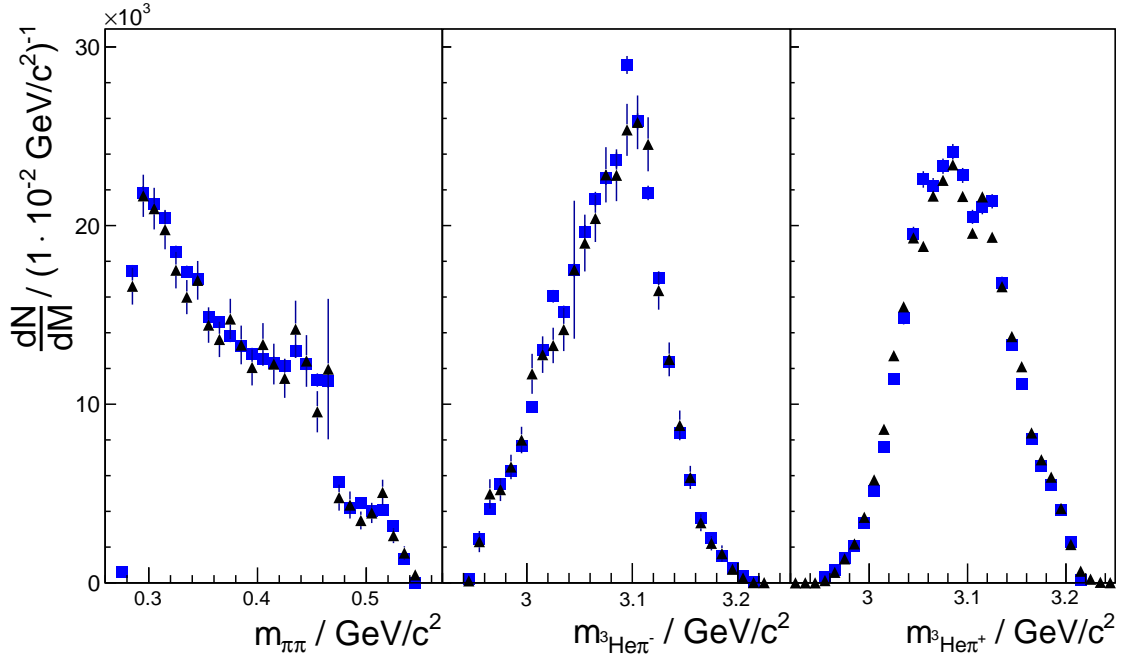


Figure 4.9.: Invariant mass distributions after correction for acceptance with the four-dimensional (black triangles) and one-dimensional (blue squares) procedure on the basis of Equation 4.1. A definition of the processed cuts can be found in the text. For convenience, statistical uncertainties of the multidimensionally corrected data points are only plotted for $m_{\pi^+\pi^-}$ and $m^3_{\text{He}\pi^-}$.

final state. In Section 3.5 it was shown, that it is possible to extract a practically background free data sample through the request of a coincident detection of all three involved charged particles. Since the total energy of 3.353 GeV, corresponding to an excess energy of $Q_{{}^3\text{He}\pi^+\pi^-\pi^0} = 130$ MeV, is just below the production threshold of the η meson, no contamination from meson resonance decays needs to be considered. In comparison to the ANKE detector acceptance of the $d p \rightarrow {}^3\text{He} \pi^+ \pi^-$ reaction it has to be regarded, however, that the necessary coincidence of three detected particles leads to a worse coverage of the accessible phase space. In addition, the presence of four particles in the final state makes the relevant acceptance map even more complex, since interdependences of 7 effective degrees of freedom would need to be considered.¹

The following considerations are therefore intended to show some selected features and limitations of the acceptance distribution, allowing to place the result presented

¹ On the lines of the considerations at the beginning of Section 4.2.1, there are in total 12 degrees of freedom, which are reduced by four-momentum conservation and isotropic distributions in the azimuthal angle.

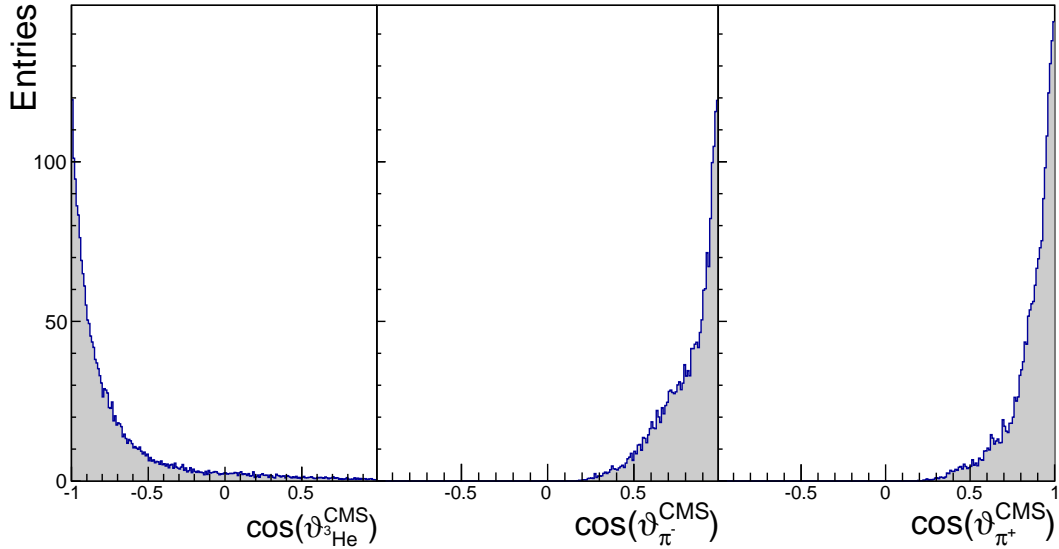


Figure 4.10.: Monte Carlo generated CMS scattering angle distributions of the ${}^3\text{He}$, π^- and π^+ particles from the $d p \rightarrow {}^3\text{He} \pi^+ \pi^- \pi^0$ reaction at $\sqrt{s} = 3.353$ GeV for the request of a coincident detection by the ANKE detector system. The momenta produced by the event generator follow a uniform distribution in the cosine of the CMS scattering angles.

in Section 4.4.3 into a proper context.

Due to their small mass, pions only reach the side detectors if they have small transversal, but high longitudinal momenta in the laboratory system. In any other case, they are too strongly deflected by the magnetic field of the spectrometer. As can be seen from Figure 4.10, only pions which are emitted under small production angles in CMS are therefore covered by the ANKE acceptance. As a consequence of the reaction kinematics, coincidentally measurable ${}^3\text{He}$ particles move predominantly into the opposite direction. There is hence only little sensitivity on angular distributions and their interdependences. The similarly limited acceptances of the π^\pm production angles affect furthermore a restriction on the observed $m_{\pi^+\pi^-}$ range, because large two particle invariant masses coincide with large relative angles. This becomes apparent from Figure 4.11, where correlations in acceptance between $m_{\pi^0\pi^+}$ and $m_{\pi^0\pi^-}$ as well as $m_{\pi^+\pi^-}$ and $m_{{}^3\text{He}\pi^+}$ are presented in terms of a juxtaposition of generated and accepted event distributions. In case of the other shown particle combinations however, the full mass range is covered.

Even on the basis of this crude acceptance analysis it can be stated, that the kinematics of the $d p \rightarrow {}^3\text{He} \pi^+ \pi^- \pi^0$ reaction are only partly accessible by the

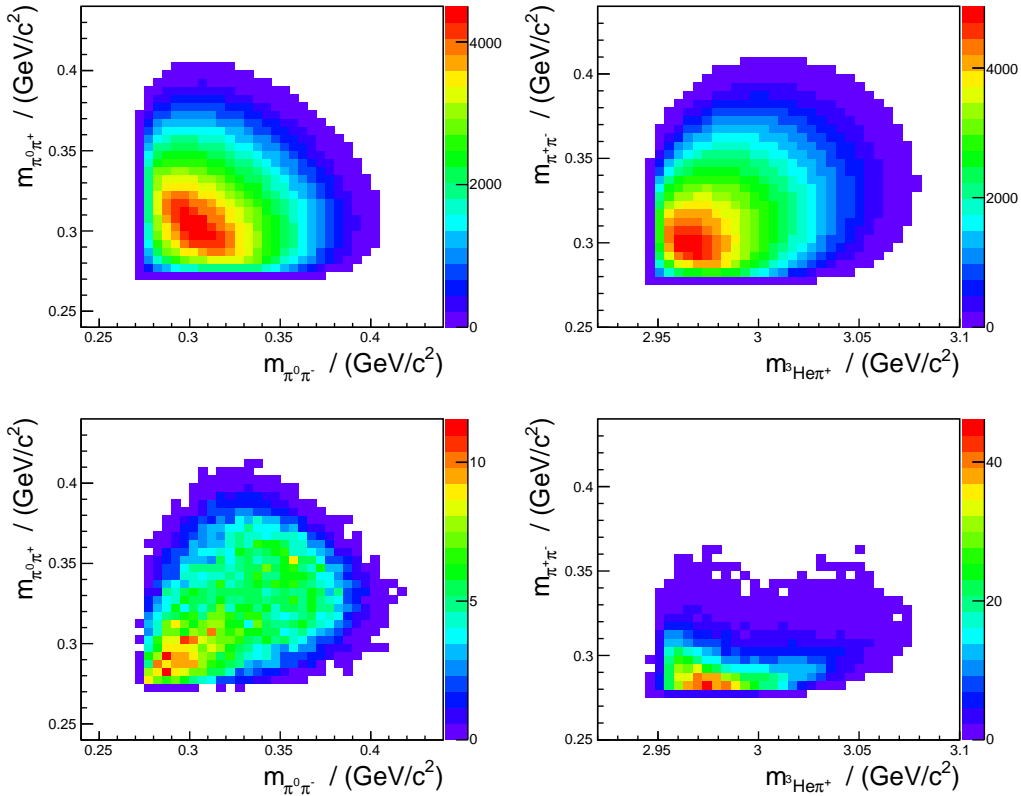


Figure 4.11.: Monte Carlo generated correlations between different two-particle invariant mass distributions for the same scenario as in Figure 4.10. The upper spectra show the distributions produced by the event generator, whereas the lower spectra reflect the ANKE acceptance. The π^0 three-momenta needed for the bottom left plot were calculated from the smeared momentum vectors of the detected particles.

ANKE detector system. A correction for the acceptance will thus suffer from a potentially strong model dependence. The little knowledge about the involved physical processes and the small amount of only 40 events that could be assigned to the reaction (see Section 3.5), do furthermore significantly hamper the development of an appropriate data description. The only available experimental data on the reaction were taken at the much higher excess energies of $Q = 386$ MeV and $Q = 432$ MeV [S⁺10], do however not reveal any significant deviations from phase space behaviour in the observed invariant mass spectra. Although this does certainly not allow for definitive conclusions on the characteristics of physical observables at the energy of the presented experiment, it may be seen as an indication for less pronounced effects in comparison to the two-pion production reactions. Hence,

to amend the sparse amount of experimental data on three-pion production, a cross section estimation on the basis of an acceptance determined with phase space simulations will be given in Section 4.4.3.

4.4. Results

The probability of a specific scattering event is described in terms of its cross section σ . From a definite number of measured events N_{meas} , which can be attributed to the investigated reaction, it can be calculated through the equation

$$\sigma = \frac{N_{meas}}{\varepsilon A} \frac{1}{L_{int}} = \frac{N_{corr(\varepsilon)}}{A} \frac{1}{L_{int}}. \quad (4.8)$$

L_{int} is the integrated luminosity of the examined data sample and was calculated to be $L_{int} = (3143 \pm 17_{stat} \pm 190_{syst}) \text{ nb}^{-1}$ (see beginning of this chapter). ε represents the combination of detector and trigger efficiencies, A the ANKE acceptance. The determination of ε is described in Section 3.6. The correction was done on an event-by-event basis, allowing to replace N_{meas}/ε by the corrected number $N_{corr(\varepsilon)}$ in the final calculation. The evaluation of A for the reaction $d p \rightarrow {}^3\text{He} \pi^+ \pi^-$ is elaborated in the previous section. Since the correction factors were considered bin-wise for each of the invariant mass spectra, these needed to be derived before integrated cross sections could be determined.

4.4.1. Invariant mass distributions for $d p \rightarrow {}^3\text{He} \pi^+ \pi^-$

As a consequence of the restriction to CMS ${}^3\text{He}$ production angles from 143° to 173° in the analysis of the $d p \rightarrow {}^3\text{He} \pi^+ \pi^-$ reaction, the invariant mass distributions were derived in terms of double differential cross sections. To extract these for each mass bin of width $0.01 \text{ GeV}/c^2$, Equation 4.8 was modified accordingly to the form

$$\left(\frac{d^2\sigma}{d\Omega dm} \right)_i = \frac{1}{2\pi \cdot (\cos(143^\circ) - \cos(173^\circ)) \cdot 0.01 \text{ GeV}/c^2} \frac{N_{corr(\varepsilon),i}}{A_i} \frac{1}{L_{int}}. \quad (4.9)$$

The dominating relative systematic uncertainties result from the choice of the model used for the acceptance correction. They were determined individually for each data point by evaluation of the relative differences between the correction factors

resulting from Equation 4.1 and various model variations which also show a reasonable agreement with the data. For this purpose Equation 4.5 was used, as well as Equation 4.1 with modest modifications of the parameters m_Δ and b . Furthermore modest variations of the 3:1 factor for the Δ^{++} and Δ^0 were tested. For all considered alternatives, the χ^2 test presented in Section 4.2.2 was required to lead to $\chi_{red}^2 < 10$ and to show besides a tendency to small χ^2 values in the regions of low acceptance. The maximum deviations from the original correction factors are taken as systematic uncertainties. Mostly these values are smaller than 5%. Not included in this calculation is the overall normalisation uncertainty of 6%. Contributions from other sources of relative or absolute systematic uncertainties are considered to be negligible.

The resulting values for $m_{\pi^+\pi^-}$, $m_{^3\text{He}\pi^+}$ and $m_{^3\text{He}\pi^-}$ at an excess energy of 265 MeV are given in table 4.2. Furthermore they are shown in Figure 4.12, together with simulated distributions according to Equation 4.1 and simple phase space.

The data show the characteristic features known from earlier measurements on the ABC effect, namely the strong enhancement at small $m_{\pi^+\pi^-}$ and the central peaking of the $m_{^3\text{He}\pi^\pm}$ distributions. They are essentially consistent with results from the CELSIUS-WASA experiment on the same reaction measured at a very close excess energy, which were however averaged over the full ^3He angular range [B⁺06, Bas06]. Since the reaction is known to show a strong dependence on the ^3He production angle, this hampers a direct comparison. An important finding is nevertheless the confirmation of a notable difference between the two $m_{^3\text{He}\pi^\pm}$ distributions. Due to a high invariant mass resolution of the ANKE results, it is possible to display this effect in high detail. The clearly identifiable shift of the $^3\text{He}\pi^+$ invariant mass distribution towards higher values allows to conclude that the $I_{\pi\pi} = 1$ production has a noticeable effect, as already pointed out in Section 1.1.2. The $m_{^3\text{He}\pi^\pm}$ spectra and their difference are very well described by the simple isobar model according to Equation 4.1, which explains the charge difference in terms of a large excess of Δ^{++} over Δ^0 excitations. It also provides a reproduction of the low mass enhancement of the $\pi\pi$ distribution, which is however less pronounced than in the data.

Thanks to high statistics and a comparatively stable acceptance distribution in the lower half of the two-pion invariant mass spectrum, the question of possible isovector contributions to the low $m_{\pi^+\pi^-}$ region, raised in Section 1.1.2, could additionally be investigated. For that purpose, the $m_{^3\text{He}\pi^\pm}$ spectra was examined for events which fulfill the condition $m_{\pi^+\pi^-} < 0.34 \text{ GeV}/c^2$. The resulting triple differential cross sections are shown in Figure 4.13. Here the charge difference becomes even more pronounced than predicted by the model, indicating an underestimation of the isovector $\pi^+\pi^-$ production at low $m_{\pi^+\pi^-}$. This evidence for further contributions to the $I_{\pi\pi} = 1$ channel is a matter of discussion in chapter 5.

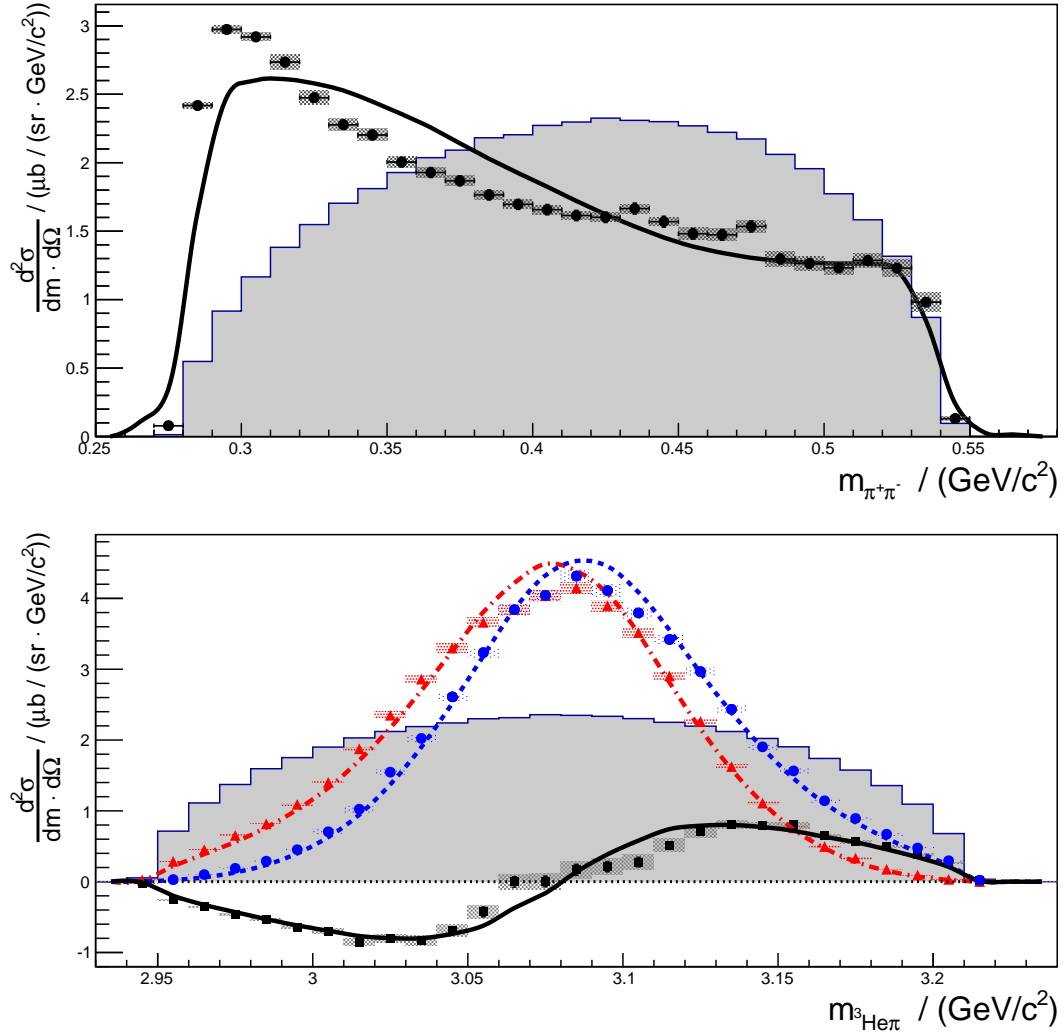


Figure 4.12.: Double differential cross sections for the reaction $dp \rightarrow {}^3\text{He} \pi^+ \pi^-$ as functions of the invariant masses $m_{\pi^+\pi^-}$ (top), $m_{^3\text{He}\pi^+}$ (bottom, blue circles) and $m_{^3\text{He}\pi^-}$ (bottom, red triangles); averaged over the CMS ${}^3\text{He}$ production angle range $143^\circ < \vartheta_{^3\text{He}}^{CMS} < 173^\circ$. The differences between the two $m_{^3\text{He}\pi}$ distributions are plotted as black squares. Horizontal error bars show the bin width, vertical ones the statistical uncertainty. The shaded rectangles around the points reflect systematic uncertainties in the acceptance correction. Not shown is the overall normalisation uncertainty of 6%. The curves correspond to Equation 4.1 and the shaded areas are phase-space distributions normalised to the integrated cross section. A similar version of this figure has been published in Reference [M⁺14].

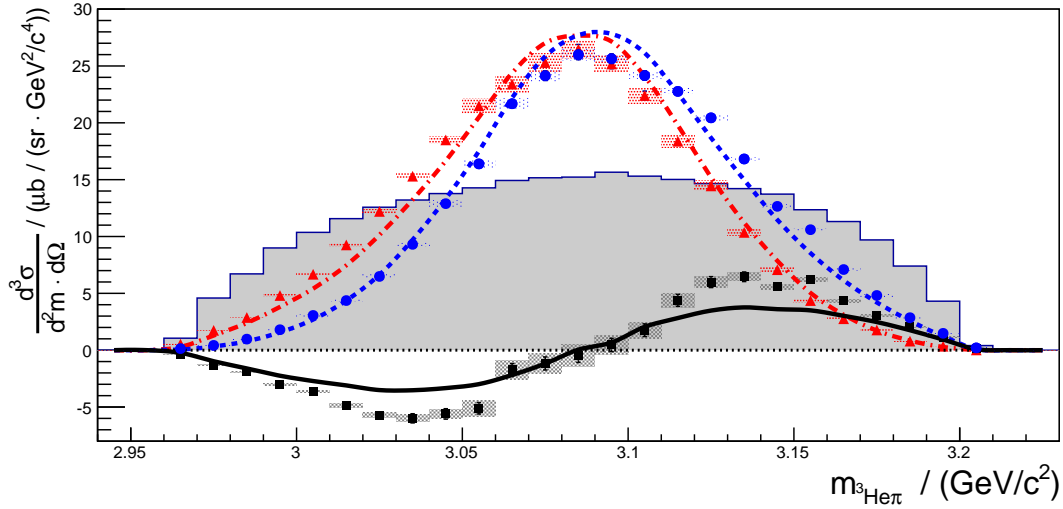


Figure 4.13.: Triple differential cross sections for the reaction $d p \rightarrow {}^3\text{He} \pi^+ \pi^-$ plotted against the invariant masses $m_{3\text{He} \pi^+}$ and $m_{3\text{He} \pi^-}$ as in Figure 4.12, but additionally averaged over the two-pion invariant mass range $2m_{\pi^\pm} < m_{\pi^+ \pi^-} < 0.34 \text{ GeV}/c^2$. A similar version of this figure has been published in Reference [M⁺14].

4.4.2. Single differential cross section for $d p \rightarrow {}^3\text{He} \pi^+ \pi^-$

On the basis of the acceptance-corrected invariant mass spectra it is possible to determine an average value of the single differential cross section for the ${}^3\text{He}$ production angle interval $143^\circ < \vartheta_{3\text{He}}^{CMS} < 173^\circ$. For that purpose, the event numbers of an invariant mass spectrum were corrected for efficiency and acceptance and integrated over all bins of the spectrum:

$$N_{corr(\varepsilon, A)} = \sum_i \frac{N_{corr(\varepsilon), i}}{A_i} = \sum_i N_{corr(\varepsilon, A), i}. \quad (4.10)$$

Using $N_{corr(\varepsilon, A)}$ the differential cross section can be calculated with the equation

$$\frac{d\sigma}{d\Omega} = \frac{1}{2\pi \cdot (\cos(143^\circ) - \cos(173^\circ))} \frac{N_{corr(\varepsilon, A)}}{L_{int}}. \quad (4.11)$$

From a comparison of different approaches for the acceptance evaluation, a systematic uncertainty of 3% could be assigned to the correction for the ANKE acceptance (see Section 4.2.3). In combination with the normalisation uncertainty of 6% the total systematic uncertainty was quadratically summed up to 7%. The value of

4. Determination of cross sections

$N_{corr(\varepsilon,A)}$ was derived independently for each of the three invariant mass spectra, with all three numbers coinciding within 1.5%. From that, the $d p \rightarrow {}^3\text{He} \pi^+ \pi^-$ differential cross section at the excess energy $Q = 265$ MeV, averaged over the ${}^3\text{He}$ production angle interval $143^\circ < \vartheta_{{}^3\text{He}}^{CMS} < 173^\circ$, could be determined to

$$\langle d\sigma/d\Omega^{CMS} \rangle = (480 \pm 3_{\text{stat}} \pm 35_{\text{syst}}) \text{ nb/sr}. \quad (4.12)$$

Differential cross sections of the investigated reaction in the same energy region as function of $\vartheta_{{}^3\text{He}}^{CMS}$ were also determined at CELSIUS-WASA [B⁺06] and Saturne [B⁺73]. In the course of the publication of the ANKE results in the European Physical Journal A [M⁺14], a comparison with the originally published CELSIUS-WASA value of $\langle d\sigma/d\Omega^{CMS} \rangle = (660 \pm 60)$ nb/sr as an average value over $141^\circ < \vartheta_{{}^3\text{He}}^{CMS} < 180^\circ$ had been done. Through consideration of an additional normalisation uncertainty of the WASA results of 20% [Bas14], the numbers were found to be in good agreement. Meanwhile, recent results from the WASA-at-COSY collaboration on the $p d \rightarrow {}^3\text{He} \pi^0 \pi^0$ reaction [PdR14a] led to a reanalysis of the original CELSIUS-WASA data on the $p d \rightarrow {}^3\text{He} \pi^0 \pi^0 / \pi^+ \pi^-$ reactions and in consequence to a reduction of the cross section values by one third [A⁺14a, PdR14b]. The revised number for the here relevant differential cross section of $\langle d\sigma/d\Omega^{CMS} \rangle = (450 \pm 50)$ nb/sr is now much closer to the ANKE result.

For a comparison to the result from the Saturne cyclotron it is necessary to consider the associated experimental and analysis conditions. Since only the ${}^3\text{He}$ momenta were measured, there is no differentiation between charged and uncharged two-pion production. From isospin relations it follows, that the isoscalar part of the $\pi^+ \pi^-$ channel contributes twice as strong as that of $\pi^0 \pi^0$. In addition, the isovector part increases the fraction of the $\pi^+ \pi^-$ cross section slightly further (see Section 1.1.2). The ratio $\sigma(\pi^+ \pi^-) / \sigma(\pi \pi)_{\text{total}}$ can hence be estimated to be in the range 0.7 – 0.75. It has furthermore to be noted, that the ABC enhancement was treated as a peak structure and therefore separated from the rest of the missing mass spectrum. The amount of subtracted two-pion events cannot be exactly reproduced from the published results. It can however be presumed, that this approach led to a significant reduction of the derived cross sections. Finally, it has to be regarded that at the energy similar to that of the ANKE experiment, the ${}^3\text{He}$ particles were only measured at $\vartheta_{{}^3\text{He}}^{CMS} = 180^\circ$. Taking all these considerations into account, the quoted differential cross section of (560 ± 70) nb/sr is compatible with the ANKE result.

4.4.3. Three-pion production

The identification of coincidentally detected ${}^3\text{He} \pi^+ \pi^-$ particle combinations allows to supplementary analyse the direct three-pion production in the $\text{d p} \rightarrow {}^3\text{He} \pi^+ \pi^- \pi^0$ reaction at an excess energy of $Q = 130$ MeV. In the missing mass analysis presented in Section 3.5, a practically background-free peak with a content of 40 events could be assigned to this process. In Section 4.3 it was shown that limitations of the ANKE angular coverage hamper an evaluation of the dependence of the results on the model used for the acceptance correction. All the cross section values given in the following are therefore estimations whose accuracy may depend significantly on similarity of the actual kinematics with pure phase space behaviour. A specification of the systematic uncertainties is not done.

The total cross section was calculated from Equation 4.8, where the overall acceptance is $A = 0.023$ and the efficiency corrected number of events $N_{\text{corr}(\varepsilon)} = (77.0 \pm 12.3)$, to $\sigma = (1.05 \pm 0.16_{\text{stat}})$ nb.

For a comparison with the result from two-pion production given in the previous section, the ratio between differential cross sections of $\pi^+ \pi^-$ and $\pi^+ \pi^- \pi^0$ production for the ${}^3\text{He}$ angular range $143^\circ < \vartheta_{3\text{He}}^{\text{CMS}} < 173^\circ$ has been determined. With $A = 0.13$ and $N_{\text{corr}(\varepsilon)} = (36.68 \pm 8.4)$, the corresponding differential cross section is $\langle d\sigma/d\Omega^{\text{CMS}} \rangle = (0.071 \pm 0.016)$ nb/sr and the resulting ratio

$$\frac{\langle d\sigma/d\Omega^{\text{CMS}} \rangle_{\text{d p} \rightarrow {}^3\text{He} \pi^+ \pi^-}}{\langle d\sigma/d\Omega^{\text{CMS}} \rangle_{\text{d p} \rightarrow {}^3\text{He} \pi^+ \pi^- \pi^0}} = 6760 \pm 1520_{\text{stat}}. \quad (4.13)$$

In addition, an attempt has been made to investigate the dependence of differential cross sections on the ${}^3\text{He}$ production angle. It needs to be stated at this point, that the model dependence of the acceptance correction could principally affect the relative distribution. Nevertheless, the results provide an estimation of possible deviations from phase space behaviour. As can be seen from Figure 4.14, the data points indicate a rising slope towards smaller angles, but are also compatible with a flat distribution in $\cos(\vartheta_{3\text{He}}^{\text{CMS}})$. For the case of two-pion production, the same distribution shows in contrast a strong decrease between $\cos(\vartheta_{3\text{He}}^{\text{CMS}}) = -1$ and $\cos(\vartheta_{3\text{He}}^{\text{CMS}}) = 0$ [B⁺06]. It seems therefore likely that the ratio of total cross sections $\langle \sigma \rangle_{\pi\pi} / \langle \sigma \rangle_{\pi\pi\pi}$ is smaller than that quoted above for the differential cross sections at large ${}^3\text{He}$ angles.

Other results for the same reaction are published only from the CELSIUS-WASA collaboration for data from a pd scattering experiment, taken at the significantly higher excess energies $Q = 386$ MeV and $Q = 432$ MeV. Total cross sections of $\sigma = (1400 \pm 17_{\text{stat}} \pm 370_{\text{syst}} \pm 410_{\text{norm}})$ nb and $\sigma = (910 \pm 7_{\text{stat}} \pm 80_{\text{syst}} \pm 110_{\text{norm}})$ nb respectively are quoted [S⁺10], with the latter uncertainties being due

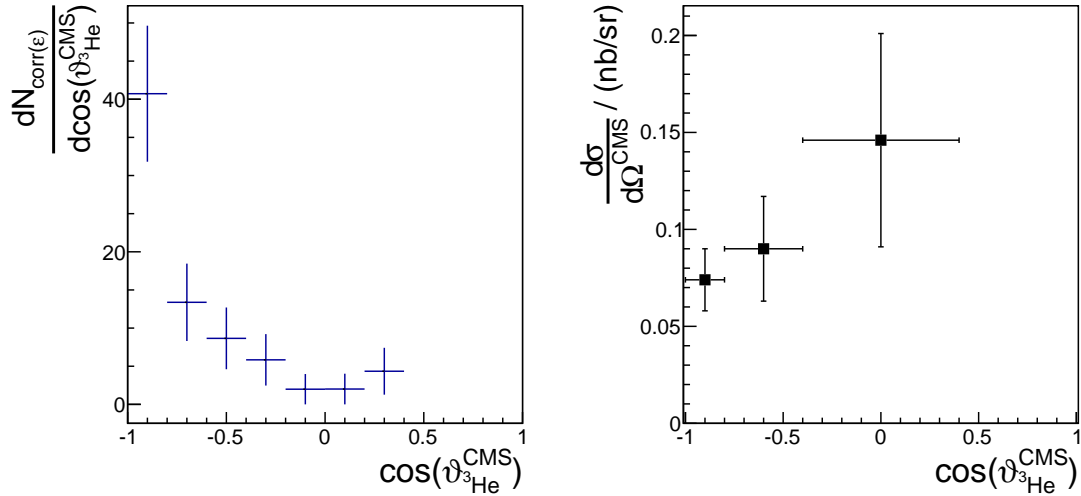


Figure 4.14.: Event distribution of the $dp \rightarrow {}^3\text{He} \pi^+ \pi^- \pi^0$ reaction measured at ANKE as function of the CMS ${}^3\text{He}$ production angle. Shown are the results after correction for detector and trigger efficiency, but without correction for the detector acceptance (left), and estimations of averaged differential cross sections after correction for the acceptance on the basis of pure phase space simulations (right). Horizontal error bars define the according bin widths, vertical ones statistical uncertainties.

to normalisation. Estimations of the ${}^3\text{He} \pi^0 \pi^0$ final state cross sections from the same measurement indicate two- and three-pion production to be of similar strength in this energy region [Sch09]. For the reaction $pp \rightarrow pp \pi^+ \pi^- \pi^0$, also measured at CELSIUS-WASA, the total cross section at $Q = 174$ MeV was found to be $\sigma = (4.6 \pm 0.3_{\text{stat}} \pm 1.2_{\text{syst}})$ nb and thus about 0.7% of that for the $pp \pi^+ \pi^-$ final state [P⁺07].

In conjunction with the estimated ANKE result, the presently available data indicate direct three-pion production to be of minor strength in the ABC energy region, but to gain strongly in importance towards higher energies. Possible conclusions will be discussed in the following chapter.

$m_{\pi^+\pi^-}$ (GeV/c ²)	$d^2\sigma/(d\Omega dm_{\pi^+\pi^-})$ ($\mu\text{b}/(\text{sr GeV}/c^2)$)	$m_{^3\text{He}\pi}$ (GeV/c ²)	$d^2\sigma/(d\Omega dm_{^3\text{He}\pi^+})$ ($\mu\text{b}/(\text{sr GeV}/c^2)$)	$d^2\sigma/(d\Omega dm_{^3\text{He}\pi^-})$ ($\mu\text{b}/(\text{sr GeV}/c^2)$)
0.275	0.079 ± 0.005 ± 0.001	2.945		0.026 ± 0.005 ± 0.000
0.285	2.418 ± 0.028 ± 0.024	2.955	0.030 ± 0.009 ± 0.001	0.287 ± 0.015 ± 0.005
0.295	2.973 ± 0.032 ± 0.030	2.965	0.100 ± 0.011 ± 0.004	0.452 ± 0.015 ± 0.0028
0.305	2.919 ± 0.033 ± 0.029	2.975	0.188 ± 0.013 ± 0.008	0.654 ± 0.017 ± 0.007
0.315	2.735 ± 0.033 ± 0.055	2.985	0.290 ± 0.015 ± 0.012	0.817 ± 0.019 ± 0.008
0.325	2.475 ± 0.033 ± 0.049	2.995	0.452 ± 0.018 ± 0.018	1.092 ± 0.022 ± 0.011
0.335	2.277 ± 0.034 ± 0.046	3.005	0.705 ± 0.021 ± 0.028	1.403 ± 0.025 ± 0.014
0.345	2.203 ± 0.035 ± 0.044	3.015	1.024 ± 0.025 ± 0.041	1.877 ± 0.031 ± 0.019
0.355	2.005 ± 0.035 ± 0.040	3.025	1.546 ± 0.031 ± 0.031	2.350 ± 0.036 ± 0.047
0.365	1.928 ± 0.036 ± 0.039	3.035	2.023 ± 0.036 ± 0.040	2.860 ± 0.041 ± 0.057
0.375	1.867 ± 0.037 ± 0.037	3.045	2.610 ± 0.042 ± 0.052	3.299 ± 0.046 ± 0.066
0.385	1.765 ± 0.037 ± 0.035	3.055	3.235 ± 0.049 ± 0.065	3.662 ± 0.050 ± 0.073
0.395	1.696 ± 0.037 ± 0.034	3.065	3.840 ± 0.053 ± 0.077	3.844 ± 0.052 ± 0.077
0.405	1.657 ± 0.038 ± 0.033	3.075	4.042 ± 0.055 ± 0.081	4.039 ± 0.053 ± 0.081
0.415	1.614 ± 0.038 ± 0.032	3.085	4.316 ± 0.055 ± 0.086	4.147 ± 0.052 ± 0.083
0.425	1.602 ± 0.038 ± 0.032	3.095	4.111 ± 0.053 ± 0.082	3.899 ± 0.050 ± 0.078
0.435	1.669 ± 0.040 ± 0.033	3.105	3.795 ± 0.049 ± 0.076	3.518 ± 0.046 ± 0.070
0.445	1.569 ± 0.040 ± 0.031	3.115	3.420 ± 0.044 ± 0.068	2.906 ± 0.042 ± 0.058
0.455	1.481 ± 0.039 ± 0.044	3.125	2.966 ± 0.040 ± 0.059	2.262 ± 0.036 ± 0.045
0.465	1.473 ± 0.039 ± 0.044	3.135	2.434 ± 0.035 ± 0.049	1.625 ± 0.031 ± 0.032
0.475	1.534 ± 0.041 ± 0.046	3.145	1.904 ± 0.030 ± 0.038	1.110 ± 0.026 ± 0.022
0.485	1.297 ± 0.037 ± 0.052	3.155	1.564 ± 0.026 ± 0.031	0.760 ± 0.022 ± 0.015
0.495	1.264 ± 0.036 ± 0.051	3.165	1.143 ± 0.022 ± 0.023	0.496 ± 0.018 ± 0.010
0.505	1.236 ± 0.034 ± 0.049	3.175	0.893 ± 0.019 ± 0.018	0.333 ± 0.016 ± 0.013
0.515	1.287 ± 0.034 ± 0.051	3.185	0.671 ± 0.017 ± 0.013	0.176 ± 0.012 ± 0.009
0.525	1.230 ± 0.034 ± 0.062	3.195	0.475 ± 0.015 ± 0.010	0.093 ± 0.008 ± 0.007
0.535	0.981 ± 0.032 ± 0.069	3.205	0.296 ± 0.013 ± 0.009	0.032 ± 0.005 ± 0.005
0.545	0.131 ± 0.006 ± 0.011	3.215	0.019 ± 0.002 ± 0.001	0.002 ± 0.000 ± 0.001

Table 4.2.: Double differential cross sections for the reaction $d p \rightarrow {}^3\text{He} \pi^+ \pi^-$ as functions of the invariant masses $m_{\pi^+\pi^-}$, $m_{^3\text{He}\pi^+}$ and $m_{^3\text{He}\pi^-}$ integrated over the CMS ${}^3\text{He}$ production angle range $143^\circ < \vartheta_{^3\text{He}}^{CMS} < 173^\circ$. The uncertainties quoted are statistical (first number) and known systematic (second number). In addition there is an overall normalisation uncertainty of 6%.

4. *Determination of cross sections*

5. Conclusions and outlook

The reactions $d p \rightarrow {}^3\text{He} \pi^+ \pi^-$ and $d p \rightarrow {}^3\text{He} \pi^+ \pi^- \pi^0$ were measured with the ANKE spectrometer at a total centre-of-mass energy of $\sqrt{s} = 3.353$ GeV, corresponding to excess energies of $Q = 265$ MeV and $Q = 130$ MeV respectively. The main motivation of the investigation was to shed more light on production mechanisms leading to the two-pion final state, particularly in the energy region where the so-called ABC effect is observed. Intensive studies on this long-standing phenomenon have in recent years also been made with the WASA setup at both the CELSIUS and the COSY accelerators. These experiments led to unexpected and interesting findings, in particular of a narrow resonance structure, which call for further research. The capability of neutral pion detection and the high geometrical acceptance of WASA can be usefully complemented by the good momentum resolution, a reliable normalisation and high statistics achieved in the current ANKE experiment, allowing to illuminate additional aspects of two-pion production processes.

In the previous chapters, the experimental conditions and the performed analysis steps have been elaborated. With the coincident detection of all three charged particles, it was possible to reconstruct kinematically complete data samples for both studied reactions. The phase space coverage for the two-pion production was improved significantly further through the additional consideration of events with only one of the pions measured in coincidence with the ${}^3\text{He}$ nucleus. For these events the precise track information of the detected particles allowed for a momentum reconstruction of the missing pion. The application of various selection steps led to very clean data samples of both reactions, each with a negligible amount of background. Strong deviations of invariant mass and angular distributions from pure phase space in the case of two-pion production necessitated an elaborate correction for the limited acceptance of the ANKE detector system. With an isobar model developed primarily for this purpose, it was possible to adequately reproduce the observed invariant mass distributions in the examined ${}^3\text{He}$ angular range and to provide an accurate acceptance correction on the basis of Geant simulations. By testing the approach with the help of model variations as well as a four-dimensional acceptance analysis, it was possible to confirm its applicability for a ${}^3\text{He}$ angular range of $143^\circ < \vartheta_{{}^3\text{He}}^{CM} < 173^\circ$. Systematic uncertainties associated with the correction method were estimated to be below 5% for most of the data points.

5.1. Two-pion production

The derived averaged differential cross section is consistent with results from earlier measurements at CELSIUS-WASA and Saturne. The two-particle invariant mass spectra are dominated by the well known ABC structure and the peaks in the $m_{^3\text{He}\pi^\pm}$ distributions. The difference between the latter two could be extracted with high precision, revealing the influence of isovector $\pi^+\pi^-$ production. An attempt to model this effect in terms of a $N^*(1440) \rightarrow \Delta(1232) \rightarrow N$ decay chain was driven by the underlying idea that the observed charge difference is caused by an excess of processes leading to $\Delta \rightarrow N\pi^+$ compared to $\Delta \rightarrow N\pi^-$. In this case, the Δ resonance would effect dominantly on the $m_{^3\text{He}\pi^+}$ spectrum, whereas the peak-like structure in the $m_{^3\text{He}\pi^-}$ distribution were to be understood as a kinematic reflection. With an analysis of the corresponding isospin relations (see Section 4.2.2), it could be shown that there is an equally strong preference of the channels $p^* \rightarrow (\Delta^{++} \rightarrow p\pi^+)\pi^-$ and $n^* \rightarrow (\Delta^0 \rightarrow n\pi^-)\pi^+$ over the other possible decay routes. Hence, only for nuclei with unequal numbers of protons and neutrons, the considered process must lead to a different appearance of the nucleus-pion invariant mass spectra. In the context of the applied model, the proton-neutron ratio of 2 : 1 in the ^3He nucleus is in agreement with the observed tendency, but is however not sufficient for a description of the size of difference observed in the data, even if the N^* is considered to dominate the two-pion production process. A good reproduction of the total results was achieved by completely neglecting the influence of neutron excitations, which supports a scenario where the nucleons in the beam deuteron remain in a bound state and only the target proton is excited.

The validity of the data description has furthermore been tested for the region of low two-pion invariant masses ($m_{\pi^+\pi^-} < 0.34\text{GeV}/c^2$). The observed underestimation of the charge difference by the isobar model provides an evidence for further contributions to the $\pi^+\pi^-$ isovector part. Such an observation is remarkable, because $I_{\pi^+\pi^-} = 1$ involves the contribution of relative p-waves (see Section 1.1.2) which have to vanish at the $\pi^+\pi^-$ threshold and were not expected to be of considerable strength in the low mass region.

As discussed in Section 1.1.2, the CELSIUS-WASA collaboration estimated the $\pi\pi$ isovector rate at almost the same energy from a comparison of the $\pi^+\pi^-$ and $\pi^0\pi^0$ cross section distributions [B⁺06] (see also left hand side of 1.4) and did only identify relevant contributions above $m_{\pi\pi} = 400$ MeV. As stated by the authors, the conclusion depends strongly on the relative normalisation, to which they assign an uncertainty of about 10% [Bas14]. However, even if this is accounted for, relatively little isovector strength can be deduced for $m_{\pi^+\pi^-} < 340$ MeV/ c^2 .

Alternative access to cross section values of the $I_{\pi\pi} = 1$ part is possible by investigating the $^3\text{H}\pi^+\pi^0$ final state. The only published results are from inclusive

measurements at much lower or higher energies ($Q_{\pi^+\pi^0} = 188$ MeV from the original ABC experiment [BAC61], $Q_{\pi^+\pi^0} = 337$ MeV and $Q_{\pi^+\pi^0} = 354$ MeV from Saturne [B⁺73]), each conducted at an individual ${}^3\text{H}$ laboratory-system angle. All three triton momentum distributions indicate slight enhancements below $m_{\pi\pi} = 400$ MeV/ c^2 , although these are small in comparison to the ABC enhancements in the ${}^3\text{He}$ momentum spectra that correspond to similar kinematic conditions. In consideration of the relation $\sigma_{I=1}({}^3\text{He} \pi\pi) = \frac{1}{2}\sigma({}^3\text{H} \pi\pi)$, following from isospin conservation, C. Wilkin extracted for the low energy data points in the region of the ABC peak the production ratio $I_{\pi\pi} = 1/I_{\pi\pi} = 0$ [Wil13, M⁺14]. Depending on the background assumptions, these seem to be compatible with an isovector rate of about 10% in the $\pi^+\pi^-$ channel for $m_{\pi^+\pi^-} < 340$ MeV/ c^2 . Similar values can be extracted roughly for both energies from the Saturne experiment. With $I_{\pi\pi} = 1$ contributions of this magnitude, it might be possible to explain the observed $m_{{}^3\text{He} \pi^\pm}$ difference. However, it has to be considered that the data presented in this work were taken at energy and angular conditions, where the isoscalar ABC effect is known to be maximal. It therefore cannot be concluded from the available information on the ${}^3\text{H} \pi^+ \pi^0$ channel and its comparison to corresponding ${}^3\text{He} \pi\pi$ results, that the extracted ratio may be extrapolated to the energy of the ANKE results. It would hence be of high value to fill the gap of available data on the double-pionic triton production by measurements in the ABC energy region.

In summary, there is currently too little experimental information available to reliably test the finding of significant contributions to the isovector $\pi\pi$ channel at low two-pion invariant masses, as indicated by the presented measurement of a large difference in the $m_{{}^3\text{He} \pi^\pm}$ spectra. If this finding is actually associated with a large influence of N^* decay channels, then these resonances should also contribute to two-pion production with $I_{\pi\pi} = 0$, which might lead to an impact on the evaluation of isoscalar results. The Roper influence has for example so far not been considered important in a description of recent results on the $d p \rightarrow {}^3\text{He} \pi^0 \pi^0$ reaction by WASA-at-COSY [PdR14a], emphasising rather on dibaryon and conventional $\Delta\Delta$ production.

In order to further study the influence of the $N^*(1440) \rightarrow \Delta(1232) \rightarrow N$ decay chain on the charge difference, exclusive measurements on the $d p \rightarrow {}^3\text{He} \pi^+ \pi^-$ reaction at much lower or higher energies could be very useful. According to the explanations in Section 4.2.2, the majority of the Δ resonances effects on the $m_{{}^3\text{He} \pi^+}$ spectrum, whereas the shape of the $m_{{}^3\text{He} \pi^-}$ distribution is mainly a reflection of that. As can be seen from Figure 5.1, the picture would change significantly for total energies that are 50 MeV lower or higher than that of the here presented measurement. The difference becomes more evident at lower energies, caused by the fact that the resonance position $m_{{}^3\text{He}} - m_p + m_\Delta$ moves towards the edge of the invariant mass spectrum. In contrast, at higher energies the apparent charge difference results predominantly from the asymmetric shape of the Delta Breit-

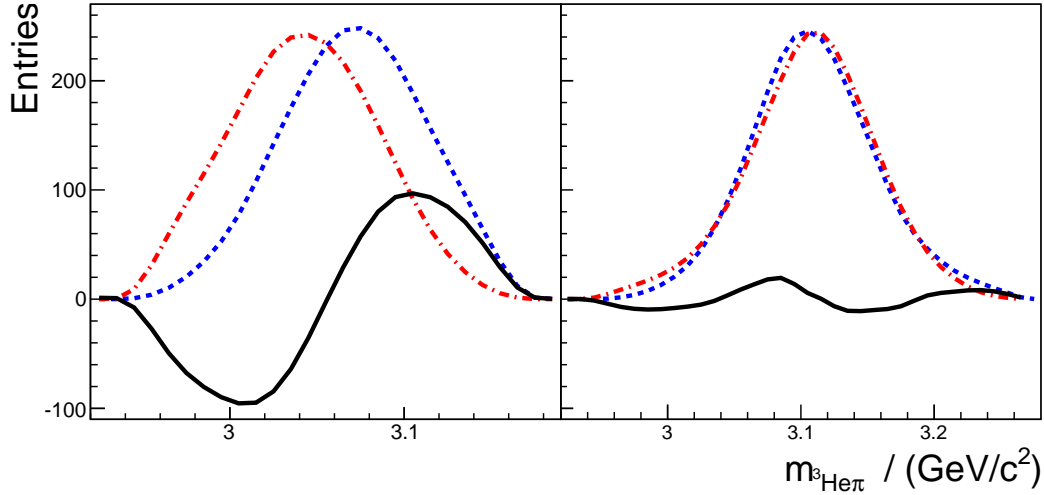


Figure 5.1.: Shapes of the $m_{3\text{He}\pi^+}$ (blue dashed curves) and $m_{3\text{He}\pi^-}$ (red dash-dotted curves) distributions of events which were generated according to the discussed isobar model (Equation 4.1) at total energies of $\sqrt{s} = 3.30$ GeV (left hand side) and $\sqrt{s} = 3.40$ GeV (right hand side). Differences are plotted as black solid curves.

Wigner function. The availability of corresponding exclusive data samples could hence be used to further investigate the suspected influence of N^* resonances.

It is however clear that their influence is not sufficient to explain the full extent of discovered isovector strength. Neither can the observed effects be explained as a consequence of isospin violation in terms of slight differences in the masses of the Δ resonances [P⁺78]. Such modifications of the applied model were tested and found to be of minor importance. This finding is in accordance with unpublished WASA-at-COSY data on $n p \rightarrow d \pi^+ \pi^-$, where no charge difference is observed [Bas14].

A general deficiency of the description according to Equation 4.1 is, that the charge difference cancels at very high $m_{\pi\pi}$, because of the limited available phase space. In contrast to that, significant contributions to the high mass region are present in the CELSIUS-WASA data [B⁺06]. It appears therefore reasonable to consider further possible effects on the isovector channel. One possible extension is the introduction of a $\pi^+\pi^-$ final state interaction [Wil14]. In contrast to the $I = 0$ two-pion interaction, which is known to be weak (see Section 1.1.1), it plays an important role in the $I_{\pi\pi} = 1$ state, where it may manifest in form of the ρ meson resonance. A respective extension of the isobar model might provide the required strengthening of the $\pi\pi$ isovector part. Whether it would lead to an increase of the $m_{3\text{He}\pi}$ difference depends then on the interference terms of the total amplitude. Further theoretical work is called for at this point.

As a further logical enhancement, one could assume that the final state interaction leads to an actual excitation of a ρ resonance. Although the presented data on the $d p \rightarrow {}^3\text{He} \pi^+ \pi^-$ reaction were measured at an energy which is about 235 MeV below the excitation threshold, the corresponding width of 150 MeV still allows for some ρ^0 contribution, predominantly in the region of high $m_{\pi\pi}$. Hence, this would support the above mentioned indications seen at CELSIUS-WASA. It is understood that the influence of the ρ meson should rise significantly if the experiment is conducted at higher energies. It should be noted in addition, that the decay of the nearby $N^*(1520)$ resonance into $N\rho$ has a branching ratio of 15-25% according to the Particle Data Group [B⁺12], and might therefore also be of importance here.

Recently conducted measurements on the $p d \rightarrow {}^3\text{He} \eta$ reaction in a total energy range of about $3.37 < \sqrt{s} < 3.44$ GeV [B⁺14] provide, through a supplementary measurement of charged and uncharged pions, the possibility to investigate the question, how strong the features observed in the ANKE results are linked with the $N^*(1440) \rightarrow \Delta(1232) \rightarrow N$ decay chain. The most effective tool for this are probably the $m_{{}^3\text{He} \pi^\pm}$ spectra.

There are furthermore ANKE data from an experiment with vector and tensor polarised deuteron beams, which was conducted to measure the deuteron tensor analysing power T_{20} of the $\vec{d} p \rightarrow {}^3\text{He} \eta$ reaction close to the production threshold [P⁺14]. Though the measurement suffered from comparably low statistics, an analysis with respect to the $d p \rightarrow {}^3\text{He} \pi^+ \pi^-$ reaction may provide additional insight into the reaction mechanism of two-pion production in the ABC energy region. During the same beam time, data were also taken at a much lower energy, corresponding to a ${}^3\text{He} \pi^+ \pi^-$ excess energy of $Q = 100$ MeV. This is of particular interest, since in the low energy region, the knowledge about two-pion production in nuclear fusion reactions is highly ambiguous (see also the discussion in Section 1.1.2). New results could provide valuable information on the strength of the $\pi\pi$ isovector channel in that range.

5.2. Three-pion production

Based on a very clean data sample of 40 events, which could be assigned to the reaction $d p \rightarrow {}^3\text{He} \pi^+ \pi^- \pi^0$, the total cross section as well as differential cross sections as function of CMS ${}^3\text{He}$ production angles in the backward hemisphere were estimated for an excess energy of $Q = 130$ MeV. So far, no such results on direct three-pion production in dp collisions were published for energies within the first 350 MeV above threshold, and only few data exist on comparable nucleon-nucleon reactions. On the other hand, in many analyses of light meson production processes,

5. Conclusions and outlook

the consideration of this reaction is an important aspect of the background treatment.^a Even a rough estimation of the quantitative contribution would in these cases allow for more precise background descriptions. Moreover, investigations on direct three-pion production are of interest by themselves, since an improvement of the experimental data base is essential for a better understanding of the corresponding production processes. Although the reliability of the here presented results depends significantly on the assumption of a phase-space-like kinematic behaviour, in particular of the particle production angles, they may provide therefore valuable information.

The absolute values, and even more the comparison to two-pion production, lead to the conclusion that direct three-pion production in the energy region of the η meson threshold is of very low strength. A similar tendency was observed by the CELSIUS-WASA collaboration for pp collisions at $Q = 160$ MeV, where the ratio $\langle\sigma\rangle_{\pi^+\pi^-}/\langle\sigma\rangle_{\pi^+\pi^-\pi^0}$ was deduced to be ≈ 140 [P⁺07]. The still considerable relative difference to the ANKE result of $\langle d\sigma/d\Omega^{CMS}\rangle_{\pi^+\pi^-}/\langle d\sigma/d\Omega^{CMS}\rangle_{\pi^+\pi^-\pi^0} = 6760 \pm 1520_{stat}$ for the ${}^3\text{He}$ angular range $143^\circ < \vartheta_{{}^3\text{He}}^{CMS} < 173^\circ$ can for a great part be explained by different properties of the respective two-pion production processes. The resonance structure associated with the ABC effect is absent in pp collisions [S⁺09], but implies a strong increase of cross sections in the ${}^3\text{He}\pi\pi$ state. The numerator of the ANKE ratio is strengthened even further by the limitation in the ${}^3\text{He}$ production angle, since differential cross sections in the ABC energy region show a clear preference of the ${}^3\text{He}$ particles being emitted in forward or backward direction in CMS.

In comparison to the presented estimation of a total cross section for $d p \rightarrow {}^3\text{He}\pi^+\pi^-\pi^0$ at $Q = 130$ MeV, total cross sections at $Q = 386$ MeV and $Q = 432$ MeV, measured with CELSIUS-WASA in inverse kinematics [S⁺10], are about three orders of magnitude higher. Such a steep rise in the strength of three-pion production cannot be explained purely by the increase of the available phase space of the reaction. A possible reason can rather be found through studies on nucleon resonance decays. According to an isobar model developed by R. M. Sternheimer and S. J. Lindenbaum [SL61], the simultaneous excitation of $\Delta(1232)$ and N^* resonances would be expected to dominate in the low energy region. The maximum of the resonance curve of the $\Delta(1232)$ - $N^*(1440)$ combination almost coincides with the lower energy of the CELSIUS-WASA experiment ($Q = 386$ MeV), for which the larger cross section had been determined. Since the ANKE experiment was conducted far below this region, only a very small tail of the excitation distribution could have contributed to three-pion production. In consideration of a hardly quantifiable systematic uncertainty of the ANKE result, the estimated cross section

^a See for example studies on the ${}^3\text{He}\eta$ final state by the ANKE [R⁺09] and WASA-at-COSY [A⁺14b] collaborations.

of about 1 nb seems plausible within the isobar model.

From the recently conducted WASA measurements on dp collisions (see previous section), also data on three-pion production in the excess energy range $150 \text{ MeV} < Q < 220 \text{ MeV}$ are available. A respective investigation could help to further verify the predictions of the discussed isobar model.

5. *Conclusions and outlook*

A. Appendix

A.1. Concepts of relativistic kinematics and associated analysis techniques

Relativistic processes in particle physics are commonly described by four-momentum vectors. With the three-momentum \vec{p} and energy E of a particle or particle system these are defined as

$$\mathbb{P} = (E, \vec{p}). \quad (\text{A.1})$$

Here and in the following, the simplifying notation with $\hbar = c = 1$ is used.

The scalar product of four-momenta is invariant under Lorentz transformation. The squared norm of a particle's four-momentum-vector

$$\mathbb{P}^2 = E^2 - \vec{p}^2 = m_{inv}^2, \quad (\text{A.2})$$

with m_{inv} denoting the invariant mass, is therefore constant in all reference frames. For single particles, m_{inv} is identical with the rest mass m_0 . This fact can be utilised to identify a particle X through its decay products $1, 2, \dots, n$. By accounting for energy and momentum conservation, which leads to

$$\mathbb{P}_1 + \mathbb{P}_2 + \dots + \mathbb{P}_n = \mathbb{P}_X, \quad (\text{A.3})$$

it can be shown that the invariant mass of the decay products is identical to the rest mass of the initial particle:

$$m_{inv}^2 = |\mathbb{P}_1 + \mathbb{P}_2 + \dots + \mathbb{P}_n|^2 = |\mathbb{P}_X|^2 = m_X^2. \quad (\text{A.4})$$

More generally, the invariant mass of a particle system is equivalent to its total energy in its particular centre-of-mass frame. It can thus be understood as the sum of the rest masses and the relative kinetic energies of the involved particles.

Two-particle invariant mass distributions of a three-body final state, like in $d p \rightarrow {}^3\text{He} \pi^+ \pi^-$, do therefore reflect the relative movement of the particles.

In the cases where from a reaction of the type $a + b \rightarrow 1 + 2 + \dots + n$, only $m < n$ ejectiles have been reconstructed, the invariant mass of the missing ejectile system Y can be determined through

$$m_Y = |\mathbb{P}_Y| = |\mathbb{P}_a + \mathbb{P}_b - (\mathbb{P}_1 + \dots + \mathbb{P}_m)|. \quad (\text{A.5})$$

m_Y , also termed as the missing mass, is commonly used for the identification of particle reactions.

A.2. Basic properties of two-pion systems produced in fusion reactions of light nuclei

The possible characteristics of a two-pion system are defined by the individual particle properties, but do furthermore depend on the specific reaction in which they were produced. In the following, an overview will be provided on the differences in the minimum values of the invariant mass $m_{\pi\pi}$, the isospin states $I_{\pi\pi}$ and the associated relative angular momenta $L_{\pi\pi}$ for the reactions discussed in the context of this thesis.

Pions are pseudo-scalar mesons with the quantum numbers $I(J^P) = 1(0^-)$. The third components of isospin are $I_3 = 1$ (π^+), $I_3 = 0$ (π^0) and $I_3 = -1$ (π^-). According to the Particle Data Group (PDG), the charged pion masses are $(139.57018 \pm 0.00035) \text{ MeV}/c^2$, that of the neutral pion is $(134.9766 \pm 0.0006) \text{ MeV}/c^2$ [B⁺12]. Since pions are bosons, their total wave function is necessarily symmetric. It can be expressed as a product of wavefunctions that depend on space-, spin-, and isospin coordinates, leading to the symmetry requirement

$$(-1)^{L+S+I} = +1. \quad (\text{A.6})$$

The spin S is zero for single pions and hence also for two-pion systems. To satisfy Equation A.6, L and I need to be therefore either both odd or both even. This means, for $I_{\pi\pi} = 0$ or 2 , only $L = 0, 2, \dots$ is possible, whereas $I_{\pi\pi} = 1$ is associated with $L = 1, 3, \dots$. The isospins can principally couple to $I_{\pi\pi} = 0, 1$ or 2 , also denoted as isoscalar ($I_{\pi\pi} = 0$), isovector ($I_{\pi\pi} = 1$) and isotensor ($I_{\pi\pi} = 2$) states.

Depending on the actual combination of pions, there are the following characteristics:

A.2. Basic properties of two-pion systems produced in fusion reactions of light nuclei

$\pi^0 \pi^0$: These are identical particles, causing the two-pion system to have solely even angular momentum numbers. $L = 1$ and, due to the above mentioned symmetry considerations, also $I_{\pi\pi} = 1$ are not allowed. The minimum value of $m_{\pi^0\pi^0}$ is $269.95 \text{ MeV}/c^2$.

$\pi^+ \pi^0$: The combination of $I_3 = 1$ and $I_3 = 0$ does not allow for a coupling to $I_{\pi\pi} = 0$. The minimum value of $m_{\pi^+\pi^0}$ is $274.55 \text{ MeV}/c^2$.

$\pi^+ \pi^-$: For this combination there are no principal restrictions on isospins and angular momenta, as long as the above mentioned symmetry condition is fulfilled. The minimum value of $m_{\pi^+\pi^-}$ is $279.14 \text{ MeV}/c^2$.

Under consideration of isospin conservation and the above given conditions, the allowed isospin states of the two-pion system are in the following deduced for each reaction that leads to a bound nucleus with a mass number up to $A = 4$.

$A = 2$:

$$\begin{array}{rcccl}
 & \text{p} & \text{n} & \rightarrow & \text{d} & (\pi^0 \pi^0) \\
 \mathbf{I} & 1/2 & 1/2 & & 0 & (0) \\
 \\
 & \text{p} & \text{n} & \rightarrow & \text{d} & (\pi^+ \pi^-) \\
 \mathbf{I} & 1/2 & 1/2 & & 0 & (0 \vee 1)
 \end{array}$$

$A = 3$:

$$\begin{array}{rcccl}
 & \text{d} & \text{p} & \rightarrow & {}^3\text{He} & (\pi^0 \pi^0) \\
 \mathbf{I} & 0 & 1/2 & & 1/2 & (0) \\
 \\
 & \text{d} & \text{p} & \rightarrow & {}^3\text{H} & (\pi^+ \pi^0) \\
 \mathbf{I} & 0 & 1/2 & & 1/2 & (1) \\
 \\
 & \text{d} & \text{p} & \rightarrow & {}^3\text{He} & (\pi^+ \pi^-) \\
 \mathbf{I} & 0 & 1/2 & & 1/2 & (0 \vee 1)
 \end{array}$$

$A = 4$:

$$\begin{array}{rcccl}
 & \text{d} & \text{d} & \rightarrow & {}^4\text{He} & (\pi^0 \pi^0) \\
 \mathbf{I} & 0 & 0 & & 0 & (0) \\
 \\
 & \text{d} & \text{d} & \rightarrow & {}^4\text{He} & (\pi^+ \pi^-) \\
 \mathbf{I} & 0 & 0 & & 0 & (0)
 \end{array}$$

Effects of isospin relations on relative production amplitudes of the ${}^3\text{He}/{}^3\text{H} \pi\pi$ final states

One approach to determine relative $I_{\pi\pi} = 1/I_{\pi\pi} = 0$ production intensities relies on a comparison of the $d p \rightarrow {}^3\text{He} \pi^+ \pi^-$ reaction, where both channels contribute, with the single $\pi\pi$ -isospin reaction $d p \rightarrow {}^3\text{He} \pi^0 \pi^0$. For this purpose, it is necessary to account for cross section differences which are caused by isospin relations. An analysis of the Clebsch-Gordan (CG) coefficients yields the following contributions

$\pi^0 \pi^0$:

$$I_{\pi\pi} = 0 \quad I_3(\pi_1) = 0 \quad I_3(\pi_2) = 0 \quad \text{CG: } -\sqrt{1/3}$$

$\pi^+ \pi^-$:

$$I_{\pi\pi} = 0 \quad I_3(\pi_1) = 1 \quad I_3(\pi_2) = -1 \quad \text{CG: } \sqrt{1/3}$$

$$I_{\pi\pi} = 0 \quad I_3(\pi_1) = -1 \quad I_3(\pi_2) = 1 \quad \text{CG: } \sqrt{1/3}$$

These lead to the cross section ratio $\sigma_{I_{\pi\pi}=0}(\pi^+ \pi^-) = 2 \sigma(\pi^0 \pi^0)$.

The same method of approach is possible for a comparison of the $I_{\pi\pi} = 1$ contributions in the ${}^3\text{He} \pi^+ \pi^-$ and ${}^3\text{H} \pi^+ \pi^0$ final states. Here the CG coefficients for the $\pi\pi$ combinations are identical. However, for the nucleus- $(\pi\pi)$ combinations one finds:

${}^3\text{He} \pi^+ \pi^-$:

$$I_{\pi\pi} = 1 \quad I_3({}^3\text{He}) = 1/2 \quad I_3((\pi\pi)^0) = 0 \quad \text{CG: } \sqrt{1/3}$$

${}^3\text{H} \pi^+ \pi^0$:

$$I_{\pi\pi} = 1 \quad I_3({}^3\text{H}) = 1/2 \quad I_3((\pi\pi)^+) = 1 \quad \text{CG: } -\sqrt{2/3}$$

This relation leads to the cross section ratio $\sigma_{I_{\pi\pi}=1}({}^3\text{He} \pi^+ \pi^-) = \sigma({}^3\text{H} \pi^+ \pi^0)/2$.

A.3. Monte Carlo generated event distributions

The Monte Carlo generated distributions, presented in Chapter 4, reflect the ANKE detector acceptance, but are influenced by the actual event distributions. For a better understanding of the shown spectra, it is helpful to know the actual detector input in form of the generated event distribution. Note that for a three-body final state, a uniform distribution in phase space implies uniform distributions in the two-dimensional squared invariant mass spectra (Dalitz Plots), but not in case of the here shown linear invariant mass distributions.

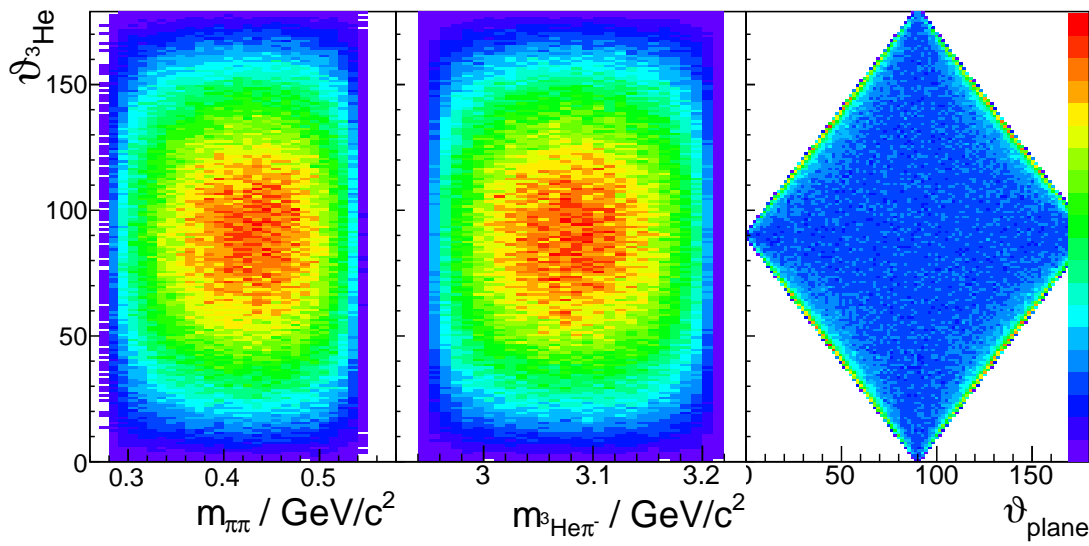


Figure A.1.: Monte Carlo generated distributions of events on the assumption of a uniformly filled phase space without request of acceptance by the ANKE detector system or other restrictions. Shown are the correlations between the ^3He production angle and the other three chosen independent variables $m_{\pi^+\pi^-}$, $m_{^3\text{He}\pi^-}$ and $\vartheta_{\text{plane}}^{CMS}$ as in Figure 4.1. The coloured scale is linear, starting at 0. The maxima of the three distributions are not necessarily identical.

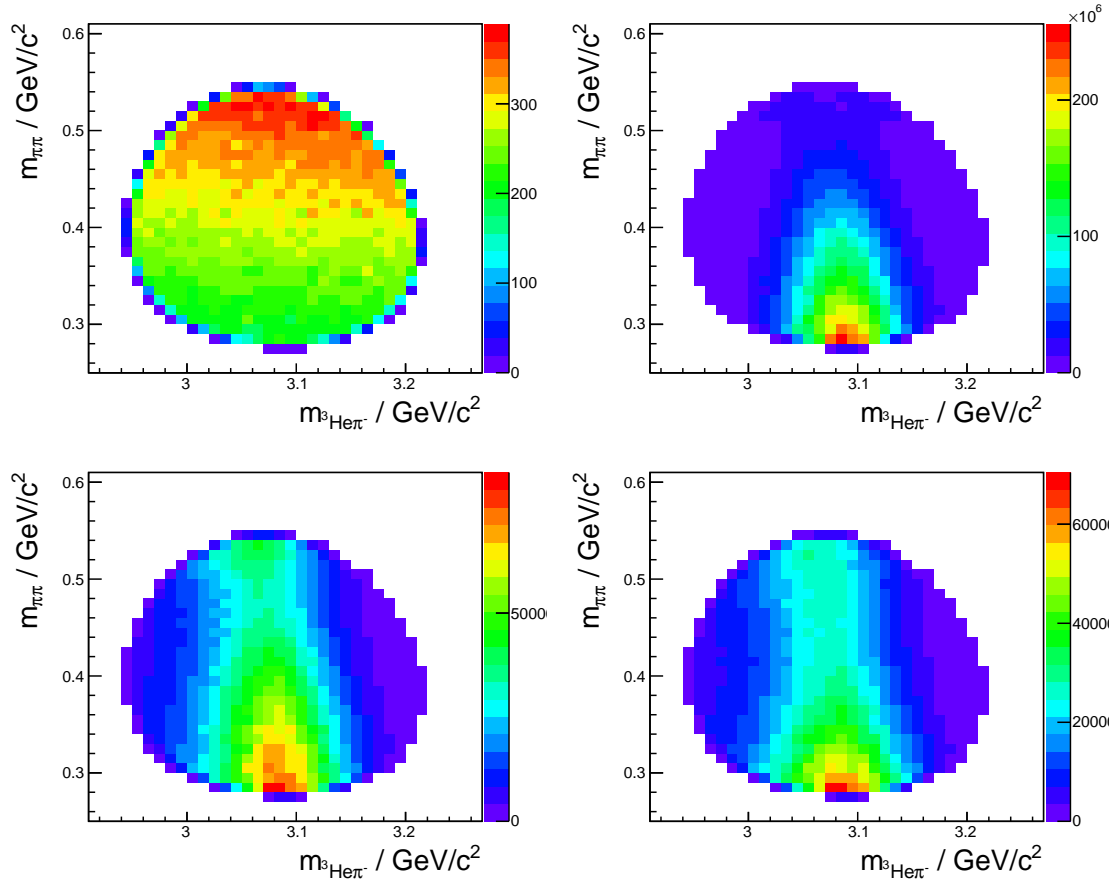


Figure A.2.: Monte Carlo generated distributions of events without request of acceptance by the ANKE detector system, but with the confinement $143^\circ < \vartheta_{3\text{He}}^{CMS} < 173^\circ$. Shown are the correlations between $m_{\pi^+\pi^-}$ and $m_{3\text{He}\pi^-}$ according to uniformly filled phase space (upper left), $\Delta\Delta$ model as explained in Section 4.2.2 (upper right), $N^*(1440) \rightarrow \Delta(1232)\pi \rightarrow N\pi\pi$ decay chain as in Equations 4.1 (lower left) and 4.5 (lower right). Except for the phase space distribution, the spectra do reflect the ABC enhancement at small $m_{\pi^+\pi^-}$ values, as well as the central peak structure in $m_{3\text{He}\pi^-}$.

Bibliography

- [A⁺00] M. Andersson et al. Isospin resolved double pion production in the reaction $p + d \rightarrow {}^3\text{He} + 2\pi$. *Physics Letters B*, 485(4):327 – 333, 2000.
- [A⁺11] P. Adlarson et al. Abashian-Booth-Crowe effect in basic double-pionic fusion: A new resonance? *Physical Review Letters*, 106:242302, Jun 2011.
- [A⁺12] P. Adlarson et al. Abashian-Booth-Crowe resonance structure in the double pionic fusion to ${}^4\text{He}$. *Physical Review C*, 86:032201, Sep 2012.
- [A⁺14a] P. Adlarson et al. ABC effect and resonance structure in the double-pionic fusion to ${}^3\text{He}$. *arXiv:1408.5744*, 2014.
- [A⁺14b] P. Adlarson et al. Cross section ratio and angular distributions of the reaction $p + d \rightarrow {}^3\text{He} + \eta$ at 48.8 MeV and 59.8 MeV excess energy. *The European Physical Journal A*, 50(6), 2014.
- [ABC60] A. Abashian, N. E. Booth, and K. M. Crowe. Possible anomaly in meson production in $p + d$ collisions. *Physical Review Letters*, 5:258–260, Sep 1960.
- [AR99] L. Alvarez-Ruso. The role of the Roper resonance in $np \rightarrow d(\pi\pi)^0$. *Physics Letters B*, 452:207 – 213, 1999.
- [AROH98] L. Alvarez-Ruso, E. Oset, and E. Hernández. Theoretical study of the $NN \rightarrow NN \pi\pi$ reaction. *Nuclear Physics A*, 633(3):519 – 543, 1998.
- [B⁺73] J. Banaigs et al. "ABC" and "DEF" effects in the reaction $d + p \rightarrow \text{He}^3 (\text{mm})^0$: Position, width, isospin, angular and energy distributions. *Nuclear Physics B*, 67(1):1 – 36, 1973.
- [B⁺76] J. Banaigs et al. A study of the inclusive reaction $d + d \rightarrow {}^4\text{He} + X$, the ABC effect, and $I=0$ meson resonances. *Nuclear Physics B*, 105(1):52–76, 1976.
- [B⁺97] Chr. Bargholtz et al. The inclusive reaction $d + d \rightarrow {}^4\text{He} + X$ 29 MeV above the $2\pi^0$ threshold. *Physics Letters B*, 398:264 – 268, 1997.

- [B⁺99] F. Bellemann et al. Pion-pion p-wave dominance in the $pd \rightarrow {}^3\text{He} \pi^+ \pi^-$ reaction near threshold. *Physical Review C*, 60:061002, Nov 1999.
- [B⁺01a] F. Balestra et al. φ and ω meson production in pp reactions at $p_{\text{lab}} = 3.67$ GeV/c. *Physical Review C*, 63:024004, 2001.
- [B⁺01b] S. Barsov et al. ANKE, a new facility for medium energy hadron physics at COSY-Jülich. *Nuclear Instruments and Methods in Physics Research Section A: Accelerators, Spectrometers, Detectors and Associated Equipment*, 462(3):364 – 381, 2001.
- [B⁺02a] W. Brodowski et al. Exclusive measurement of the $pp \rightarrow pp \pi^+ + \pi^-$ reaction near threshold. *Physical Review Letters*, 88(19):192301, 2002.
- [B⁺02b] M. Büscher et al. Identification of K^+ -mesons from subthreshold pA collisions with ANKE at COSY-Jülich. *Nuclear Instruments and Methods in Physics Research Section A: Accelerators, Spectrometers, Detectors and Associated Equipment*, 481:378 – 396, 2002.
- [B⁺06] M. Bashkanov et al. Exclusive measurements of $pd \rightarrow {}^3\text{He} \pi \pi$: The ABC effect revisited. *Physics Letters B*, 637(4-5):223 – 228, 2006.
- [B⁺12] J. Beringer et al. Review of particle physics. *Physical Review D*, 86:010001, 2012.
- [B⁺14] F. Bergmann et al. Investigation of total cross section structures in the $pd \rightarrow {}^3\text{He} \eta$ reaction at WASA-at-COSY. COSY Proposal # 220, 2014.
- [BA63] N. E. Booth and A. Abashian. Meson production in $p + d$ collisions and the $I = 0 \pi - \pi$ interaction. IV. Double-pion production and pion-pion scattering. *Physical Review*, 132:2314–2322, 1963.
- [BAC61] N. E. Booth, A. Abashian, and K. M. Crowe. Anomaly in meson production in $p + d$ collisions. *Physical Review Letters*, 7:35–39, Jul 1961.
- [Bas06] M. Bashkanov. *Double Pionic Fusion: Towards an Understanding of the ABC Puzzle by Exclusive Measurements*. PhD thesis, Eberhard-Karls-Universität Tübingen, 2006.
- [Bas14] M. Bashkanov. Private communication, 2014.
- [C⁺66] K. R. Chapman et al. Observation of the reaction $d + d \rightarrow {}^4\text{He} + 2\pi$ at 1.69 GeV/c. *Physics Letters*, 21(4):465 – 467, 1966.
- [D⁺68] V. Dalhagav et al. *Yadernaya Fizika*, 8:342, 1968.
- [D⁺80] Ya. S. Derbenev et al. Accurate calibration of the beam energy in a storage ring based on measurement of spin precession frequency of polarized particles. *Particle Accelerators*, 10:177–180, 1980.

-
- [D⁺97] H. Dombrowski et al. The Münster cluster target for internal storage ring experiments. *Nuclear Instruments and Methods in Physics Research Section A: Accelerators, Spectrometers, Detectors and Associated Equipment*, 386:228 – 234, 1997.
- [D⁺04] S. Dymov et al. The forward detector of the ANKE spectrometer. Tracking system and its use in data analysis. *Particles and Nuclei, Letters*, 119(2):40–53, 2004.
- [D⁺09] S. Dymov et al. Observation of an ABC effect in proton-proton collisions. *Physical Review Letters*, 102:192301, 2009.
- [Dym09] S. Dymov. FD momentum calibration for March08 beam time. Internal notes of the ANKE collaboration, 2009.
- [Eve12] M. Evelt. Identifikation des $^3\text{He} \pi^0$ Endzustandes in Deuteron-Proton-Kollisionen am ANKE-Experiment. Bachelor's thesis, Westfälische Wilhelms-Universität Münster, 2012.
- [F⁺07] I. Fröhlich et al. Pluto: A Monte Carlo simulation tool for hadronic physics. *PoS, ACAT2007:076*, 2007.
- [FGW00] G. Fäldt, A. Gårdestig, and C. Wilkin. Production of isoscalar pion pairs in the $p d \rightarrow ^3\text{He} \pi \pi$ reaction near threshold. *Physics Letters B*, 496:185 – 189, 2000.
- [Fri11] C. Fritzscht. Energy calibration for the ANKE experiment. Bachelor's thesis, Westfälische Wilhelms-Universität Münster, 2011.
- [Fri14] C. Fritzscht. Untersuchung verschiedener Normierungsreaktionen für dp-Kollisionen am ANKE-Experiment. Master's thesis, Westfälische Wilhelms-Universität Münster, 2014.
- [FTW06] G. Fäldt, U. Tengblad, and C. Wilkin. Two-pion production in deuteron-deuteron collisions at low energies. *The European Physical Journal A - Hadrons and Nuclei*, 28(2):245–249, 2006.
- [G⁺91] E. Gülmez et al. Absolute differential cross section measurements for proton-deuteron elastic scattering at 641.3 and 792.7 MeV. *Physical Review C*, 43:2067–2076, May 1991.
- [GFW98] A. Gårdestig, G. Fäldt, and C. Wilkin. An explanation of the ABC enhancement in the $d d \rightarrow \alpha X$ reaction at intermediate energies. *Physics Letters B*, 421:41 – 45, 1998.

- [Gos08] P. Goslawski. Hochpräzise Impulsbestimmung des COSY-Beschleunigerstrahls im Rahmen der Messung zur Bestimmung der η -Masse am Experimentaufbau ANKE. Diplomarbeit, Westfälische Wilhelms-Universität Münster, 2008.
- [Gos13] P. Goslawski. *High precision measurement of the η meson mass at COSY - ANKE*. PhD thesis, Westfälische Wilhelms-Universität Münster, 2013.
- [Gri14] S. Grieser. The cluster-jet target MCT1S and the analysis of cluster beams. Master's thesis, Westfälische Wilhelms-Universität Münster, 2014.
- [H⁺82] C. L. Hollas et al. Deuteron spectrum in $np \rightarrow d(\pi\pi)^0$ at 1.46 GeV/c. *Physical Review C*, 25:2614–2618, May 1982.
- [Her13] A.-K. Hergemöller. Präparation von Clusterstrahlen und der Aufbau der finalen Clusterquelle für das PANDA-Experiment. Master's thesis, Westfälische Wilhelms-Universität Münster, 2013.
- [HHM02] V. Hejny, M. Hartmann, and A. Mussgiller. RootSorter: a new analysis framework for ANKE. Forschungszentrum Jülich Annual Report, 2002.
- [I⁺83] F. Irom et al. Measurements of small angle elastic $\vec{p}d$ scattering at 796 MeV using a recoil method. *Physical Review C*, 28(6):2380, 1983.
- [Jun00] H. Junghans. *Bestimmung der Impulsspektren von K^+ Mesonen aus Proton-Kern-Reaktionen bei Projektilenergien unterhalb der freien NN-Schwelle*. PhD thesis, Universität zu Köln, 2000.
- [K⁺99] A. Khoukaz et al. Systematic studies on hydrogen cluster beam production. *The European Physical Journal D - Atomic, Molecular, Optical and Plasma Physics*, 5(2):275–281, 1999.
- [K⁺01] V. Koptev et al. Forward K^+ production in subthreshold pA collisions at 1.0 GeV. *Physical Review Letters*, 87:022301, 2001.
- [K⁺09] S. Keleta et al. Exclusive measurement of two-pion production in the $dd \rightarrow {}^4\text{He} \pi\pi$ reaction. *Nuclear Physics A*, 825:71 – 90, 2009.
- [K⁺10] F. Kren et al. Exclusive measurements of $pp \rightarrow d\pi^+\pi^0$: Double-pionic fusion without ABC effect. *Physics Letters B*, 684:110 – 113, 2010.
- [Köh] E. Köhler. *In preparation*. PhD thesis, Westfälische Wilhelms-Universität Münster.

-
- [Köh10] E. Köhler. Das Münsteraner Cluster-Jet Target MCT2, ein Prototyp für das PANDA-Experiment, und die Analyse der Eigenschaften des Clusterstrahls. Diplomarbeit, Westfälische Wilhelms-Universität Münster, 2010.
- [M⁺70] T. Maung et al. S - wave pion - pion scattering length from reaction $\pi^- p \rightarrow \pi^0 \pi^0 n$ at 378 MeV. *Physics Letters B*, 33(7):521 – 524, 1970.
- [M⁺01] I. Mohos et al. New Schottky-Pickup for COSY-Jülich. In *Proc. DIPAC 2001 - ESRF, Grenoble, France*, 2001.
- [M⁺07] T. Mersmann et al. Precision study of the $\eta^3\text{He}$ system using the $dp \rightarrow {}^3\text{He}\eta$ reaction. *Physical Review Letters*, 98:242301, Jun 2007.
- [M⁺13] M. Mikirtychyants et al. The polarized H and D atomic beam source for ANKE at COSY-Jülich. *Nuclear Instruments and Methods in Physics Research Section A: Accelerators, Spectrometers, Detectors and Associated Equipment*, 721(0):83 – 98, 2013.
- [M⁺14] M. Mielke et al. Isospin effects in the exclusive $dp \rightarrow {}^3\text{He}\pi^+\pi^-$ reaction. *The European Physical Journal A*, 50(6):102, 2014.
- [Mai97] R. Maier. Cooler synchrotron COSY - Performance and perspectives. *Nuclear Instruments and Methods in Physics Research Section A: Accelerators, Spectrometers, Detectors and Associated Equipment*, 390:1 – 8, 1997.
- [MB79] J. Myrheim and L. Bugge. A fast Runge-Kutta method for fitting tracks in a magnetic field. *Nuclear Instruments and Methods*, 160(1):43 – 48, 1979.
- [Mch13] D. Mchedlishvili. *Studies of the neutron-proton charge-exchange amplitudes at COSY using the ANKE spectrometer*. PhD thesis, Tbilisi State University, 2013.
- [Mer03] T. Mersmann. Untersuchungen zur Proton-Deuteron-Streuung an einem Deuteriumclusterstrahl am Magnetspektrometer ANKE. Diplomarbeit, Westfälische Wilhelms-Universität Münster, 2003.
- [Mie07] M. Mielke. Untersuchung des ABC-Effekts in der Reaktion $dp \rightarrow {}^3\text{He}\pi^+\pi^-$ am Magnetspektrometer ANKE. Diplomarbeit, Westfälische Wilhelms-Universität Münster, 2007.
- [Mus04] A. Mussgiller. A new Geant4 based simulation framework for ANKE. Forschungszentrum Jülich Annual Report, 2004.

- [P⁺78] E. Pedroni et al. A study of charge independence and symmetry from π^+ and π^- total cross sections on hydrogen and deuterium near the 3, 3 resonance. *Nuclear Physics A*, 300(2):321 – 347, 1978.
- [P⁺00] D. Prasuhn et al. Electron and stochastic cooling at COSY. *Nuclear Instruments and Methods in Physics Research Section A: Accelerators, Spectrometers, Detectors and Associated Equipment*, 441:167 – 174, 2000.
- [P⁺03] J. Pätzold et al. The $pp \rightarrow pp \pi^+ + \pi^-$ reaction studied in the low-energy tail of the Roper resonance. *Physical Review C*, 67:052202, May 2003.
- [P⁺07] C. Pauly et al. The $pp \rightarrow pp\pi\pi\pi$ reaction channels in the threshold region. *Physics Letters B*, 649:122 – 127, 2007.
- [P⁺14] M. Papenbrock et al. Absence of spin dependence in the final state interaction of the reaction $\vec{d}p \rightarrow {}^3\text{He}\eta$ reaction. *Physics Letters B*, 734(0):333 – 337, 2014.
- [Pap] M. Papenbrock. *In preparation*. PhD thesis, Westfälische Wilhelms-Universität Münster.
- [PdR13] E. Perez del Rio. Private communication, 2013.
- [PdR14a] E. Pérez del Río. *ABC effect and d^* resonance in double-pionic fusion to ${}^3\text{He}$* . PhD thesis, Eberhard Karls Universität Tübingen, 2014.
- [PdR14b] E. Perez del Rio. Private communication, 2014.
- [Pil67] H. Pilkuhn. *The Interactions of Hadrons*. North-Holland Publishing Co. Amsterdam, 1967.
- [R⁺09] T. Rausmann et al. Precision study of the $dp \rightarrow {}^3\text{He}\eta$ reaction for excess energies between 20 and 60 MeV. *Physical Review C*, 80:017001, Jul 2009.
- [RS73] T. Risser and M.D. Shuster. Anomalous enhancements in multiple-pion production with deuterons. *Physics Letters B*, 43(1):68 – 72, 1973.
- [S⁺08] R. Stassen et al. The HESR RF-system and tests in COSY. *EPAC08, Genoa, Italy*, 2008.
- [S⁺09] T. Skorodko et al. Two-pion production in proton–proton collisions – experimental total cross sections and their isospin decomposition. *Physics Letters B*, 679(1):30–35, 2009.

-
- [S⁺10] K. Schönning et al. Production of η and 3π mesons in the $pd \rightarrow {}^3\text{He}X$ reaction at 1360 and 1450 MeV. *The European Physical Journal A*, 45(1):11–21, 2010.
- [S⁺11] T. Skorodko et al. $\Delta\Delta$ excitation in proton–proton induced $\pi^0\pi^0$ production. *Physics Letters B*, 695:115 – 123, 2011.
- [Sch99] V. Schwarz. *Kontinuierliche Messung der Polarisation eines Synchrotronstrahls während der Hochbeschleunigung*. PhD thesis, Rheinische Friedrich-Wilhelms-Universität Bonn, 1999.
- [Sch09] K. Schönning. *Meson Production in pd Collisions*. PhD thesis, Uppsala University, Sweden, 2009.
- [Sch12] D. Schröer. Strahlzeitvorbereitungen zur Untersuchung der schwelennahen Produktion von η -Mesonen in der quasifreien Reaktion $pd \rightarrow d\eta p_{spec}$ bei ANKE. Diplomarbeit, Westfälische Wilhelms-Universität Münster, 2012.
- [SL61] R. M. Sternheimer and S. J. Lindenbaum. Extension of the Isobaric Nucleon Model for Pion Production in Pion-Nucleon, Nucleon-Nucleon, and Antinucleon-Nucleon Interactions. *Physical Review*, 123:333–376, July 1961.
- [T⁺11] A. Täschner et al. High density cluster jet target for storage ring experiments. *Nuclear Instruments and Methods in Physics Research Section A: Accelerators, Spectrometers, Detectors and Associated Equipment*, 660(1):22 – 30, 2011.
- [Täs12] A. Täschner. *Entwicklung und Untersuchung von Cluster-Jet-Targets höchster Dichte*. PhD thesis, Westfälische Wilhelms-Universität Münster, 2012.
- [V⁺88] G.N. Velichko et al. Elastic pd scattering at small angles in the energy range of 700-1000 MeV. *Yadernaya Fizika*, 47:1185–1192, 1988.
- [W⁺73] C. Wilkin et al. A comparison of π^+ and π^- total cross sections of light nuclei near the $3-3$ resonance. *Nuclear Physics B*, 62:61–85, 1973.
- [W⁺80] E. Winkelmann et al. Proton-deuteron elastic scattering at 800 MeV. *Physical Review C*, 21:2535–2541, Jun 1980.
- [W⁺99] R. Wurzinger et al. Study of the ABC enhancement in the $dd \rightarrow \alpha X^0$ reaction. *Physics Letters B*, 445(3):423–427, 1999.
- [Wei66] S. Weinberg. Pion scattering lengths. *Physical Review Letters*, 17:616–621, 1966.

[Wil13] C. Wilkin. Private communication, 2013.

[Wil14] C. Wilkin. Private communication, 2014.

Danksagung – Acknowledgements

Das Folgende ist ein sicherlich unvollkommener Versuch, die Beiträge der vielen Menschen zu würdigen, die zum Gelingen dieser Arbeit beigetragen haben.

Als erstem in dieser Reihe danke ich Prof. Dr. Alfons Khoukaz, der mir die Möglichkeit gegeben hat, mich an einer herausfordernden Aufgabenstellung zu beweisen. Seine ruhige und sachliche Herangehensweise, verbunden mit einem freundlichen und zugewandten Umgang, war eine große Hilfe bei der Lösung vieler Probleme und haben meine eigene Arbeitsweise stark beeinflusst.

Herrn Prof. Dr. Johannes P. Wessels bin ich sehr dankbar, dass er sich als Zweitgutachter zur Verfügung gestellt hat. Gleiches gilt für Priv.- Doz. Dr. Jochen Heitger, der freundlicherweise die Rolle des Drittprüfers übernommen hat.

I am deeply indebted to Prof. Dr. Colin Wilkin, whose patience, profound understanding of particle physics and never-ending support were invaluable for this work and have widened my own knowledge.

A large number of members of the ANKE collaboration supported my work in many different ways. Special thanks go to Dr. Andro Kacharava for his commitment, to Dr. Sergey Dymov for the forward momenta, furthermore to Dr. Michael Hartmann for all the hints and the nice conversations.

Thanks a lot also to Dr. Mikhail Bashkanov and Dr. Elena Perez del Rio for the support from Tübingen.

Durch stetiges Wachstum, insbesondere nach Einführung der Bachelor- und Masterstudiengänge, sieht und sah die Arbeitsgruppe während meiner Zeit inzwischen so viele Gesichter, dass ich unmöglich die Namen all dieser Menschen aufzählen kann, ohne irgendwen ungerechtfertigterweise zu unterschlagen. Euch allen ein großes Dankeschön für die Zeit, wo immer Ihr jetzt auch steckt.

Ein besonderer Dank geht an Timo Mersmann für das intensive Vorablesen meiner Arbeit, die nie nachlassende Unterstützung, das Antreiben (vor allem zum Laufen) und die Freundschaft, die aus all dem erwachsen ist.

Ähnliches gilt für Paul Goslawski, der sich seine ansteckende Begeisterungsfähigkeit zum Glück nie ganz hat nehmen lassen und dem ich viele

positive Anregungen zu verdanken habe. Sowohl im Bezug auf die Arbeit, als auch auf "das Leben".

Ein weiteres Extra-Dankeschön geht an Michael Papenbrock, Mitsinger beim Ersti-Wochenende, Praktikumpartner fürs Leben, Tischnachbar im Büro, Reisebegleiter in Polen und Italien, sowie Anschubser und Gestalter unseres kleinen Softwareprojekts. So viele gemeinsame Erlebnisse und prägende Erfahrungen. Danke für all das, aber jetzt müssen wir mal alleine klarkommen. Eine letzte besondere Erwähnung in der Reihe ehemaliger Bürokollegen möchte ich nicht unterschlagen, denn Michael Evelt hat es sogar geschafft, die Gute-Nacht-Geschichten meiner Kinder zu prägen. Danke für vieles, und besonders für den Faust.

Zum Abschluss auch ein Dank an meine Familie; meine Brüder, meine Eltern und natürlich vor allem an Nicole, Tammo und Tilo, die mich in den letzten Monaten und in der ganzen Zeit davor so eng begleitet haben wie es sonst wohl niemand ausgehalten hätte. Nichts, was ich hier schreiben könnte, würde Euch gerecht werden.